



Bernardo Cruz Varzielas

BSc in Sciences of Mechanical Engineering

# ROBOTIZING THE CONVENTIONAL AND HOT-FORGING WIRE ARC ADDITIVE MANUFACTURING PROCESSES FOR PRODUCING 3D PARTS WITH COMPLEX GEOMETRIES

MASTER IN MECHANICAL ENGINEERING

NOVA University Lisbon

September, 2022



# ROBOTIZING THE CONVENTIONAL AND HOT-FORGING WIRE ARC ADDITIVE MANUFACTURING PROCESSES FOR PRODUCING 3D PARTS WITH COMPLEX GEOMETRIES

**Bernardo Cruz Varzielas**

BSc in Sciences of Mechanical Engineering

**Adviser:** Nuno Alberto Marques Mendes  
Assistant Professor, NOVA University Lisbon

**Co-advisers:** Telmo Jorge Gomes dos Santos  
Full Professor, NOVA University Lisbon

## **Examination Committee:**

**Chair:** Carla Maria Moreira Machado,  
Assistant Professor, NOVA University Lisbon

**Rapporteurs:** Valdemar Rebelo Duarte,  
Invited Assistant Professor, NOVA University Lisbon

**Adviser:** Nuno Alberto Marques Mendes  
Assistant Professor, NOVA University Lisbon



**Robotizing the conventional and Hot-Forging Wire Arc Additive Manufacturing processes for producing 3D parts with complex geometries**

Copyright 2022 Bernardo Cruz Varzielas, NOVA School of Science and Technology, NOVA University Lisbon.

The NOVA School of Science and Technology and the NOVA University Lisbon have the right, perpetual and without geographical boundaries, to file and publish this dissertation through printed copies reproduced on paper or on digital form, or by any other means known or that may be invented, and to disseminate through scientific repositories and admit its copying and distribution for non-commercial, educational or research purposes, as long as credit is given to the author and editor.



*To my family*





## ACKNOWLEDGMENTS

First of all, I would like to express my sincere gratitude to Professor Nuno Mendes and Professor Telmo Santos for all the guidance and support throughout this work. They gave me the opportunity to work in an area that I find interesting and important, and inspired me to improve myself every day.

To Professor Valdemar Duarte, Mr. António Campos, and Mr. Paulo Magalhães, for their support, patience, and advice during this study.

To the NOVA School of Science and Technology, in particular to the Department of Mechanical and Industrial Engineering for all the knowledge and skills that provided me.

To my parents, for allowing me to focus on myself and on my studies, without other concerns, providing me all the conditions to have a wonderful university experience.

To my brother, for all the patience he had and for all the support throughout this journey.

To my girlfriend, for the love, friendship, patience, and motivation she gave me. She is my special person, and it would have been almost impossible to make this journey without her.

To my dear friends, who accompanied me from the beginning and made my university times memorable. Best friends in the world.

This activity has received funding from the European Institute of Innovation and Technology (EIT) RawMaterials through the project Smart-WAAM: Microstructural Engineering and Integrated Non-Destructive Testing. This body of the European Union receives support from the European Union's Horizon 2020 research and innovation program.



## ABSTRACT

Wire Arc Additive Manufacturing (WAAM) is an Additive Manufacturing (AM) process which has high deposition rates at reduced costs, being suitable to produce large size components. Hot-Forging WAAM (HF-WAAM) is a WAAM variant which uses an oscillating hammer to forge the material as it is deposited, improving mechanical properties and the microstructure of the produced parts.

This study aimed to use and validate the WAAM and HF-WAAM to robotize the production of compact metallic and complex geometry parts. Thus, a welding torch capable of performing forging was redesign, developed and assembled in a 6 degree-of-freedom (6-DoF) manipulator robot. 316LSi stainless steel parts were produced using WAAM and HF-WAAM processes. During their production, the vibration signal of the robot was acquired and then processed and compared.

The AM robotic system demonstrated to be suitable to build these parts, since the tool tip speed and tool tip to substrate distance are controlled, and the tool path optimized. It was also observed that vibration did not negatively affect the built parts quality.

**Keywords:** Robotic Additive Manufacturing, Wire Arc Additive Manufacturing, Hot-Forging - Wire Arc Additive Manufacturing, Vibration signal.



## RESUMO

O Wire Arc Additive Manufacturing (WAAM) é um processo de Manufatura Aditiva (MA) que apresenta elevadas taxas de deposição a custos reduzidos sendo adequado para produzir peças de grandes dimensões. O Hot-Forging WAAM (HF-WAAM) é uma variante do WAAM que usa um martelo oscilante para forjar o material à medida que este vai sendo depositado, melhorando as propriedades mecânicas e a microestrutura das peças produzidas.

Este trabalho tem como objetivo usar e validar o WAAM e HF-WAAM para robotizar a produção de peças metálicas com geometria complexa. Para isto, uma tocha de soldadura com capacidade de realizar forjamento foi redesenhada, fabricada, e montada num robô manipulador de 6 graus de liberdade (6-DoF). Foram produzidas peças em aço inoxidável 316LSi utilizando os processos de WAAM e HF-WAAM. Durante a sua produção, o sinal de vibração do robô foi adquirido e posteriormente processado e comparado.

O sistema robótico de MA demonstrou ser adequado para produzir peças quando a velocidade da ponta da ferramenta e a distância da ponta da ferramenta ao substrato estavam controladas e o percurso da ferramenta otimizado. Também se observou que a vibração não afetou negativamente a qualidade das peças produzidas.

**Palavras chave:** Manufatura Aditiva robótica, *Wire Arc Additive Manufacturing*, *Hot-Forging* - *Wire Arc Additive Manufacturing*, Sinal de vibração.



# CONTENTS

<b>ABSTRACT .....</b>	<b>XI</b>
<b>RESUMO .....</b>	<b>XIII</b>
<b>1 INTRODUCTION .....</b>	<b>1</b>
1.1 Motivation .....	1
1.2 Objectives .....	2
1.3 Structure.....	2
<b>2 STATE-OF-THE-ART .....</b>	<b>3</b>
2.1 Additive Manufacturing .....	3
2.2 Metal Additive Manufacturing.....	5
2.3 Wire Arc Additive Manufacturing.....	6
2.4 Hot-Forging WAAM .....	10
2.5 Automatization of the process.....	12
2.5.1 WAAM manipulator.....	12
2.5.2 Workflow for a WAAM integrated system.....	13
2.5.3 Online-Monitoring system.....	16
2.6 Robot vibration .....	17
<b>3 IMPROVEMENT OF A WAAM ROBOTIC CELL .....</b>	<b>19</b>
3.1 Development of the welding tool .....	19
3.2 Controlling system .....	26

3.2.1	Industrial robot.....	26
3.2.2	Controlling system.....	26
3.3	Data acquisition system .....	28
<b>4</b>	<b>EXPERIMENTAL PROCEDURE AND RESULTS .....</b>	<b>31</b>
4.1	Material and parameters .....	31
4.2	Process steps .....	32
4.3	Two-dimensional linear torch movement .....	37
4.4	Two-dimensional non-linear torch movement .....	39
4.5	Three-dimensional torch movement .....	43
4.6	Vibration analysis and results .....	48
4.6.1	Magnetic Pulse Forming vibration comparison.....	54
<b>5</b>	<b>CONCLUSIONS AND FUTURE WORK.....</b>	<b>57</b>
5.1	Conclusions.....	57
5.2	Future work.....	58
	<b>REFERENCES.....</b>	<b>61</b>
<b>6</b>	<b>APPENDIX.....</b>	<b>68</b>



## LIST OF FIGURES

Figure 2.1 - Current main AM processes [6].....	4
Figure 2.2 - Components suitable to be built by AM processes [17]. (a) Printed prosthetic limb. (b) Metallic turbine. ....	5
Figure 2.3 - Hybrid system with a welding robot and machining robot [31]. (a) Robot with Fronius welder for AM, (b) Robot with motor spindle for machining. ....	8
Figure 2.4 - Part built using WAAM [19]. (a) Part before surface milling, (b) Part after surface milling.....	9
Figure 2.5 - HF-WAAM torch developed by Duarte et al. [5] in its working position. ..	11
Figure 2.6 - Building strategy of a part model with a complex geometry [42]. (a) The usual build direction of the part, (b) Supports required due to overhangs, (c) Multi-direction deposition strategy reducing the needs for supports. ....	13
Figure 2.7 - Schematic proposed approach of an integrated system[43].....	14
Figure 2.8 - Robotic cell with programmed auto-path [49]. ....	15
Figure 2.9 - Schematic representation of a 6-DoF robot with represented joint motion [53]. ....	17
Figure 3.1 - (a) CAD model of the torch developed by Duarte [15], (b) CAD model of the torch developed in this project. ....	20
Figure 3.2 - Developed AM torch. Identification of the components of the torch indicated in Table 3.1. ....	22
Figure 3.3 - Schematic model of the connection between Bakelite plates and other components in the torch. ....	23

Figure 3.4 - Comparison of the distance from the back plate to the wire between (a) the torch by [17], (b) and the new torch.....	24
Figure 3.5 - Comparison of the size of the handle and the plate between (a) the torch by [17], (b) and the new torch. ....	24
Figure 3.6 - The AM torch built in this study. (a) torch assembled. (b) Torch attached to the robot in its working position. ....	25
Figure 3.7 - Assembly scheme of the controlling system [57].....	27
Figure 3.8 - (a) Scheme of the data acquisition architecture. (b) Scheme of connection of the accelerometers to the Arduino. Adapted from [58]. ....	28
Figure 3.9 - Schematic representation of the combining <i>MATLAB</i> program to obtain reference and maximum values. ....	29
Figure 4.1 - AM robotic cell .....	34
Figure 4.2 - zig-zag strategy used in material deposition. ....	34
Figure 4.3 - Schematic representation of the deposition process using the robot.....	36
Figure 4.4 - Proof test with 20 layers obtained in Test 1 - WAAM.....	37
Figure 4.5 - Proof test with 20 layers obtained in Test 3- HF-WAAM.....	39
Figure 4.6 - Proof test with 10 layers obtained in Test 4 - WAAM. The path between Points 1 and 2 has twice the material than the rest of the path, being points with excessive heat.....	40
Figure 4.7 - Proof test obtained in Test 5 - HF-WAAM.....	41
Figure 4.8 - Proof test obtained in Test 4.9 - HF-WAAM. ....	42
Figure 4.9 - Proof test with three-dimensional torch movement. The part to build by AM is the top, in dark. (a) CAD view of the part to build. (b) Front view of the part with the indicated measures. ....	44
Figure 4.10 - Representation of the 9 marked points to build the path of the torch. ..	44
Figure 4.11 - Proof test obtained in Test 7 - HF-WAAM.....	45
Figure 4.12 - Proof test obtained in Test 8 - HF-WAAM.....	46
Figure 4.13 - Proof test obtained in Test 9 - HF-WAAM.....	48

Figure 4.14 - Accelerometers position in the AM robotic system.....	49
Figure 4.15 - Graph of the vibration acquired when the robot is immobilized. ....	50
Figure 4.16 - Graph of the vibration acquired during Test 2 - WAAM proof test. ....	51
Figure 4.17 - Graph of the vibration acquired during Test 3 - HF-WAAM proof test...52	
Figure 4.18 - Graph of the vibration acquired during Test 9 - HF-WAAM proof test...53	
Figure 4.19 - Graph of the vibration acquired during Magnetic Pulse Forming. ....	55



## LIST OF TABLES

Table 3.1 - List of the components used to build the AM torch in this project.....	21
Table 3.2 - Triggers of the controlling system and their outputs number .....	26
Table 4.1 - Chemical composition of the ER316LSi wire (wt.%). Adapted from [58, 59]. .....	31
Table 4.2 - Mechanical and thermal properties of the ER316LSi wire. Adapted from [16]. YTS - Yield Tensile Strength; UTS - Ultimate Tensile Strength.....	32
Table 4.3 -Parameters of the WAAM and HF-WAAM processes. WFS - Wire Feed Speed; TS - Travel Speed; DAC - Distance to Arc Center. Is the distance from the arc to the hammer; CTWD - Contact Tip to Work Distance; GFR - Gas Flow Rate.....	32
Table 4.4 - Parameters utilized in Test 2 - WAAM.....	37
Table 4.5 - Parameters utilized in Test 3 - HF-WAAM.....	38
Table 4.6 - Parameters utilized in Test 4 - WAAM.....	39
Table 4.7 - Parameters utilized in Test 5 - HF-WAAM.....	40
Table 4.8 - Parameters utilized in Test 6 - HF-WAAM.....	42
Table 4.9 - Parameters utilized in Test 7 - HF-WAAM.....	43
Table 4.10 - Parameters utilized in Test 8 - WAAM.....	46
Table 4.11 - Parameters utilized in Test 9 -WAAM.....	47
Table 4.12 - Values of the vibration of the robot when it is stationary, and all the equipment is disconnected, in g (9.81 m/s <sup>2</sup> ).....	49
Table 4.13 - Values of the vibration during Test 2 - WAAM, and Test 3 - HF-WAAM, in g (9.81 m/s <sup>2</sup> ). .....	50

Table 4.14- Values of the vibration during Test 9 - HF-WAAM, in g ( $9.81 \text{ m/s}^2$ ).....	52
Table 4.15 - Values of the vibration during Magnetic Pulse Forming, in g ( $9.81 \text{ m/s}^2$ ). .....	55

## ABBREVIATIONS

AM	International Business Machines.
AutomationML	North Atlantic Treaty Organization.
CAD	Computer Aided Design
CAM	Computer Aided Manufacturing
CMT	Cold Metal Transfer
CNC	Computer Numerical Control
CTWD	Contact Tip to Work Distance
DED	Direct Energy Deposition
DoF	Degree-of-Freedom
EWI	Effective Wall Thickness
FPGA	Field Programmable Gate Array
GFR	Gas Flow Rate
GTAW	Gas Tungsten Arc Welding
GUI	Graphical User Interface
HA	Height Adjustment
HF	Hot Forging

<b>MAG</b>	Metal Active Gas
<b>MAM</b>	Metal Addictive Manufacturing
<b>MIG</b>	Metal Inert Gas
<b>NDT</b>	Non-Destructive Testing
<b>PAW</b>	Plasma Arc Welding
<b>PBF</b>	Powder Bed Fusion
<b>SL</b>	Stereolithography
<b>TS</b>	Travel Speed
<b>UTS</b>	Ultimate Tensile Strength
<b>WAAM</b>	Wire Arc Addictive Manufacturing
<b>WFS</b>	Wire Feed Speed
<b>YTS</b>	Yield Tensile Strength



## SYMBOLS

$f_F$	Forging Frequency
$F_F$	Forging Force
$F_S$	Forging Step
$V_{deposition}$	Travel Speed

# INTRODUCTION

## 1.1 Motivation

In order to remain competitive, organizations and companies must have innovative technologies which increase profits, reduce production times, and can easily customize and personalize products. The world is facing an industrial revolution, Industry 4.0. This one is characterized by digitalization, optimization, automation, artificial intelligence, customization of products and production, value added services and businesses and real-time communication [1]. To face the challenges created by the Industry 4.0, Addictive Manufacturing (AM) processes have been widely accepted as some of the most important, because they allow to produce components directly from Computer Aided Design (CAD) in a full-digital operation [2, 3].

Wire Arc Addictive Manufacturing (WAAM) is an AM technique suitable to build large metallic parts, in reduced times, with high deposition rates and low material waste [4]. Therefore, several studies and research have been developed by the academia and the industry, showing the viability of this process and its advantages comparing to other AM processes.

Hot-Forging WAAM (HF-WAAM) is a WAAM variant which uses an oscillating hammer to locally forge the material at high temperatures, in order to use the viscoplastic deformation behavior to improve mechanical properties and microstructure, by promoting the grain refinement, collapsing the defects, and reducing material anisotropy [5]. Comparing to cold-work WAAM variants, such as inter-layer rolling, which consists of imposing a load onto a roller that travels over the deposited layer, promoting the plastic deformation, HF-WAAM involves smaller forces, and equipment with lower stiffness, because the deformation occurs at high temperatures, making this technique suitable to be incorporated into conventional equipment such as XYZ table or a 6 degree-of-freedom (6-DoF) robot [3, 5].

To take full advantage of AM processes, 6-DoF robots have been used as alternatives to Computer Numerical Control (CNC) machines, because they can move in all directions, making complex three-dimensional tool paths. However, 6-DoF robots are more compliant than CNC machines, making them more suitable to be affected by vibrations. So, it is very important to acquire and study the influence of tool tip vibrations generated during the process in order to reduce and eliminate them.

A well understanding of all variants, such as robot vibration, parameters and their relation to the microstructure and material properties is of the major importance to develop WAAM process and use it as a competitive manufacturing technique for the factories of the future.

## **1.2 Objectives**

In this study, it is pretended to use WAAM and HF-WAAM to robotize the production of compact metallic and complex geometry parts, using 316LSi stainless steel as feedstock, and a 6-DoF robot to move a WAAM's torch. Different paths will be investigated and analyzed, and material deposition problems during path changes will be identified. Furthermore, it is pretended to identify the AM process and robot parameters that lead to the manufacture of high-quality parts. Ultimately, the vibration signal will be acquired and processed in order to study the vibration of the robot, and its influence in the built parts quality.

## **1.3 Structure**

This thesis is structured in 6 chapters. Chapter 1 contains a brief introduction to the research, the fundamentals of it, and the structure of the paper. Chapter 2 includes an AM, WAAM and HF-WAAM review, defining concepts and presenting studies that have been developed by the academia and the industry, and linking them with robotization. Chapter 3 describes the equipment built and used in experimental procedure. Chapter 4 focus on experimental procedure itself, explaining the AM process and robot parameters used, and the different proof tests studied, and then presents the results and quality analysis of the proof tests, and the vibration data acquired during the experiments. Chapter 5 summarizes the main conclusions from the experiments and gives suggestions for the future work to develop.

## STATE-OF-THE-ART

This Chapter presents a literature review of main technologies and concepts of this dissertation. Begins with a brief introduction to AM, its history and potential. Then, it is presented an AM process, WAAM and its variant HF-WAAM. Their fundamentals, advantages and disadvantages are detailed. In the following section is shown the status of the robotization of these processes, and finally, a review of the vibration analysis in 6-DoF robots in different processes and its importance.

### 2.1 Additive Manufacturing

To produce metallic components, there are two main groups of manufacturing processes: Subtractive Manufacturing, e.g., machining, drilling, among others; and AM. The first ones are the traditional approach, in which the material is removed from a primary stock. AM consists of adding material, layer-by-layer to produce near-net shape components [6].

AM processes first emerged in the 1980's, by the stereolithography (SL) process, with the purpose to create complex shapes, which could be very difficult or even impossible to build by conventional manufacturing, with a time and cost reduction [7, 8]. SL consists in converting a liquid photosensitive resin into a solid state by exposing the resin to an ultraviolet light, depositing layer-by-layer [8].

AM technology is capable of creating three-dimensional and complex components in a layer-by-layer deposition process in one stage and full-digital operation, almost without the interaction of an operator [3]. It is possible to produce components directly from Computer-Aided Design (CAD), with a high personalization, customization, low material usage and reduced costs. AM technology has the potential to reduce almost 50% machining costs of high strength alloys. However, it presents some challenges, mainly with the performance and structural quality issues in the built parts [9]. In Fig. 2.1 it is possible to see the current main AM processes for metallic materials.

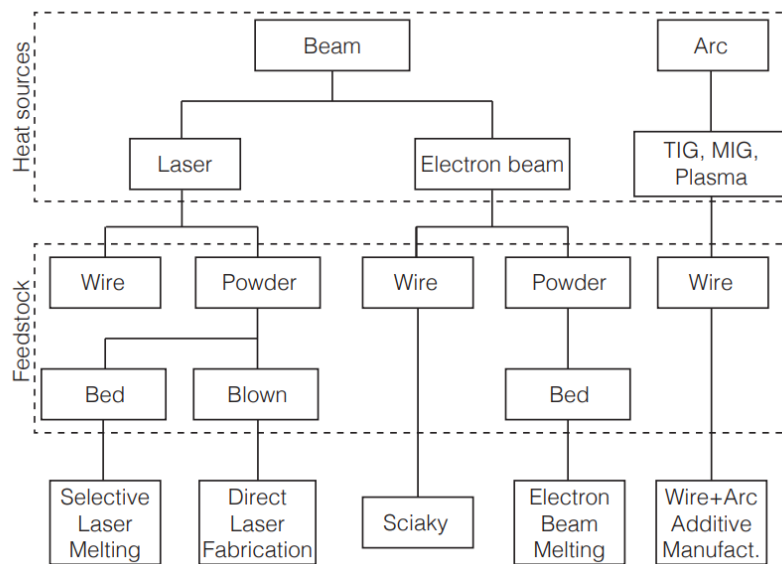


Figure 2.1 - Current main AM processes [6].

AM processes are used in most industry sectors, such as automotive, aerospace, military, medical, and architectural, despite all its limitations. For example, in the automotive industry it is really important to produce complex lightweight structures in order to reduce the weight of automotive parts while maintaining strengths. This includes components such as engine valves and turbocharger turbines. In the healthcare industry, like the dental one, AM is used to manufacture custom, complex, accurate and fully dense objects, such as dental crowns, bridges, and implants [8]. In Fig. 2.2 it is possible to visualize some components suitable to be built by AM processes.

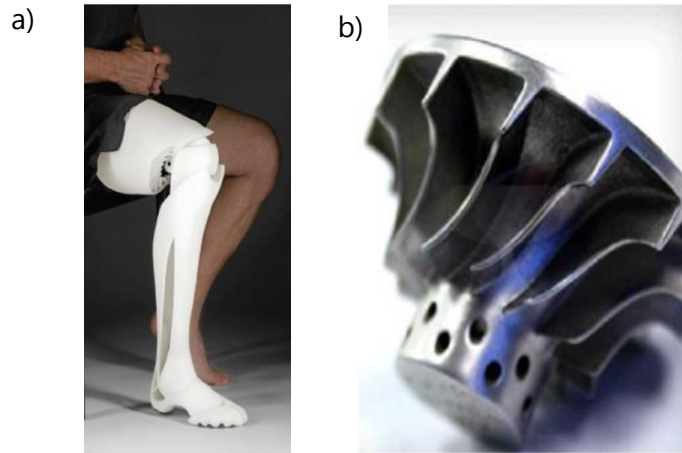


Figure 2.2 - Components suitable to be built by AM processes [17]. (a) Printed prosthetic limb. (b) Metallic turbine.

There is a significant growth in the investment in AM technologies. For example, in 2014 \$4 billion were invested, and in 2020 this number was about \$21 billion [10]. This is due to the improvements in technologies, materials and because of the necessity of having a flexible production and customized products in order companies can remain competitive [2].

## 2.2 Metal Additive Manufacturing

It is possible to use different materials in AM processes, including polymers, ceramics, and metals, however, metallic materials have more potential and interest in industrial applications [11]. There are four main categories of Metal Additive Manufacturing (MAM): Powder Bed Fusion (PBF), Direct Energy Deposition (DED), Binder Jetting and Sheet Lamination [12]. PBF systems are the most used MAM processes based on fusion, because of its high precision to make complex geometries, high-quality surface finishing and because it is possible to use a wide range of materials. Nevertheless, this process is relatively slow (up to 1 kg/h), it requires high power usage and is limited to build small components [13]–[15]. DED process uses a powder or wire as feedstock which is spread by a nozzle and melted as it is deposited by either a laser, electron beams, an electric arc as thermal energy. DED process mainly uses Metal Active Gas (MAG), or Metal Inert Gas (MIG) as arc-welding process fundamentals [13, 15]. This process

can be applied by a robotic arm with multiple axis, being suitable for repairing and remanufacturing metallic parts, such as automotive and aerospace components, due its high deposition rates and production flexibility; allows to build large components with high deposition rates (up to 6 kg/h); and can achieve up to 99.9% theoretical density of the material. Although, comparing to the previous process, it is applicable to a reduced range of materials, because of the reliance on dense support structure it is not ideal to build parts from scratch, and it has high surface roughness [16, 17].

## 2.3 Wire Arc Additive Manufacturing

DED is one of the MAM categories that stands out. Its techniques have enabled cost effective AM of large and medium complexity metallic parts, with a higher deposition rate than alternative approaches, and, theoretically, without building volume limitations [18].

One of the most MAM promising processes, with a lot of potential in industry is WAAM, which is a DED technique that uses an electric arc as a heat source and a metallic wire as feedstock [3]. Using WAAM it is possible to build large size components, reducing material waste (efficiency up to >90%), at high deposition rates (1-4 kg/h) with an increased energy efficiency [19, 20]. This process is based on existing fusion welding technology, and to produce electric arc, there are used three main technologies: MIG/MAG, Plasma Arc Welding (PAW), and MIG/MAG being MIG/MAG the most used for WAAM, because, comparing to others, it provides high deposition rates, low equipment costs, allows to weld a wider range of materials and the filler wire is aligned with the welding torch, simplifying the deposition strategy planning [21].

Despite all the research that has been done, some challenges must be addressed to produce high quality components and mitigate defects, so that WAAM can be more adopted by the industry. Until now, WAAM is used to produce simple parts, however, the industry challenges have to deal with complex geometries. So, it is especially important to find the best deposition path strategy, to understand the weld bed geometry deposited and its relation to the process parameters, to understand the microstructural evolution control during the layer-by-layer deposition, and the temperature effect between layers. It is necessary to control so many variables and aspects of the process, such as bead width, penetration, bead size, and

deposition rate, which becomes fundamental to establish and understand the parameters of the process and their influence in the bead geometry [22]–[24]:

- Current intensity: Penetration
- Voltage: Bead width
- Torch travel speed: Bead width
- Wire feed rate: Penetration and bead size
- Working distance: Effectiveness of shielding gas
- Shielding gas
- Wire diameter
- Torch angle: Effectiveness of shielding gas
- Tool path

Despite all the advantages and potential of WAAM, it presents disadvantages and aspects that can be improved. The main defects of WAAM are porosity, delamination, poor surface quality, distortion, and cracking [25]. These defects are directly connected to the parameters and process variants.

The material is subject to complex thermal cycles, and excessive heat input induces non-uniform expansion and contraction of the material, leading to residual stresses, which will induce deformations and can cause a premature failure of the component by cracking [26]. In order to minimize residual stresses, different strategies have been studied, such as Pre-Heating of the Substrate, Active Inter-Layer Cooling and/or Heating and Post-Thermal Treatments [27]. Porosity is more common in aluminum alloys, due its low hydrogen solubility when in solid-state contrasting with the high solubility when in molten phase, forming bubbles that, when are unable to escape to the melt surface during cooling, can lead to small pores which will ascend, maybe combine with other pores, and create larger pores. Porosity can also be caused from turbulent flow in the weld pool, by the shielding gas or from the quality of the feedstock. This defect can lead to a mechanical properties decreasing and cracking [28]. To mitigate porosity, some techniques have been studied, such as Inter-Layer Rolling and Hot-Forging.



One of the major disadvantages of WAAM is its poor surface finish. Therefore, a post-machining process is recommended to reduce or eliminate waviness on the surface of a part and reduce propensity for crack formation and propagation. CNC machining, which is a subtractive method, is used when it comes to high quality components, but it demands a considerable human intervention (to generate CNC programs) and it is a slow and costly process.

Thus, a hybrid solution has been developed and studied, Fig. 2.3, because it combines in the same tool two processes: the speed of the addition-material process (WAAM) with the quality of a subtractive-material method (e.g., machining, drilling), making the building and finishing machining happening in the same station [29]. The part obtained in this solution is represented in Fig. 2.4. This solution allows, for example, to machine internal cavities of hollow parts while they are being manufactured by a WAAM process. Machining internal cavities is difficult due to the fact that the machining tools collide with part surfaces and walls [30].

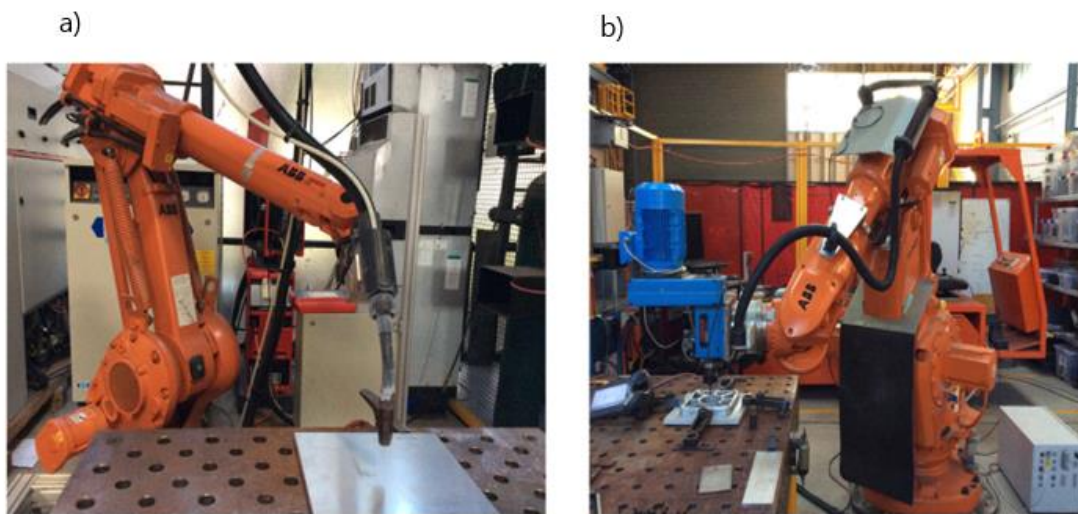


Figure 2.3 - Hybrid system with a welding robot and machining robot [31]. (a) Robot with Fronius welder for AM, (b) Robot with motor spindle for machining.

The aerospace sector has been identifying WAAM as a promising technology because it allows the production of parts made from high value materials with a significant complexity, reducing costs, and minimizing weight while keeping its functionality [32]. In this industry, some components made from materials such as titanium and nickel alloys can be very difficult to machine by subtractive methods, like CNC. So, AM processes are replacing these methods. E.g., Norsk Titanium has already produced the first titanium component, approved by the

Federal Aviation Administration, and installed in the Boeing 787 Dreamliner, reducing material waste and energy consumption, as costs and times production up to 30% and 75%, respectively, comparing to the previous production system that involved forging and a subtractive method [3, 33].

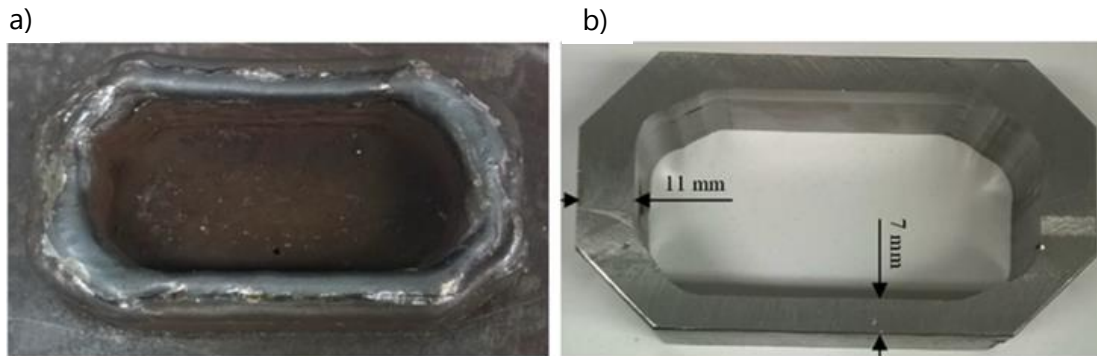


Figure 2.4 - Part built using WAAM [19]. (a) Part before surface milling, (b) Part after surface milling.

Another challenge of WAAM is the production of curved geometries parts maintaining mechanical properties and building free-defects parts. One of the industries that have been researching this is the shipbuilding industry. To meet all ships operating requirements, it is necessary to use curved parts and blocks, however, they are difficult to produce, time consuming and costly. The development of WAAM could allow ship propellers and spare parts production on board, avoiding their unnecessary transportation and reducing supply times [34].

Kazanas et al. [35] investigated the production of horizontal and inclined wall features using an inclined torch position and the effect of travel speed on part quality for inclined walls. It is concluded that walls in directions from  $0^\circ$  to  $90^\circ$  can be deposited with Cold Metal Transfer (CMT) using empirical process control models; that the tool can be inclined to produce angled walls; that WAAM can produce closed shapes so they can be used as hollow features; and that either gas mixture and wall angle affect the Effective Wall Thickness (EWT) and must be included as factors in empirical models.

Different industry sectors find potential, advantages, and viability in WAAM. Despite all research and investigations, WAAM still presents defects and difficulties that must be addressed. A well understanding of all parameters and their relation to the material behavior, of

the complex thermal cycles of the deposited material, and to find the best deposition path strategy is essential to have free-defects parts and take full advantage of this process.

## 2.4 Hot-Forging WAAM

WAAM has a lot of potential in industry. However, it is necessary to optimize the process and minimize, or eliminate some microstructural features that exist in the fabricated parts, such as large grain structures, and pores, which can lead to defects [36]. To avoid this, researchers have developed some variants of this process.

HF-WAAM is a WAAM variant based on forging the material after the deposition, using viscoplastic deformation behavior at high temperatures to reduce residual stresses, to eliminate post-heat treatment operations and to refine and homogenize grain structure. HF-WAAM aims to reduce grain size and to collapse pores that may exist in the deposited layer, avoiding down times between layers deposition and requiring reduced loads, tooling, and equipment stiffness to deform the deposited material, because once this process is applied at high temperatures, there is no need to wait for the material to cool down [5].

Duarte et al. [5], developed a WAAM torch, Fig. 2.5, used a 1 mm diameter AISI316L wire and compared a one as-built sample to samples with forging forces of 17 and 55 N, using a cylindrical hammer of diameter 10 mm and a forging frequency of 10 Hz. It was observed, comparing to the as-built part, an improvement of mechanical properties, mostly when forging forces are higher, because there is a grain refinement effect due to plastic deformation at high temperatures. Thus, Yield strength increased from 360 to 450 MPa, ultimate strength increased from 574 to 622 MPa, elongation to fracture reduced from 32% to 28%, and internal pores collapsed under the forging force.

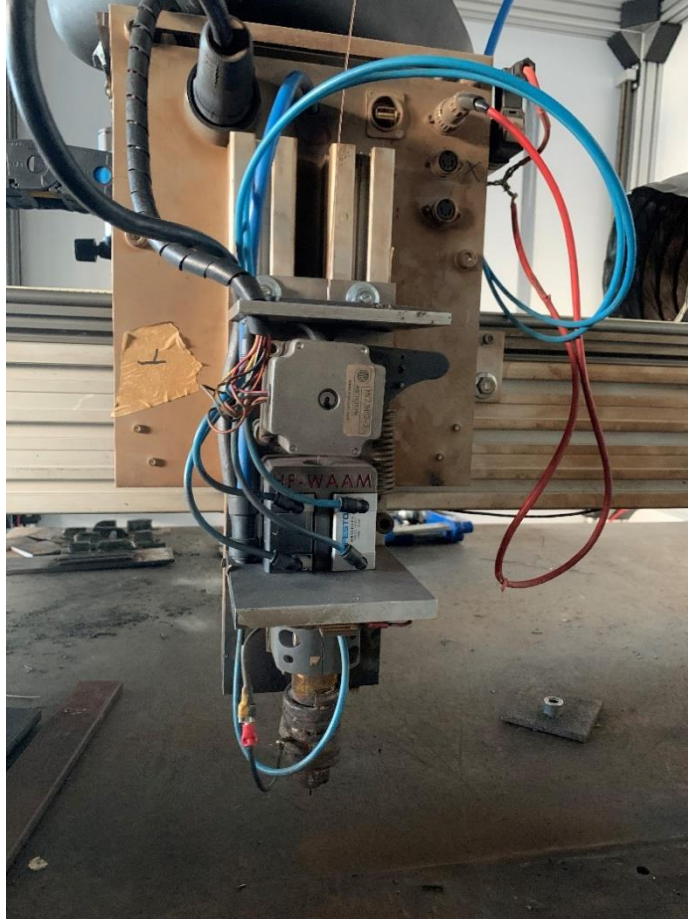


Figure 2.5 - HF-WAAM torch developed by Duarte et al. [5] in its working position.

This technology introduces some new parameters to the process, that includes forging force,  $F_F$  [N], forging frequency,  $f_F$  [Hz], distance to arc center, DAC [mm], hammer geometry, the forging step,  $F_S$  [mm/cycle], and travel speed,  $V_{deposition}$  [mm/min]. Forging step is the distance travelled by the hammer in one cycle, and it depends on the forging frequency and travel speed Equation 2.1. The area forged in each cycle depends on the bottom surface geometry of the hammer and on the forging step [5, 36].

$$F_S = \frac{60 \times V_{deposition}}{f_F} \quad [\text{mm/cycle}] \quad \text{Eq. 2.1}$$

This process presents some disadvantages, such as changing the part geometry, making it difficult to predict the final geometry, the possibility of the hammer getting stuck in the weld pool and the induction of vibrations in the structure. However, it showed potential to be applied in industrial applications, and incorporated in equipment such as XYZ table or 6-DoF robot.

## **2.5 Automatization of the process**

The industry 4.0 is leading the industries and manufacturers to take new businesses approaches and find solutions to beat the challenges. AM promises to overcome many of the boundaries and challenges of the conventional manufacturing technologies, allowing the production of complex geometry parts, reducing waste material, production times, costs, and human intervention [37]. Thus, it is necessary to integrate the different areas of the production process in order to build an integrated system with a high level of intelligence and decision-making, capable of generating the robot code directly from the slicing code, building free-defects and high-quality components [33].

### **2.5.1 WAAM manipulator**

As a motion manipulator, WAAM uses a Computer Numerical Control (CNC) machine or a robot up to 6-axis, [38]. 6-DoF robots have more degree of freedom than conventional machines, allowing production of large-size components, production of complex geometries with minimum or no support structures, and with a free collision deposition [34]. These support structures increase the fabrication time, material consumption, and fabrication costs, and with a multi-direction deposition strategy is possible to reduce the need for them, as it is represented in Fig. 2.6. Furthermore, CNC is expensive, has high maintenance costs, and has physical limitations (most of it only has 3-DoF), making some projects impractical using this, such as rotational paths keeping the extruder nozzle correctly oriented during the movements. As shown, the robotic approach, because of its flexible functionality, is desirable to serve the dynamic demands of manufacturing [39]–[41].

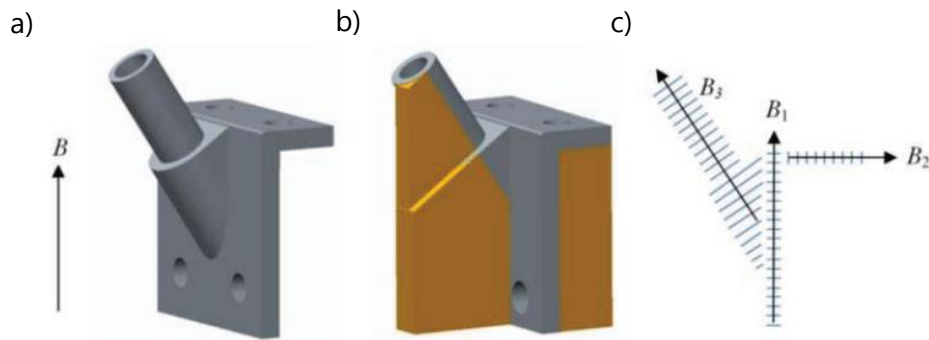


Figure 2.6 - Building strategy of a part model with a complex geometry [42]. (a) The usual build direction of the part, (b) Supports required due to overhangs, (c) Multi-direction deposition strategy reducing the needs for supports.

### 2.5.2 Workflow for a WAAM integrated system

A planning integrated system to build parts almost without human intervention includes the path generation from CAD model of the part, the best parameters generation to the path planning, simulation, robot code generation and the production of the real part [43]. As a result of having different stages and tools during the process, there is a big exchange of data and information between them that must be neutral, practical, fast, and errors-free. Automation Markup Language (AutomationML) is a system which connects and integrates all engineering processes, allowing the data exchanging and editing in a neutral format, and has a lot of potential to simplify and develop WAAM automatization [44]. In Fig. 2.7, it is possible to observe a schematic approach of an integrated system.

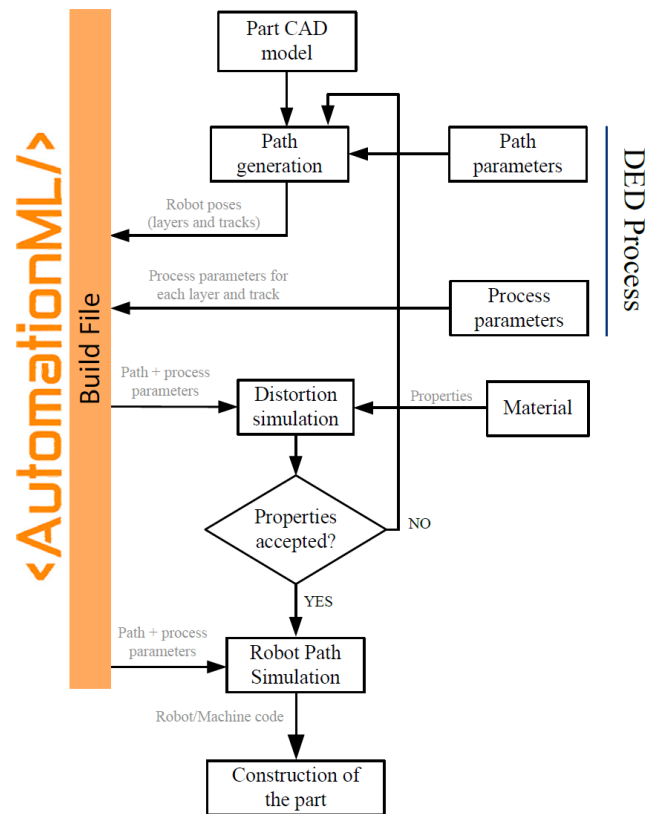


Figure 2.7 - Schematic proposed approach of an integrated system[43].

The process starts with the three-dimensional CAD model of the component to be built. Then, it is important to choose the best process-driven parameters to slice the geometry to be built and obtain the layer-by-layer model. The parameters given as inputs in this stage are the bead width, layer height, the deposition strategy, and a step over distance. The slicing strategy to build these layers has a great influence on the consistent quality of the part, and must be optimized to achieve fully filled, with low porosity and free-defects parts [33, 43]. To have an optimum tool-path planning strategy, some requirements must be satisfied: First, it must provide geometrical accuracy, fabricating the outlines by contour patterns; then, minimize the number of tool-path passes, reducing starting-stopping sequences within each layer; also, minimize the number of tool-path elements and adjust the wire feed rate until the end of each element, avoiding rapid changes of tool-path travel direction; and at last, a simple algorithm with rapid implement, so the pre-processing computational time can be reduced [45].

The simulation of the process is very important to avoid errors during the production of the part. It is possible to run the same operating system software as the real controllers and to optimize dynamic models so that they can be implemented in the process [37]. Using a Graphical User Interface (GUI), it is possible to interface with the simulation and configure operations. The most advanced GUI have automation tools that use computer vision and machine learning to process events in real time, emulating to the user interactions in reaction to those events [46].

Babcinski et al. [47] proposed an approach to exchange data between different engineering tools using a neutral data format, based on AutomationML, from CAD to path planning, process parameters definition and robot programming, in a MAM process. The approach passes by importing, to an AutomationML file, the data from path generator combined with the process parameters. The path is divided into tracks and layers, which allows a better process control because the user is able to manipulate the parameters at layer or track level, leading to better-quality components. They concluded that, in an off-line stage, the AutomationML file contains all the necessary information to simulate the building strategy and to build the part, simplifying the data exchange and making the process more efficient, as shown in Fig. 2.8.

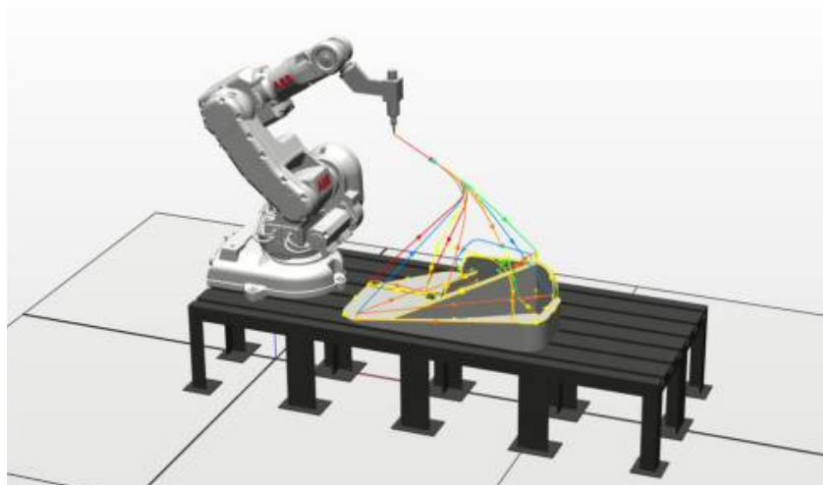


Figure 2.8 - Robotic cell with programmed auto-path [49].



### 2.5.3 Online-Monitoring system

In AM processes, parameters cannot be held constant due to differences in thermal behavior throughout parts fabrication, geometric variations, and mechanical properties, so it is necessary to adjust them to get free-defects parts.

In order to mitigate defects formation and to reduce costs and production times, it is really important to develop on-line integrated control systems with sensors capable of detecting defects deformation and non-destructive testing technologies. This allows parts rectification as they are being still built [3]. Real-time inspection involves signals provided by sensors and processed by algorithms that are the decision-maker [48]. When well established, this real time inspection can lead to other applications for WAAM, such as components reparation, decreasing costs associated with the need to renew a part. Many researchers adopted vision sensor to monitor the weld pool quality, because the welding pool captured images provide important weld deviation information [49]. Although, this cannot solve problems related to the variation of material composition, such as the accurate shielding gas flow rate or impurities inclusions.

Guo et al. [50] presented a classification method for monitoring the quality of WAAM builds based on spectrum, which can, simultaneously, monitor quality defects and evaluate the weld pool status. They used an integrated circuit, the Field Programmable Gate Array (FPGA), to trigger the spectrometer in the peak current within one welding current period, obtaining thus a spectrum with the information. It was concluded that this online monitoring system can detect more quality problems and has higher recognition, however, it is still limited by the actual band range and the sensitivity of the spectrometer.

Overall, WAAM provides a lot of potential and advantages, such as high degree of flexibility, reduced production costs, low material waste, energy efficiency and the capability to build high-quality and complex large metal components with high deposition rates [34]. However, it is necessary more investigation with the aim to mitigate defects and identify the feasibility for various materials, shapes, and applications [51]. It is necessary do develop in-situ monitoring, non-destructive inline evaluation, and an WAAM CAD/Computer Aided Manufacturing (CAM) software capable of providing a full automated process.

## 2.6 Robot vibration

The 6-DoF robots, Fig. 2.9, are widely used in different industry sectors, like in automotive industry, with different applications, such as handling, painting, and welding. Actually, they began being used in other applications, such as drilling, riveting, fiber placement and Non-Destructive Testing (NDT). For some of these applications, position, orientation, and path precision of the tool center point of the robot are required to get the machining operation correctly done [52]. The lack of stiffness and stability of industrial manipulators, mainly in processes and applications that require significant forces or fast-rotating elements, can become one of the primary sources of errors, so it is necessary to investigate, to obtain the dynamical information and to overcome the positioning error due to deflections of the robot in order to achieve high quality welded parts.

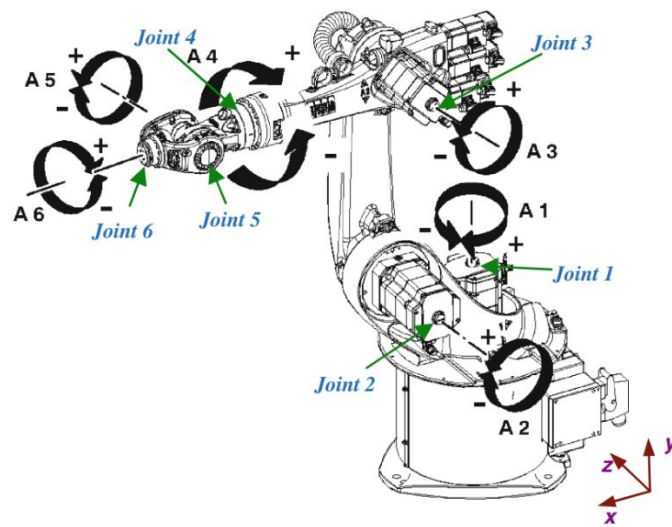


Figure 2.9 - Schematic representation of a 6-DoF robot with represented joint motion [53].

So that the robots can have a relative motion between the connected links, must exist some clearance for the joints at link connections. These clearances are inevitable due to the assembly, manufacturing errors and wear, however, reduce the stiffness and causes to impulse type contact force which has high frequency and amplitude [53].

In order to improve accuracy, minimizing tool tip vibrations, two main methods have been investigated: off-line and on-line methods. Off-line techniques estimate robot's joint

stiffnesses, estimate or measure the forces that will be involved in the machining operations, and then generate a path correction and select machining parameters. On-line methods involve external sensors to measure the tool tip position and to perform adjustments in the generated path and in the parameters originally generated [54].

Kaldestad et al. [55] developed an off-line method to compensate tool deflections and reduce vibrations in an industrial robot in an aluminum milling operation. It was considered the joint stiffness and force estimation for the machining operation to develop an off-line path correction. They also installed a passive micro damping system based on a sandbag, that when combined to the off-line path correction, reduced position error and vibrations by 50%.

Nguyen et al. [54] developed a method based on a data-driven model for active vibration suppression in robotic milling with a 6-axis robot characterized by pose-dependent modal parameters consisting of the modal stiffness, undamped natural frequency, and damping ratio. They demonstrated the controller reduced vibrations and showed to be correlated with a decrease in the machined surface deviations. The pose-dependent optimal controller was demonstrated to outperform constant gain controllers, because the gain value computed at the start of the path do not consider the change in stability conditions as the arm moves towards its base, because the robot is more compliant at the start point than at the end of the path, and therefore, the gains computed at the start configuration require larger control gains. Applying the gains to more compliant regions will not produce significant vibration suppression.

It is observed that, in order to improve robot tool tip accuracy, it is necessary to maintain the vibration of the robot and the tool reduced and controlled, identifying the sources of vibration and by accounting the calibration inaccuracies.

## IMPROVEMENT OF A WAAM ROBOTIC CELL

This Chapter describes the equipment developed and used in this project. Begins with the welding torch to forge used in this project, its operating fundamentals, and improvements relatively to the previous existing torch. Then, the existing controlling system and data acquisition system are described.

### 3.1 Development of the welding tool

The first task of this project was to redesign, manufacture and validate a WAAM and HF-WAAM torch suitable for attaching to a 6-DoF robot. This torch was adapted from the torch developed by Duarte et al., [15]. In that torch, [15], the welding wire enters from above and crosses the components straight. The wire is fixed between a bearing in the handle and a roller in the motor shaft due to the strength of a spring, and it moves due to the contact between them, when the stepper motor starts the rotation. To melt the wire, a cable from the welding machine is connected to a metallic plate, however, to conduct the current directly to the wire to perform the electric arc, avoiding the current to flow by other metallic components, a resistance was fixed and connected to metallic components that must not have current passage. The system includes two pneumatic cylinders responsible for creating the oscillating movement to the hammer, to forge the material, which are activated by a 5/2-way bi-stable solenoid valve. This movement is guide by a carriage in a linear guide. The welding gas is released in the nozzle support. The components in the torch are isolated with 2 mm of thickness plates of Teflon. To change the welding wire, it is necessary to open space between the bearings,

pushing the handle, and then to take out one wire and putting another, aligning the wire with its passage.

The biggest concern to rebuild this torch was to improve some features so its usage become more simple and stable during motion, avoiding functional problems, such as instability of the liner movement of the carriage in the linear guide during forging, lack of stiffness between components and its insulators, leading to isolation problems, difficulties changing the wire, and excessive strength needed to move the handle that fixes the wire against the bearing that is in the motor shaft. In the Fig. 3.1, it is possible to visualize a CAD model comparison between the equipment built by [15], and the one built in this project.

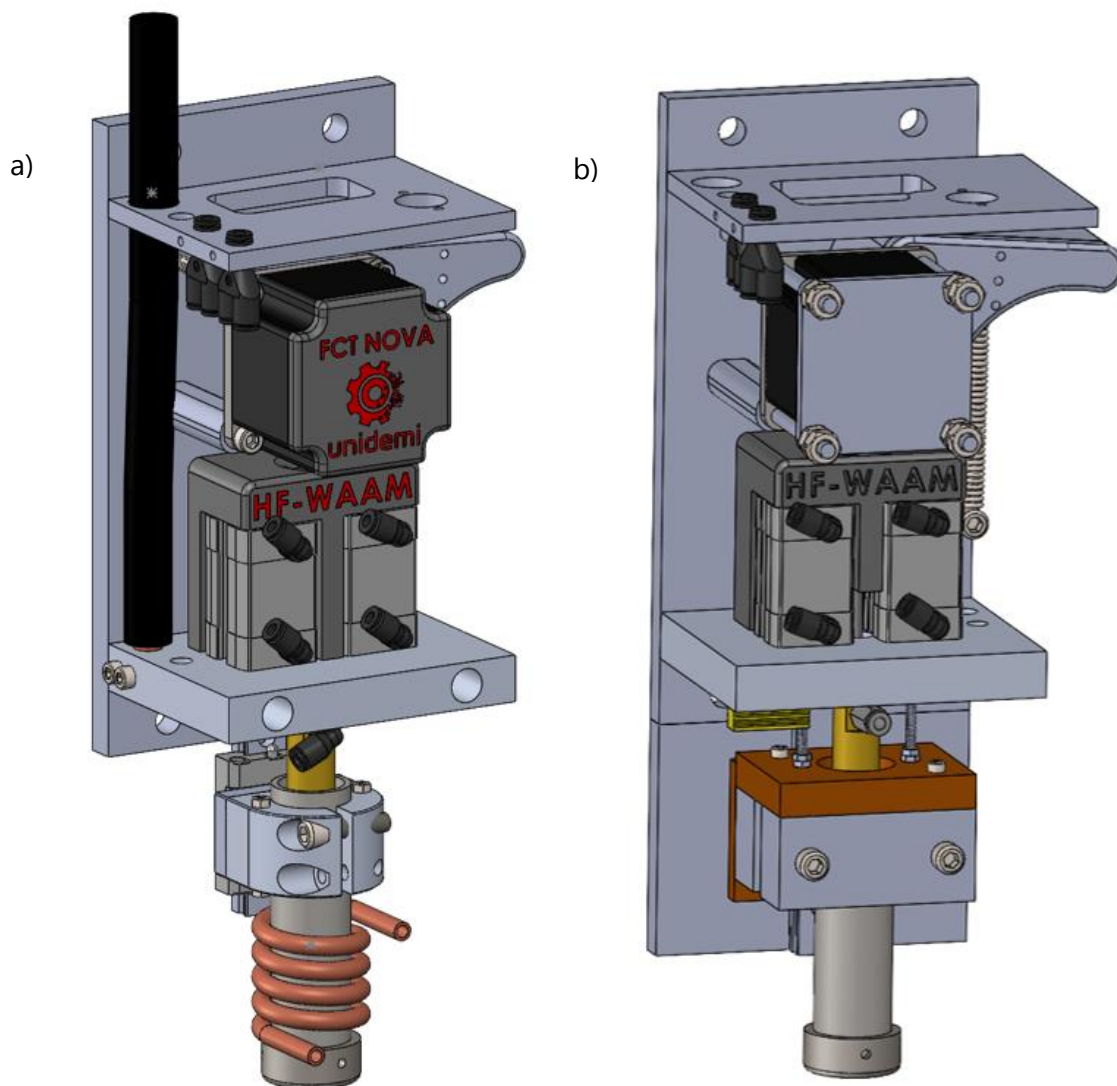


Figure 3.1 - (a) CAD model of the torch developed by Duarte [15], (b) CAD model of the torch developed in this project.

The operating principles of this torch are similar to the torch by [15], however, due to the modifications, some components were replaced, and others were introduced. A list of the components used to build the torch in this project is presented in the Table 3.1, and they can be visualized in Fig. 3.2, in their work position.

Table 3.1 - List of the components used to build the AM torch in this project.

Components	Description	Identification
1x Stepper motor	RS PRO, 2.5 V, 1.26 Nm	1
1x Bearings	SKF, Ø int. 6.35 mm, Ø ext. 15 mm	2
2x Pneumatic cylinders	<i>Festo ADN-12-10-I-P-A</i>	3
4x Aluminum plates	-	4
1x Resistance	Arcol, 10 kΩ, 25 W	5
2x Baklite plates	65 mm x 45 mm	6
1x Spring	Fanamol	7
1x Linear guide and carriage	NSK, 24 mm x16 mm	8
2x Spindles	Ø 3 mm	9
1x Welding nozzle	Ø int. 1 mm	10
1x Welding difuser	-	11
1x Hammer	Ø int. 25 mm, Ø ext. 35 mm	12
1x Noozle support	Ø int. 4 mm	13
3x 3D printed components	PLA	14
1x Spacer	Ø int. 6 mm, Ø ext. 8 mm	15
1x Nozzle support	-	16

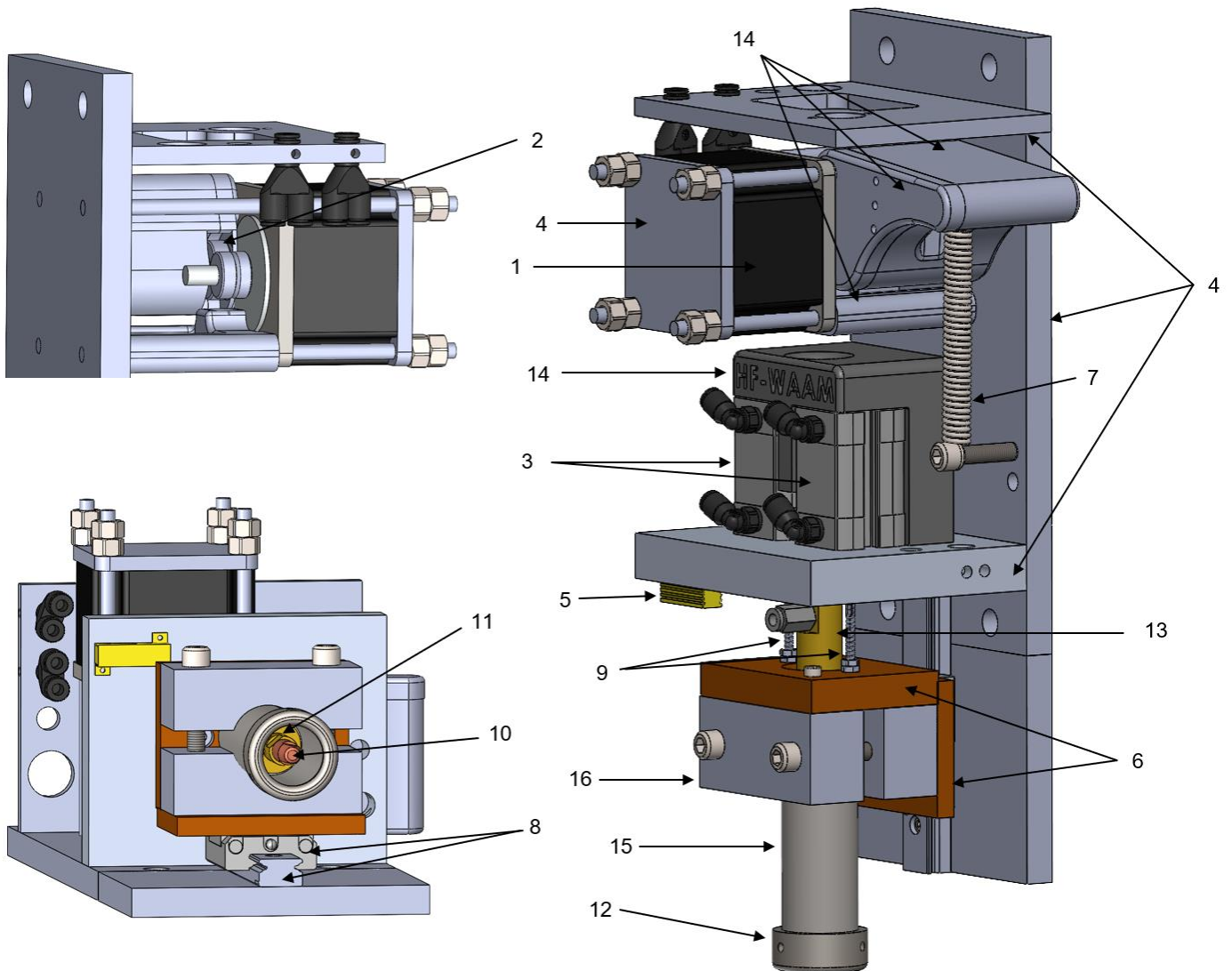


Figure 3.2 - Developed AM torch. Identification of the components of the torch indicated in Table 3.1.

In the torch proposed in [15], three plates of Teflon with 2 mm of thickness each connected the carriage of the linear guide to the nozzle support. The lack of stiffness of the plates created clearances between the screws and the holes, and between plates, creating isolation and stability problems. To solve them, it was used Bakelite plates between the carriage and the nozzle support that fixes the spacer, allowing the ascendent-descendent movement, and between the ring nozzle and the guides of the pneumatics, Fig 3.3. The carriage of the linear guide is fixed to the Bakelite plate by 4 bolts. Bakelite is a synthetic resin based on a chemical combination of phenol and formaldehyde. It has high stiffness and excellent insulating properties [56].

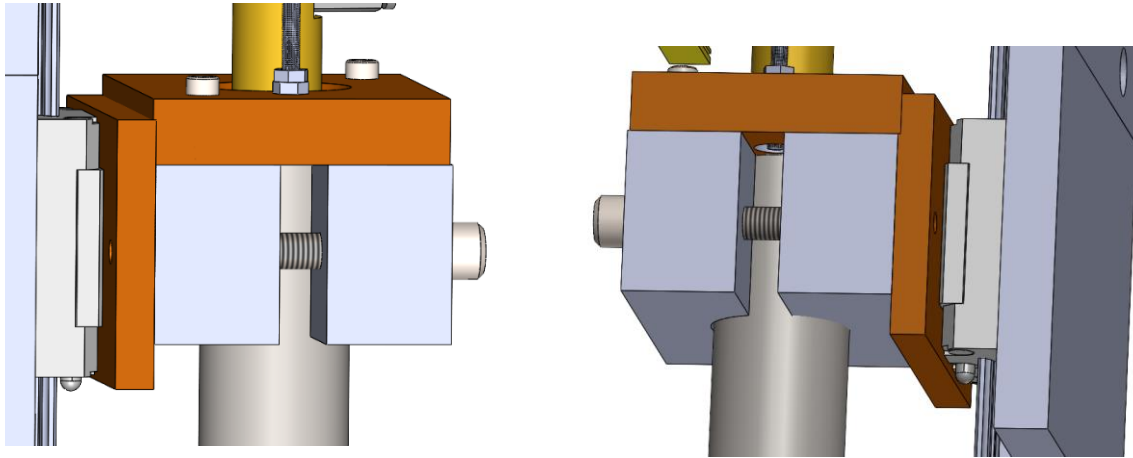


Figure 3.3 - Schematic model of the connection between Bakelite plates and other components in the torch.

In order to avoid current passage between components, despite of the insulators, the distance between the wire and the back plate was increased. The distance from the back of the ring nozzle to the hole was increased in 10 mm, forcing all the components that guide the wire to move 10 mm forward, readjusting all the design, Fig. 3.4.

The contact between the roller in the motor shaft and the bearing fixed in the handle must exert a normal force that can provide the necessary friction to move the wire, without slipping. However, this led to an excess of strength needed to open space between the bearing and the roller using the handle. To facilitate the changing of the wire, three modifications were made. First, the length of the handle was increased 15 mm, leading to an increasing of moment arm and a decreasing of the force needed. The upper cross plate length was also increased, but 20 mm. Thus, when opening space in the bearing and roller, it was possible to better support the hand in the plate, making the process easier. Second, the spring used was less strong. The last modification was to make a connection between the wire guide in the middle of the pneumatics and the nozzle support, allowing the wire to go directly into the nozzle support, not failing the entrance. This modification is presented in Fig. 3.5.



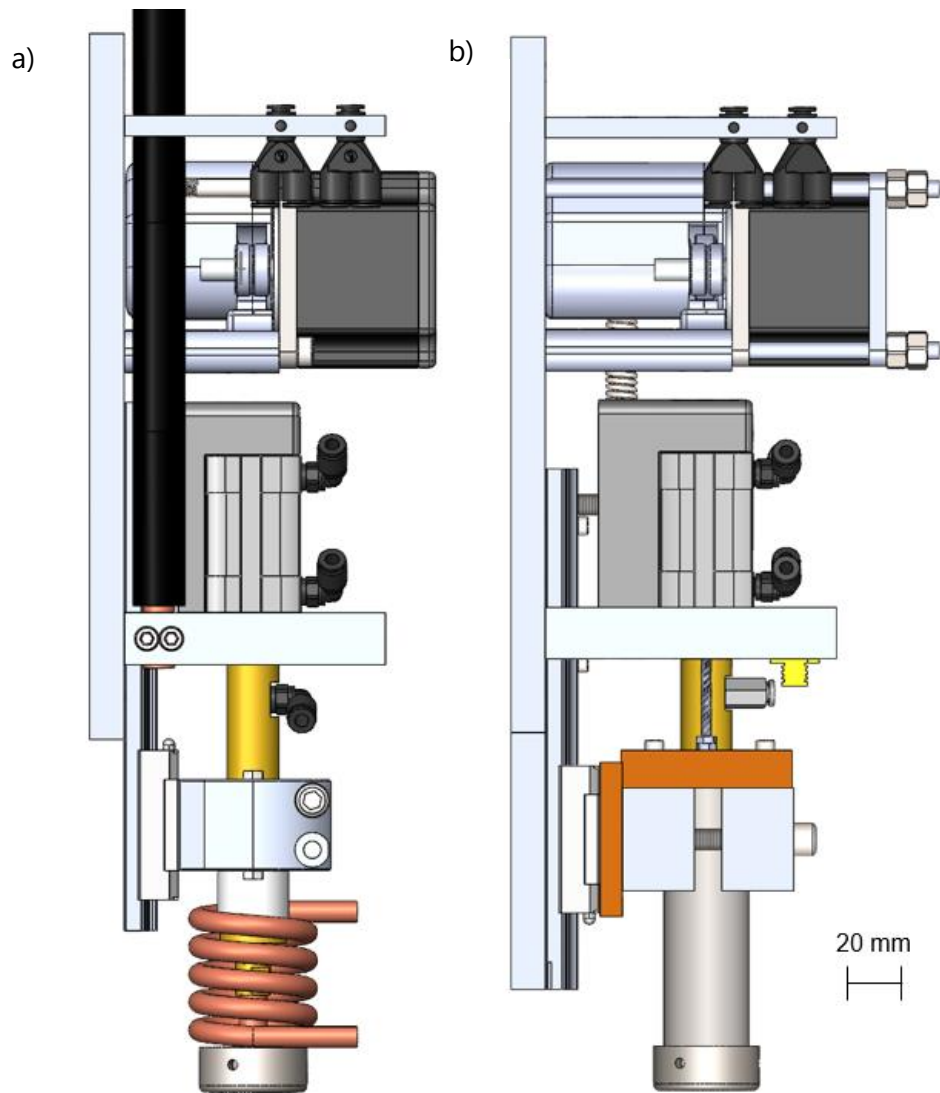


Figure 3.4 - Comparison of the distance from the back plate to the wire between (a) the torch by [17], (b) and the new torch.

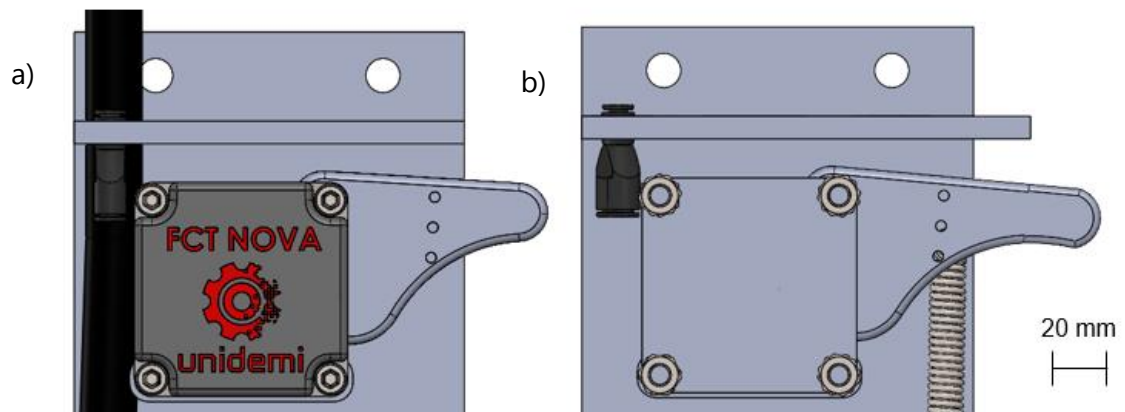


Figure 3.5 - Comparison of the size of the handle and the plate between (a) the torch by [17], (b) and the new torch.

After designing the torch in the CAD software *SolidWorks*, with all the modifications, the components were produced and the torch assembled, and it can be visualized in Fig. 3.6.

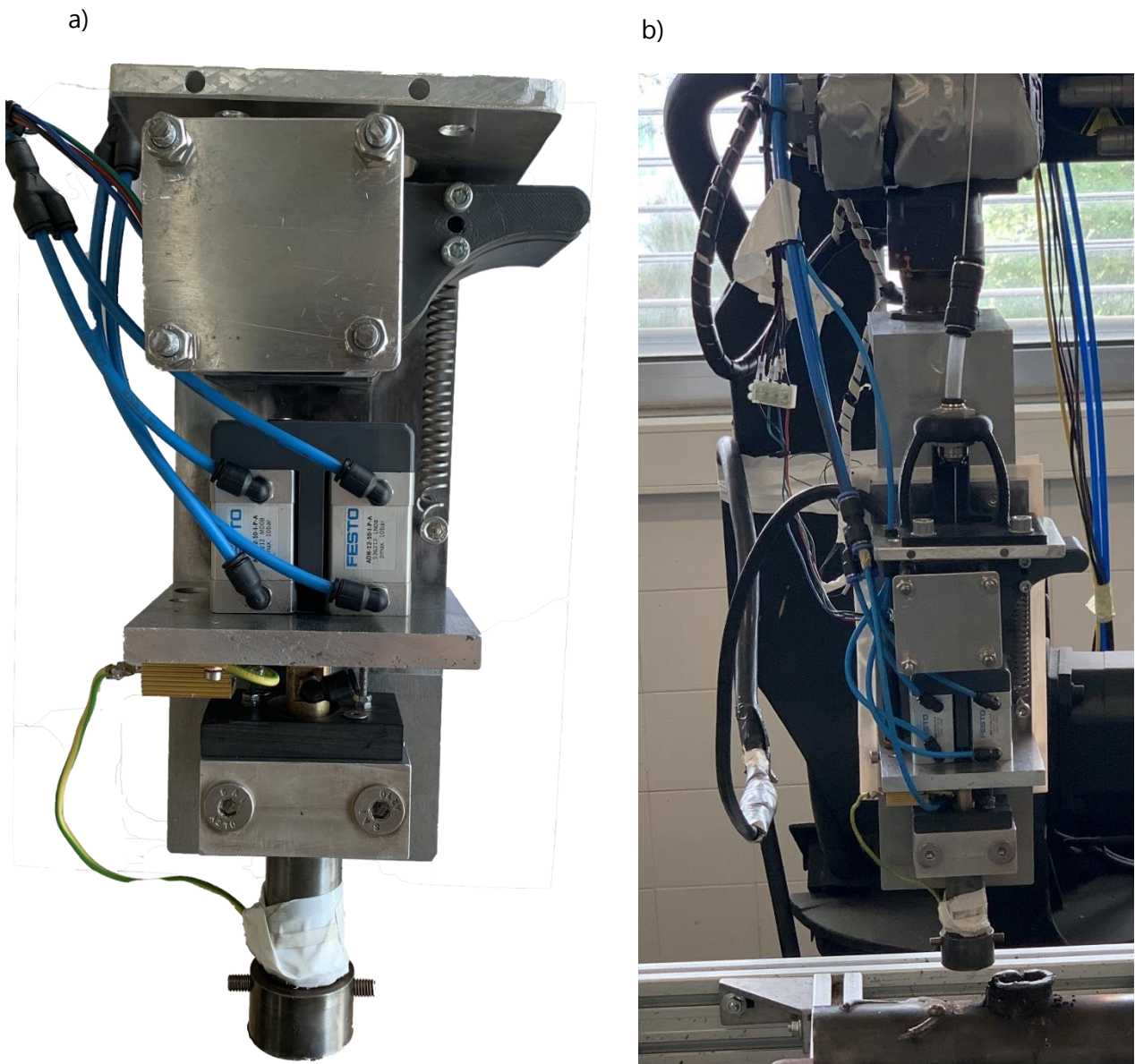


Figure 3.6 - The AM torch built in this study. (a) torch assembled. (b) Torch attached to the robot in its working position.

## 3.2 Controlling system

Once the welding torch was developed, it is necessary to connect it to an industrial 6-DoF robot, and to use the controlling system developed by [57], so that it is possible to start the experiments.

### 3.2.1 Industrial robot

A *KUKA KR6* robot with 6-DoF and capacity until 6 kg. It provides good flexibility, performance, and is widely used in a variety of applications such as machining, assembly, and handling in low payload projects. The *KUKA KRC1 SmartPad* is used to manipulate the robot, control the process equipment and the functionalities. The robot uses KRL (*KUKA Robot Language*) as programming language.

In this research, the robot is responsible for moving the torch and controlling the four triggers of the system, which are the welding equipment, the protection gas, the forging tool, and the wire feeding motor. To perform the movement, the strategy used was to save different points, marked manually, so the robot could follow them and build a path. Then, the files with the points were edited in the computer, with loop cycles, points adjustments and turning on and off the triggers. All robot programming is offline.

### 3.2.2 Controlling system

The controlling system consists of four independent systems with a relay activated by a 24 V signal. These systems, Table 3.2, are triggered during the process, based on the torch tip position.

Table 3.2 - Triggers of the controlling system and their outputs number

Trigger	Protection gas	welding equipment	Forging tool	Wire feed motor
Output	1	2	3	4



### 3.3 Data acquisition system

In order to validate the process of adding a forging torch to a 6-DoF robot to produce parts with complex geometries, it is important to study the effect of the vibration in the part quality. Thus, a system based on the Bus I2C protocol (which allows the communication between the controller device - master, and the controlled devices - slaves), and composed by 4 accelerometers MPU6050, 1 Arduino UNO, 1 Arduino nano, and 1 *Hub USB2.0* (that allows to send the data from the two Arduinos simultaneously), was installed to acquire these values, and the installation scheme can be visualized in Fig. 3.8.

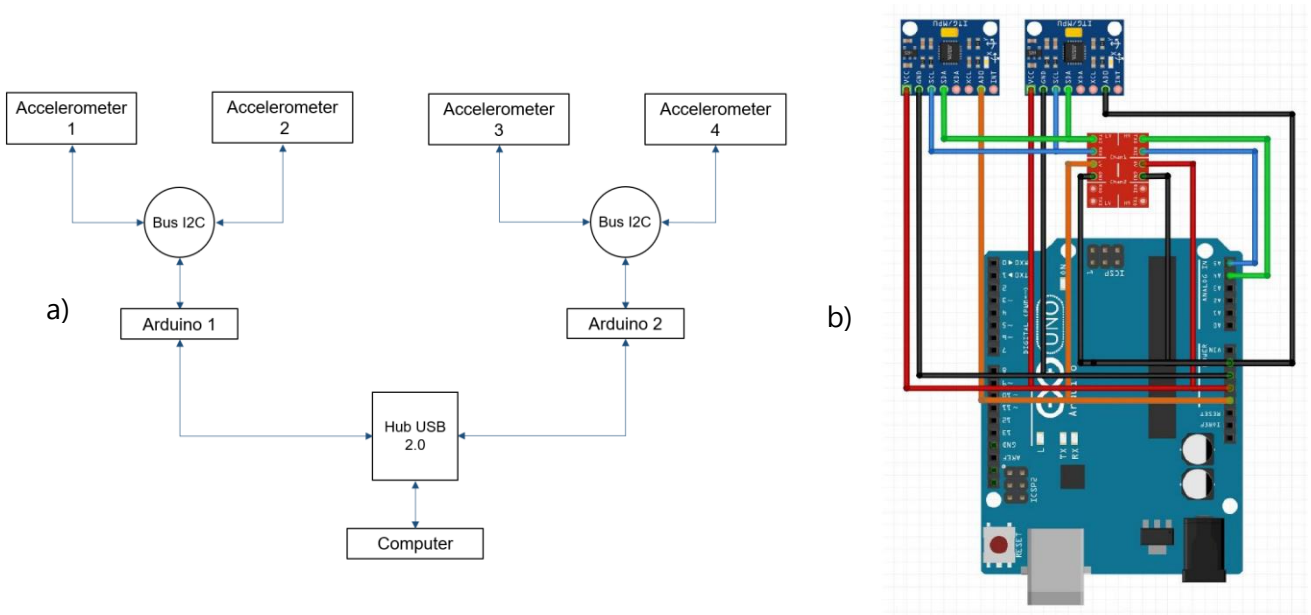


Figure 3.8 - (a) Scheme of the data acquisition architecture. (b) Scheme of connection of the accelerometers to the Arduino. Adapted from [58].

The Arduinos are responsible for sending the data from the sensors. One *MATLAB* program, *Reader*, reads and registers the data which was sent. Then, another *MATLAB* program, *Converter*, converts the values in the sensor scale acquisition (16 bit) to values with physical meaning ( $g$  ( $9.81 \text{ m/s}^2$ )), structuring them according to each accelerometer and axis. Finally, a *MATLAB* program, *Combiner*, combines all values from the three acceleration components in one and does the final data processing. To this value, it is removed the gravitational acceleration, so that it is possible to fully characterize the effect introduced by the robotic arm. All these programs are executed offline. In Appendix A.1, is possible to visualize a scheme of the process.

The Arduinos are powered by the computer. Because there are two Arduinos, the *Reader* is opened twice to acquire simultaneously the data from each Arduino, saving it in two separated files (one for each Arduino). Then, the *Converter* gather the two files, and treats the data for each accelerometer individually at once.

The *Combiner*, generates graphics, and indicates the maximum and the mean values. A vibration is an oscillation about a reference point, thus, there are pulses in the positive and negative direction, according to that point. The maximum value to study is the maximum pulse from the reference point, regardless of the direction, not the absolute maximum value, because this last one is relative to the absolute scale (the reference value can be different from zero) and does not include negative pulses. First, an acquisition with the robot motionless was performed, and the mean values were used as reference values (because these pulses are similar between them) for the acquisitions with motion. To acquire the maximum values when the robot is performing WAAM and HF-WAAM, the vibration values were ascending sorted, and it was measured the highest difference from the furthest points to the reference value. In Fig. 3.9 a), the mean values when the robot is motionless is obtained and used as reference value to obtain the maximum value when the robot is performing WAAM, Fig. 3.9 b). The maximum vibration value in modulus is  $3.71 \text{ g (m/s}^2\text{)}$ .

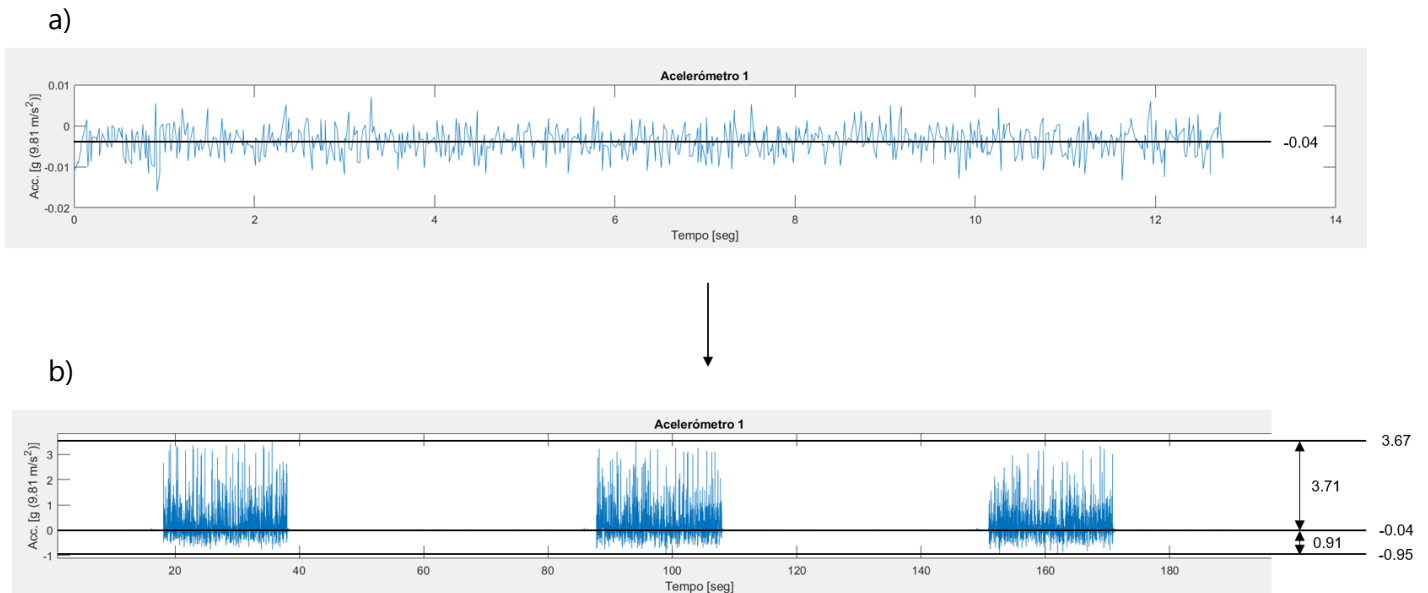


Figure 3.9 - Schematic representation of the combining *MATLAB* program to obtain reference and maximum values.



## EXPERIMENTAL PROCEDURE AND RESULTS

This Chapter presents a description of the experimental procedure. First, the parameters used are indicated and the choice criteria detailed. Then, the different stages of the process and how the robot program was created are explained. Next, the performed proof tests are presented, such as proof tests with a two-dimensional and three-dimensional torch movement for WAAM and HF-WAAM. Finally, a vibration analysis is performed, comparing values from the different processes and proof tests.

### 4.1 Material and parameters

The experimental procedures during this research were performed using, as feedstock material, the stainless steel 316L (ER316LSi) with 1 mm of diameter. This material is low carbon and has high corrosion resistance. In Table 4.1, it is possible to visualize the nominal composition of the ER316LSi, and its mechanical and thermal properties are shown in Table 4.2.

Table 4.1 - Chemical composition of the ER316LSi wire (wt.%). Adapted from [58, 59].

Material, wt.%	C	Mn	Si	S	P	Cr	Ni	Mo	Cu
ER316LSi	0.03	1-2.5	0.65-1	0.03	0.03	18.0-20.0	11.0-14.0	2.0-3.0	0.75



Table 4.2 - Mechanical and thermal properties of the ER316LSi wire. Adapted from [16]. YTS - Yield Tensile Strength; UTS - Ultimate Tensile Strength.

	YTS [MPa]	UTS [MPa]	Elongation at Break [%]	Thermal conductivity [W/mK]	Melting Temperature range [°C]
ER316LSi	248	538	50	15	1375-1400

This research involves WAAM process and its variant HF-WAAM, and in order to have free-defects and high mechanical properties parts, the parameters of the process and their influence in the deposited material must be investigated and established. Table 4.3 presents the parameters chosen, based on the previous investigation by [15, 57].

Table 4.3 -Parameters of the WAAM and HF-WAAM processes. WFS - Wire Feed Speed; TS - Travel Speed; DAC - Distance to Arc Center. Is the distance from the arc to the hammer; CTWD - Contact Tip to Work Distance; GFR - Gas Flow Rate

WFS [m/min]	Voltage [V]	Current [A]	TS [mm/s]	GFR [l/min]	Welding mode	Forging frequency [Hz]	Pneumatic pressure [bar]	DAC [mm]	CTWD [mm]
3	19	98-120	6	17	Synergistic	8	5	12.5	10

To keep the Contact Tip to Work Distance (CTWD) constant, the Height Adjustment (HA) of the manipulator between layers was also investigated, so that it is possible to generate a full robot code able to produce a complete part. The shielding gas used was Argon 99.99%.

## 4.2 Process steps

One of the aims of this research is to generate a full robot code program that is able to build a complete part, without interruptions to perform manual adjustments during the process, such as HA between layers. To achieve this, it is very important to understand the behavior of the material, the layers, and the differences between WAAM and HF-WAAM, because the parameters depend on them.

The experimental procedures can be divided in three categories, and for each one, WAAM and HF-WAAM are performed. First, simple geometries are studied, with a two-dimensional linear torch movement, then, geometries whose torch movement is two-dimensional non-linear, and finally, complex geometries with three-dimensional torch movement are performed. To each proof-test, it is pretended to validate the capacity of the AM robotic system and the torch to produce it. The robotic cell used in this study can be visualized in Fig. 4.1.

When the process is HF-WAAM, the first two layers are deposited without forging, only with WAAM. This was applied to all samples, avoiding the material to be immediately spread over the substrate, allowing the part to gain shape. The fixation plate, which connects the torch to the robot, is parallelly aligned to the direction of the closer joint of the robot. In the previous investigation, performed by [58], it was concluded that when the fixation plate is perpendicularly, the vibration amplitude is higher, causing welding electric arc extinction, instability, and interruptions in the robot's movement, due to the reaching of the allowable torque at the joint.

To program the AM robotic cell to produce parts with two-dimensional and three-dimensional torch movement, it is necessary to develop a methodology that can be reproduced. The strategy adopted in this study was to save points manually, moving the robot. So, the path to build one layer (one level of deposited material) is divided in 6 steps, because to change a signal state (on and off) in this robot, two points are needed. This change happens when the robot reaches one reference point, not in the middle of the path between these two points. These steps are repeated during the deposition, in a loop that only adjusts the height quota of the points. The deposition direction is changed between layers. It starts from right to left, and then goes from left to the right - zig-zag strategy, Fig. 4.2.

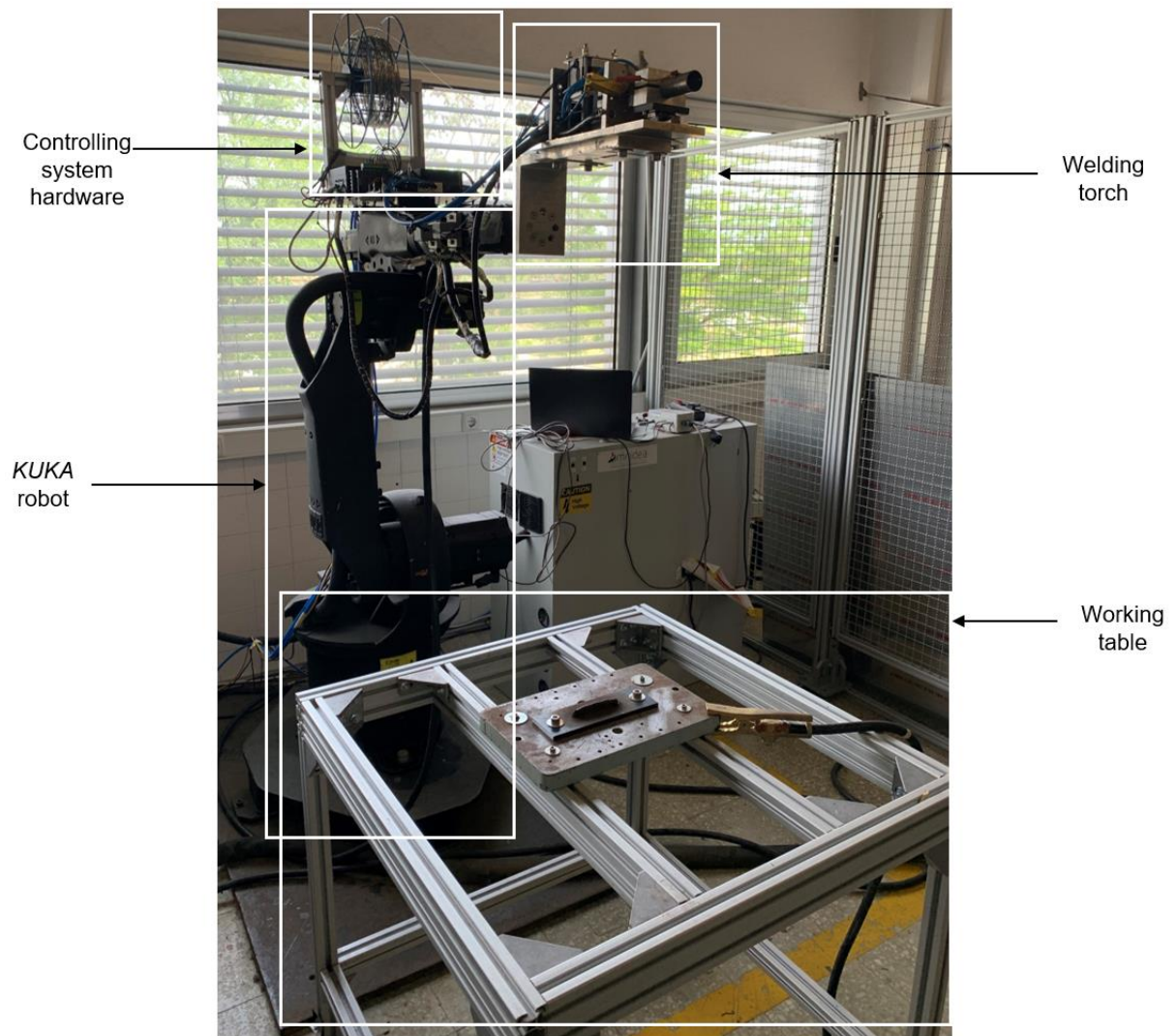


Figure 4.1 - AM robotic cell

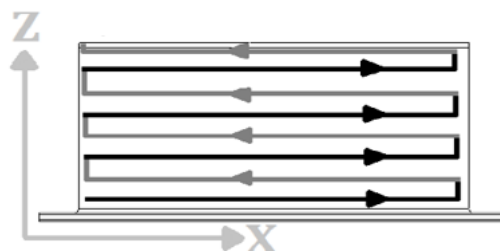


Figure 4.2 - zig-zag strategy used in material deposition.

In order to better understand the steps of the one-layer deposition process, a schematic representation was performed, Fig. 4.1. Between each layer, a 30 s wait was carried out to let the deposited material to cool down, so it is possible to deposit a new layer over it keeping the wall's shape. The steps are explained in the following points.

- **Point 1 -> Point 2:**

- During this movement, all activation signals and equipment are switched off. Point 1 is the point where the tool tip is at right distance from the substrate (10 mm) and is the point that activates the timer and adjusts the height quota, with all signals disactivated, when the torch moves in the opposite direction. The distance between these two points (1 and 2) is 3 mm.

- **Point 2 -> Point 3:**

- Point 2 is the point where the gas is activated. It is activated first so that when the welding starts, the fusion bath is already protected. The distance between these two points (2 and 3) is 5 mm.

- **Point 3 -> Point 4:**

- In Point 3 the welding, the forging system and the wire feed are activated, and the gas keeps turned on. The material deposition happens in this step. When the process is only WAAM, the forging system is not activated. This is a simple example with deposition only between two points. However, if the path has a complex geometry and needs many points, those points are placed here between these two points (3 and 4). The distance between them depends on each sample.

- **Point 4 -> Point 5:**

- In Point 4, the welding and the wire feed are disactivated, but the gas keeps turned on, guaranteeing that all the fusion bath is protected. If it was disactivated at the same time of welding, some material could be deposited without

protection gas, causing defects. The hammer keeps activated also to guarantee that all the deposited material is forged. The distance between these two points (4 and 5) is 5 mm.

- **Point 5 -> Point 6:**

- In Point 5 the gas and the hammer are turned off. Between these points (5 and 6), all signals are disconnected and the distance between them is 3 mm.

- **Point 6:**

- Once reached the Point 6, the timer starts counting and when it finishes, a height quota adjustment is done, preparing the torch to build another layer, but in the opposite direction, starting in the Point 6. This height adjustment is different for the first layers, for the middle layers and for the final ones, because of the material behavior during the process. These parameters are indicated in each proof test.

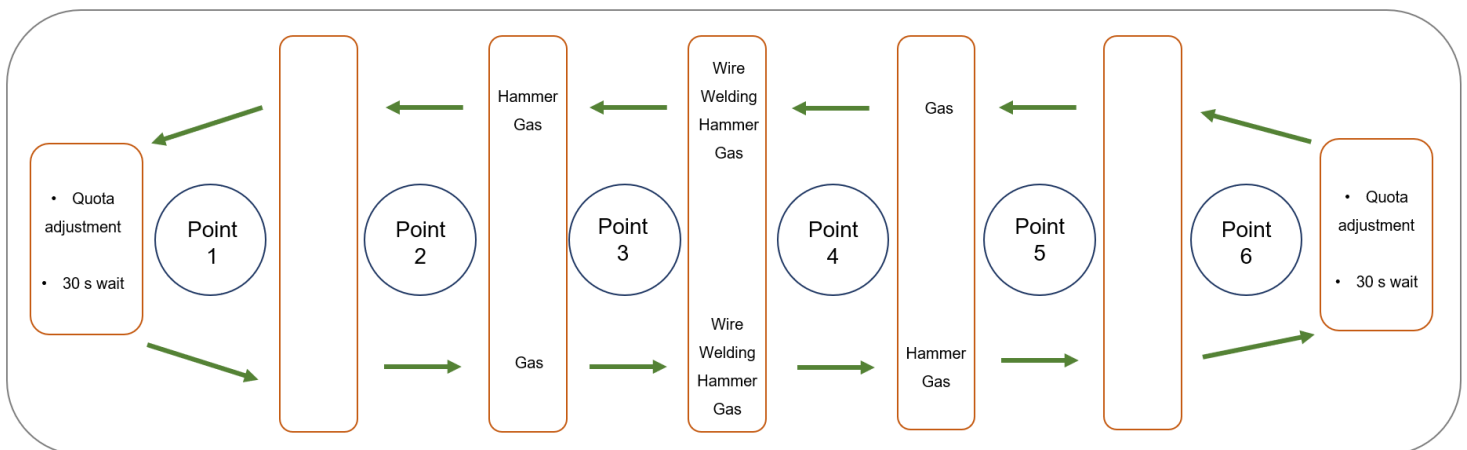


Figure 4.3 - Schematic representation of the deposition process using the robot.

Before the process starts, a simulation is run, with all activation signals and equipment turned off, only with the movement of the robot, in order to verify the correct functioning, positioning and alignment of the tool tip, so the deposition can be correctly done, without errors.

## 4.3 Two-dimensional linear torch movement

- **Test 1 - WAAM**

In order to validate the usage of the AM robotic system to produce parts in a two-dimensional plane, it was built a linear wall with 20 layers and 120 mm length. The AM and robot parameters shown in Table 4.4 were used to perform Test 1.

Table 4.4 - Parameters utilized in Test 2 - WAAM.

WT [s]	TS [mm/s]	GFR [l/min]	HA [mm]
30	6	16	1.7

In Fig. 4.4, it is possible to see the built wall. This wall does not have visible pores, excessive deformations, or copper from the welding tip, meaning the parameters are adjusted to the process, and the AM robotic system was successful producing this part.



Figure 4.4 - Proof test with 20 layers obtained in Test 1 - WAAM.

- **Test 2 - HF-WAAM**

Once WAAM parameters are adequate to the process, HF-WAAM tests are performed to study the material behavior when forging is applied. So, a 20-layer and 120 mm length wall was produced. In Table 4.5 is possible to see the parameters used during the process. The GFR was increased, when compared to Test 1, because due to the higher instability caused by the hammer movement, more shielding gas was expected to fully cover the welding area.

Table 4.5 - Parameters utilized in Test 3 - HF-WAAM.

WT [s]	TS [mm/s]	GFR [l/min]	layers: HA [mm]	Forging frequency [Hz]	Pneumatic pressure [bar]
30	6	18	1-4: 1.7	8	5
			5-10: 1.1		
			11-20: 0.9		

Before the process starts, the robot code was programmed to have a constant HA of 1.7 mm. However, after the first 4 layers (2 layers without forging, and then 2 layers with forging), it was found that this HA was not enough, because in the first layers the base material is cooler and there is reduced dilution of material between layers, so it was necessary to modify it during the production of this wall to 1.1 mm. Then, in layer 10, it was necessary to modify it again, because this HA was not enough, and the hammer was not reaching the material. To write a full robot code to build a part, it is necessary to understand these modifications so they can be anticipated and put into the code before the AM process starts, avoiding interruptions to perform modifications in the parameters during the part building. In Fig. 4.5 it is possible to visualize the proof test obtained.

The proof tests 1 and 2 allowed to validate the used parameters, and the usage of this AM robotic system and the torch to produce linear walls, and allowed to identify parameters, such as HA in HF-WAAM, that must vary as the part is being built due to the behavior of the material.



Figure 4.5 - Proof test with 20 layers obtained in Test 3- HF-WAAM.

## 4.4 Two-dimensional non-linear torch movement

- **Test 3 - WAAM**

The Test 3 aims to validate the usage of the AM robotic system and the torch to produce a WAAM part with the torch performing a non-linear trajectory. Thus, it was designed a 10-layer part whose path contemplates curves, straight lines, and points with excessive heat. In Table 4.6 it is possible to see the parameters used.

Table 4.6 - Parameters utilized in Test 4 - WAAM.

WT [s]	TS [mm/s]	GFR [l/min]	HA [mm]
30	6	16	1.7

The deposition starts on point 1, passes by point 2 and goes on anticlockwise direction, reaching point 2 and point 1 again. In the next layer, after the point 2, the deposition is on clockwise direction. From point 1 to 2, the deposited material is twice than the rest of the path, because in every layer, the material is deposited in the beginning and at the end, leading to an excessive of heat.



As it is possible to see in Fig. 4.6, there is no visible pores or excessive deformations, however, the accumulation of material between points 1 and 2 led to an increase of the wall height, decreasing the CTWD. With more depositions, this distance could not be enough to assure the correct functioning of the tool.



Figure 4.6 - Proof test with 10 layers obtained in Test 4 - WAAM. The path between Points 1 and 2 has twice the material than the rest of the path, being points with excessive heat.

- **Test 4 - HF-WAAM**

This test aims to study the performance of the AM robotic system and the torch when building geometries with corners during HF-WAAM. The path changing creates excessive heat points that can affect the deposition of material. Thus, a 20-layer rectangular geometry was designed, and the parameters used are shown in Table 4.7.

Table 4.7 - Parameters utilized in Test 5 - HF-WAAM.

WT [s]	TS [mm/s]	GFR [l/min]	layers: HA [mm]	Forging frequency [Hz]	Pneumatic pressure [bar]
30	6	16	1-2: 1.7	8	5
			3-6: 1.1		
			7-20: 0.9		

The HA between layers was established considering Test 2 - HF-WAAM, but with some differences. The 1.7 mm HA was implemented in the first two layers, built by WAAM. Then, between layers 3 to 6, built by HF-WAAM, the HA was 1.1 mm, and from layers 7 to 20, built by HF-WAAM, the HA is 0.9 mm. As the forging starts, the layers are getting compacted (with a height reduction), and this HA reduction allows the hammer to keep reaching the material.

As it is possible to see in Fig. 4.7, the hammer reached the material during all path, and the part does not have excessive deformations. The deposition had no constraints or difficulties in the corners, concluding that the parameters are adjusted to the process.



Figure 4.7 - Proof test obtained in Test 5 - HF-WAAM.

- **Test 5 - HF-WAAM**

In the fifth test, it was used HF-WAAM to study the performance of the AM robotic system and the torch to build circular geometries. The strategy used to generate the path was to save points manually, and for curved paths, the robot has a command called *CIRC*, which needs a previous marked point to start, and then is necessary to mark two more points. These three points are the starting, middle, and ending points of a curved path, and the robot connects them. However, the path the robot follows is not completely predictable. It can move in the most far direction, in the closer one, or even to follow a three-dimensional path. For this

reason, it was always necessary to simulate the path before the deposition. In Appendix B, it is possible to visualize the robot's code, including the command *CIRC*, and in Table 4.8, the parameters used are indicated.

Table 4.8 - Parameters utilized in Test 6 - HF-WAAM.

WT [s]	TS [mm/s]	GFR [l/min]	layers: HA [mm]	Forging frequency [Hz]	Pneumatic pressure [bar]
30	6	16	1-2: 1.7 3-6: 1.1 7-20: 0.9	8	5

As it is possible to see, in Fig. 4.8, the parameters are adequate to the process, however, in the final layer, the hammer did not reach all the deposited material, suggesting that the HA value parameter is not appropriate. In order to this, it has to be modified, or even the TS must be reduced.



Figure 4.8 - Proof test obtained in Test 4.9 - HF-WAAM.

## 4.5 Three-dimensional torch movement

The advantage of using a 6-DoF robot comparing to a CNC machine is the possibility to build parts with complex geometries moving the torch in three-dimensional trajectories. To study the viability of using HF-WAAM in three-dimensional deposition paths, with variation in Z-axis, circular trajectories over a steel cylinder were performed.

- **Test 6 - HF-WAAM**

In this test, it was defined a 50 mm diameter circle, which led to a 11 mm difference of height between the points in the top of the cylinder and the points below, due to the curvature of the cylinder, as it is possible to visualize in Fig. 4.9. The biggest challenge was to keep the CTWD, with the robot following the pretended path and with the hammer always perpendicular to the substrate.

To build the path, 9 points were marked, as it is represented in Fig. 4.10. The deposition starts in point 1, which is 1.5 mm from point 2, because the deposition does not start immediately when the welding trigger is activated. Although, it is turned off in point 2, closing the circular path with deposited material. The process parameters are shown in Table 4.9.

Table 4.9 - Parameters utilized in Test 7 - HF-WAAM.

WT [s]	TS [mm/s]	GFR [l/min]	layers: HA [mm]
30	6	16	1-2: 1.7
			3-6: 1.1
			7-20: 0.9

The results of Test 6, shown in Fig. 4.11, presents a discontinuity in the deposition and it is possible to find copper from the welding tip in the deposited material. This indicates that the parameters are not appropriate to the process, namely the TS, because was not hold constant. The robot movement could not hold predictable and constant during the three-dimensional circular path, because part of the speed is transferred to the adjustments of the joints of the robot, so it can keep perpendicular to the cylinder. This led to points with excessive heat

due to robot stops during its movement, and the melting of the welding tip due to the low CTWD between marked points when the robot is in motion.

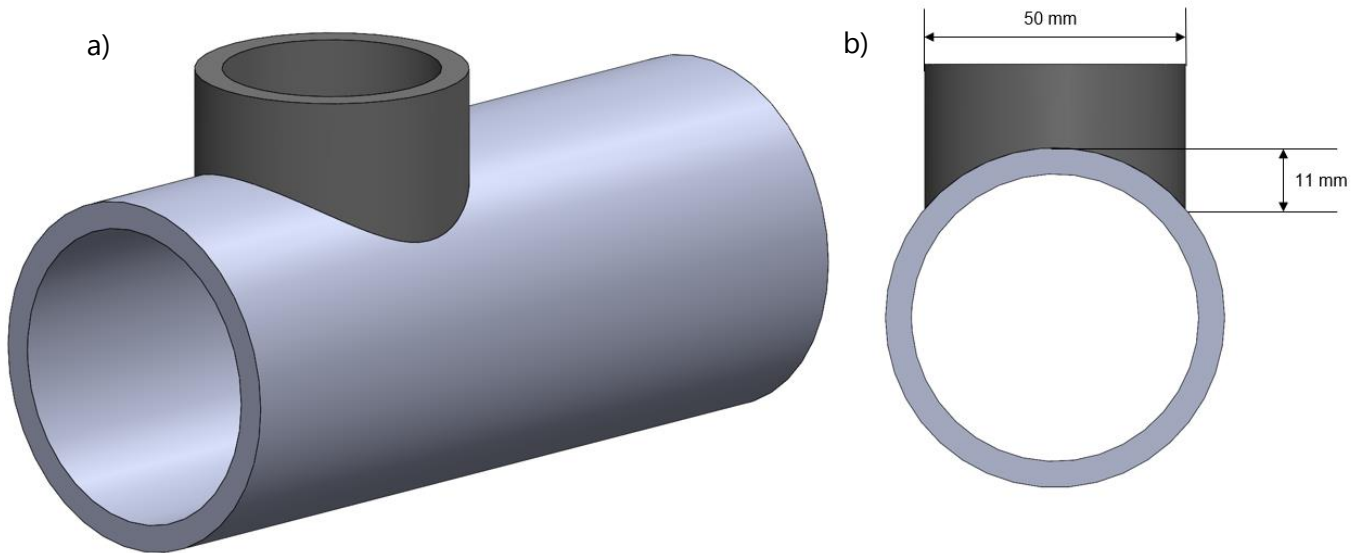


Figure 4.9 - Proof test with three-dimensional torch movement. The part to build by AM is the top, in dark. (a) CAD view of the part to build. (b) Front view of the part with the indicated measures.

Figure 4.10 - Representation of the 9 marked points to build the path of the torch.

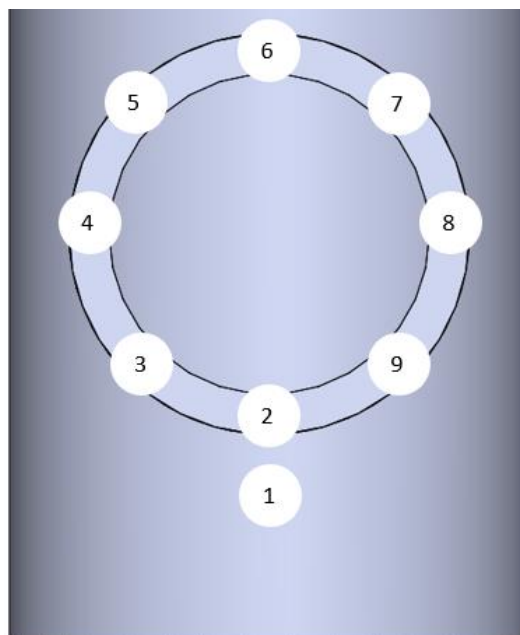




Figure 4.11 - Proof test obtained in Test 7 - HF-WAAM.

For the next proof tests, some parameters were modified, and the diameter of the geometry was reduced, so that the height between upper and lower points was reduced, and to control the robot becomes less difficult.

- **Test 7 - HF-WAAM**

In Test 7, a different strategy to build the trajectory was tried. The circular path was designed with only 5 points, instead of 9 as in the Test 6. Using the Fig. 4.10 as reference, the marked points in this test were 1, 2, 4, 6, and 8.

The first two layers were built using WAAM. Then, before HF-WAAM starts, the deposition was interrupted, and the reference points of the path were manually remarked so the torch could follow the path with less slope (getting more vertical), because after the first two layers deposition, it is expected a height difference reduction between the upper and the lower points (upper - 1, 2, 6; lower - 4, 8; Fig. 4.10). The part was built with 20 layers, all deposited clockwise.



In Table 4.10 is possible to see the parameters used, however, the GFR was increased, comparing to Test 6, because during the three-dimensional movement, once the substrate is not flat, it is necessary more gas to full cover the welding area.

Table 4.10 - Parameters utilized in Test 8 - WAAM.

WT [s]	TS [mm/s]	GFR [l/min]	layers: HA [mm]
30	6	18	1-2: 1.7
			3-6: 1.1
			7-20: 0.9

The obtained part in this test, shown in Fig. 4.12, does not have pores or excessive deformations, and the hammer reached all the deposited material. However, the part has a slope caused by the remarking of the points, that were not exactly aligned with the first marking once they are marked manually.



Figure 4.12 - Proof test obtained in Test 8 - HF-WAAM.

- **Test 8 - HF-WAAM**

In Test 8, a circular path with 5 marked points was designed. However, the height difference between upper and lower points was just of 2.5 mm, by reducing the diameter, so that the tool tip can be hold almost perpendicular to the XY plane, with a reduced tool orientation change. This allows to better control the tool path once the joints do not have to rotate considerable. The strategy was to deposit the first two layers using WAAM, then to adjust the height between layers increasing the upper points in 1.2 mm and the lower points in 3.5 mm, so they can be kept in the same quota, approximately. In the rest of the deposition, the HA is as the previous parameters, Table 4.11. The material is deposited, alternately, on clockwise and anticlockwise, allowing to uniform the layer, filling the differences of height between it.

Table 4.11 - Parameters utilized in Test 9 -WAAM.

WT [s]	TS [mm/s]	GFR [l/min]	layers: HA [mm]
30	6	18	1-2: 1.7
			3-6: 1.2 / 3: 3.5
			7-20: 0.9

As it is possible to see, Fig. 4.13, the layers are uniformed, due to the forging and the alternating deposition direction. The wall does not have excessive deformations, it is regular and has no lack of material, suggesting the parameters are adjusted to the process. The last layer was not properly forged because, a mechanical problem has arisen in the torch and the process has to be stopped. The carriage of the linear guide came off the equipment and the hammer could not reach the layer. However, the other layers of the part produced in Test 8 were forged, and it is possible to see they are aligned and compact.





Figure 4.13 - Proof test obtained in Test 9 - HF-WAAM.

The fact of the deposition was almost two-dimensional allowed to build a component without interruptions and manual adjustments during the process. In Appendix A.2 is possible to see this part during building., and in Appendix B, is possible to see this part's robot code.

## 4.6 Vibration analysis and results

In order to study the influence of the vibration from the WAAM and HF-WAAM processes in the quality of the proof tests and the in the performance of the robotic arm, four sensors were fixed along the robot in three different locations. Then, the data acquired from the sensor was processed using *MATLAB* software, which converts the raw acquired data to vibration values in g ( $9.81 \text{ m/s}^2$ ).

The accelerometer 4 is located in the fixation plate, which is in direct contact with the torch. The accelerometer 1 and 2 are fixed between the joint A4 and joint A5, and the accelerometer 3 is fixed between joint A2 and joint A3, Fig. 4.14.

It is expected that the vibration increases as the accelerometer is closer to the torch. The joints along the robotic arm cause a minimization of efforts and moments. Beyond this, the joints dimension increases as they get away from the arm tip (joint A6 is smaller than joint A1), which means the vibration values decrease, because as the joints are getting bigger, they

can support better the vibration, absorbing it and damping it. So, it is expected the accelerometer 4 to have the higher vibration, followed by accelerometer 1, 2 and 3 respectively.

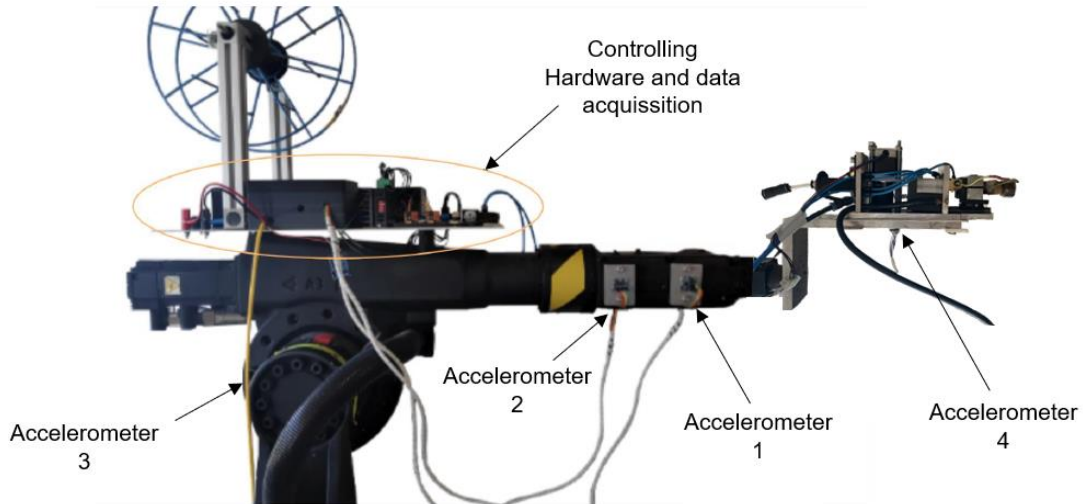


Figure 4.14 - Accelerometers position in the AM robotic system.

In Table 4.12 it is possible to visualize the vibration values acquired when the AM robotic system is off, and the robot is not moving. Before every vibration data acquisition during the AM process, this acquisition is repeated and the acquired values are used as reference values, as explained in Chapter 3.3.

Table 4.12 - Values of the vibration of the robot when it is stationary, and all the equipment is disconnected, in g ( $9.81 \text{ m/s}^2$ ).

Accelerometer		1	2	3	4
	Reference values	-0.004	0.036	-0.053	0.032
	Maximum values	0.012	0.010	0.014	0.013

As it is seen, all the maximum values are similar between them, because the acquiring conditions were constants, with no movements, and equal along the entire robotic arm. The Fig. 4.15 is the scale graphical representation of the acquired data.

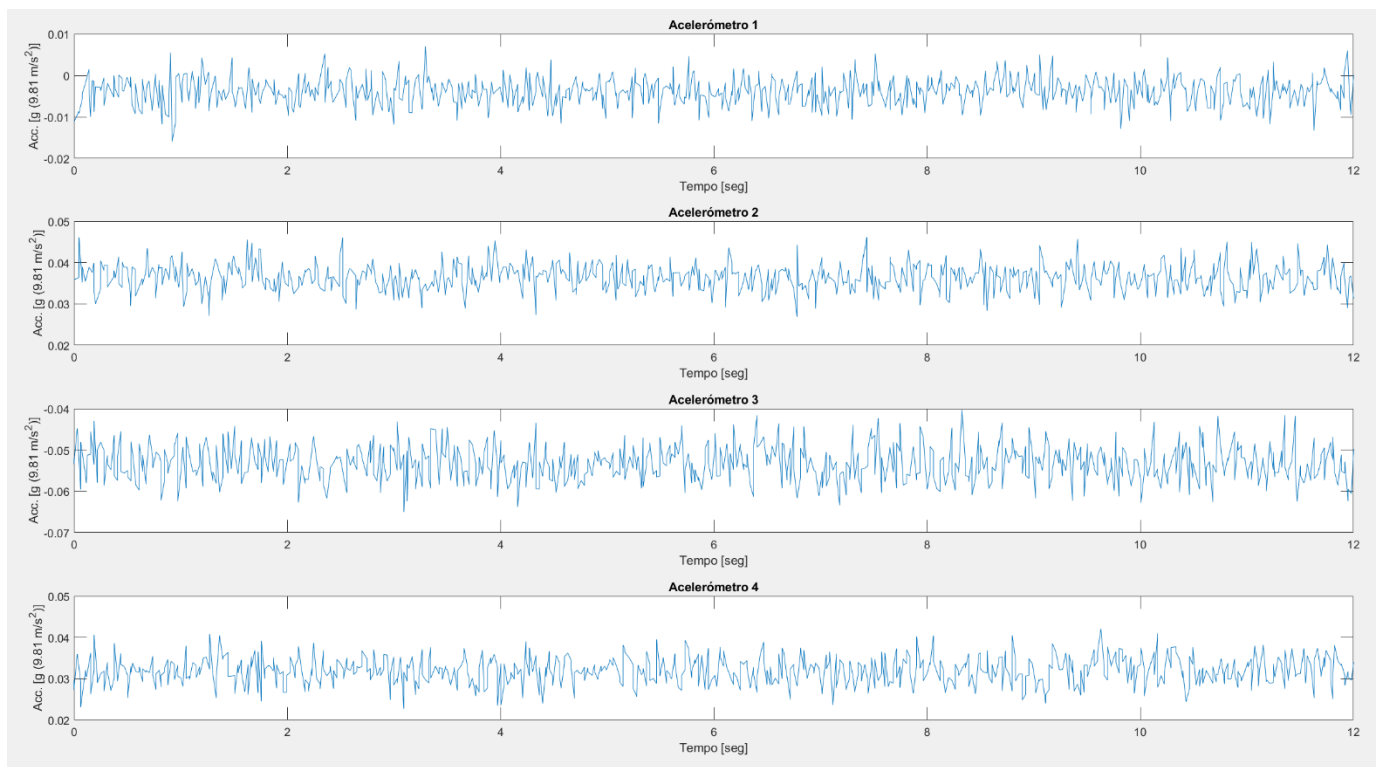


Figure 4.15 - Graph of the vibration acquired when the robot is immobilized.

A comparison of acquired vibration data between Test 2 - WAAM, and Test 3 - HF-WAAM is performed, Table 4.13. When the welding is on, it was not possible to acquire simultaneously the data from all four accelerometers, due to equipment issues. So, the data was acquired in pairs, first from sensors 1 and 2, and then sensors 3 and 4.

Table 4.13 - Values of the vibration during Test 2 - WAAM, and Test 3 - HF-WAAM, in g ( $9.81 \text{ m/s}^2$ ).

Accelerometer		1	2	3	4
Test 2 WAAM	Reference values	-0.002	0.031	-0.002	-0.010
	Maximum values	0.266	0.216	0.060	0.418
Test 3 HF-WAAM	Reference values	-0.002	0.031	-0.002	-0.010
	Maximum values	2.700	3.097	0.605	8.915

As it was expected, accelerometer 4 has the highest vibration, followed by the accelerometer 1, 2 and 3. This last one presents a significant low vibration because it is fixed in the body of the robot, in a stable position and distant from the torch.

The difference from WAAM to HF-WAAM values is in the scale of one order of magnitude, however that difference is higher in accelerometer 4. This is because, it is fixed almost in the source of vibration, leading to movements with low damping and vibration absorption compared to the other accelerometers.

In Fig. 4.16 is possible to visualize a representation of the vibration data when WAAM is applied. In Fig. 4.17, this representation corresponds to the vibration data when HF-WAAM is applied.

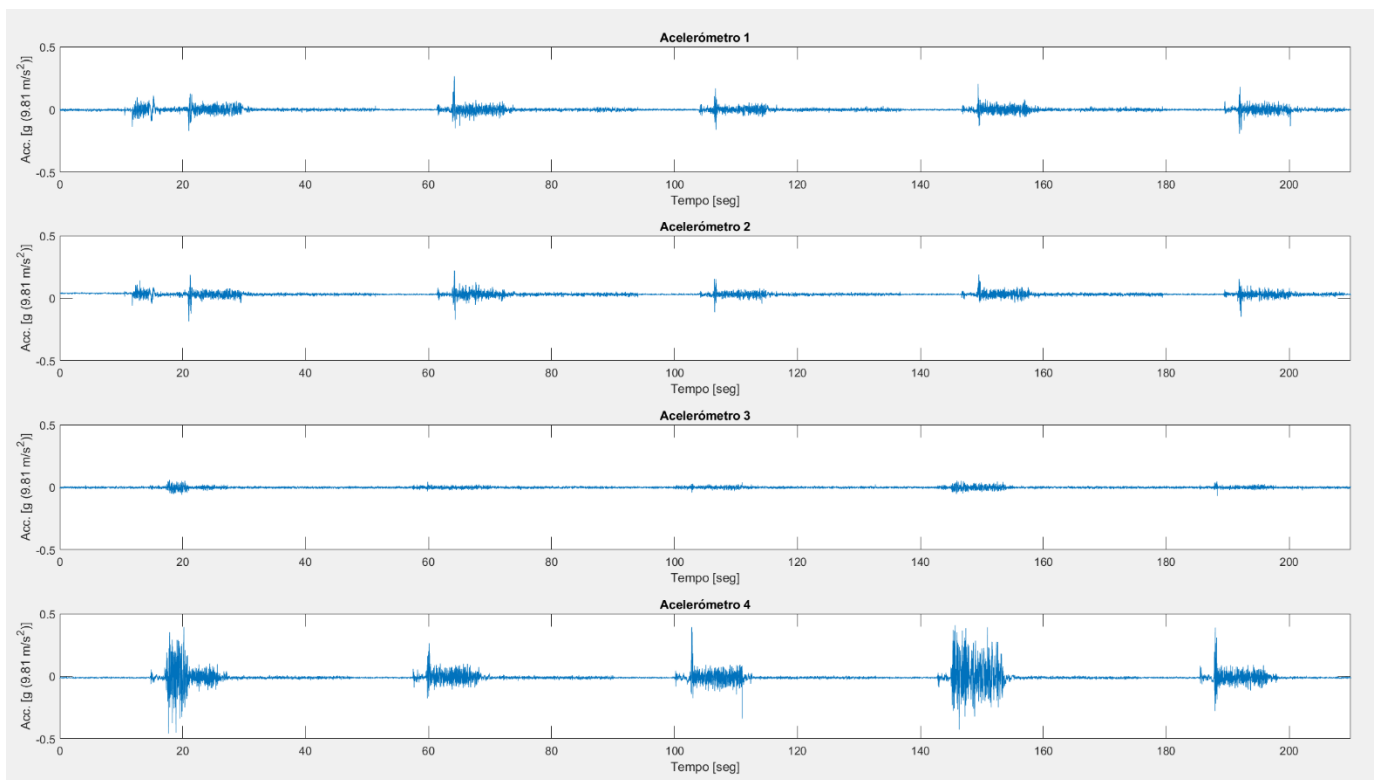


Figure 4.16 - Graph of the vibration acquired during Test 2 - WAAM proof test.

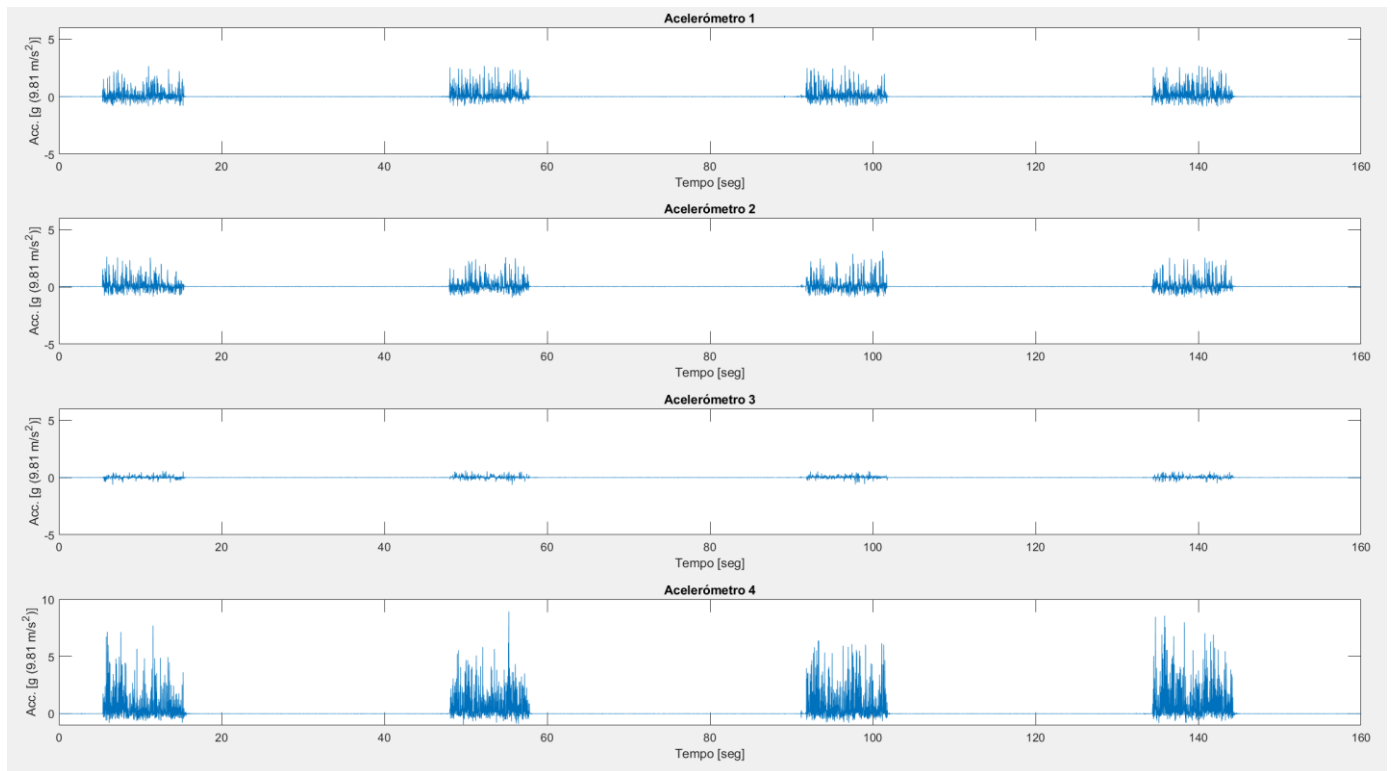


Figure 4.17 - Graph of the vibration acquired during Test 3 - HF-WAAM proof test.

Like the previous analysis, during the Test 9 - HF-WAAM the vibration data was acquired, Table 4.14. The maximum value of the accelerometer 4 is 14.4% lower than in Test 3 - HF-WAAM, because the height between the torch and the substrate is reduced in Test 9, to ensure all material is forged, reducing the vibration values in the torch. The maximum values of the other accelerometers are higher, up to 44.4%, because during the three-dimensional movement, the distance from the robot base to the torch increases, increasing the vibration values along the robotic arm. Fig. 4.18 presents the representation of the vibration data.

Table 4.14- Values of the vibration during Test 9 - HF-WAAM, in g ( $9.81 \text{ m/s}^2$ ).

Accelerometer		1	2	3	4
HF-WAAM	Reference values	-0.002	0.031	-0.002	-0.001
	Maximum values	3.905	3.528	0.712	7.792

In the vibration graphs of the accelerometers 1 and 2, Fig. 4.18, it is possible to observe a non-constant resting times between layers deposition, because due to problems such as stuck wire, sometimes it was necessary to intervene during the resting times, stopping the process longer than scheduled. Once the data from accelerometers 3 and 4 was acquired separately from the 1 and 2, they do not present this difference.

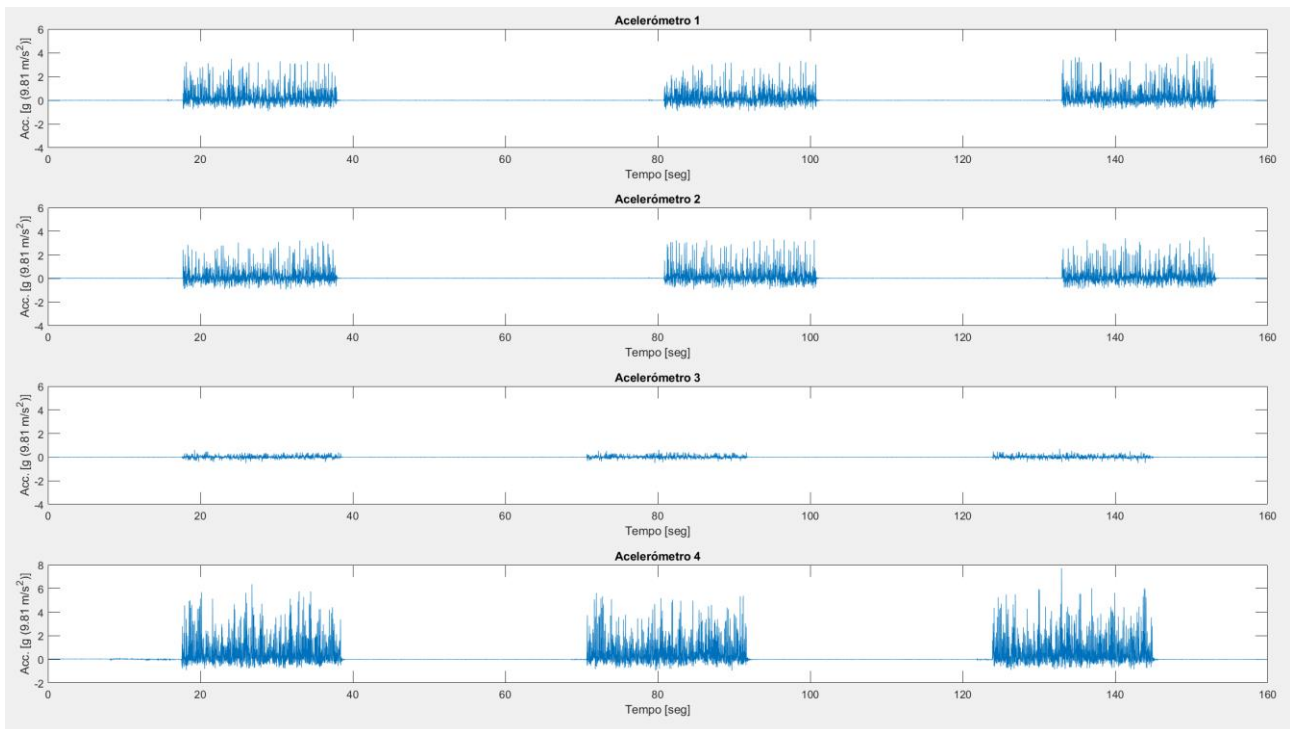


Figure 4.18 - Graph of the vibration acquired during Test 9 - HF-WAAM proof test.

Analysing the previous results, it is possible to have an idea of the vibration values that the torch and the robot are subject during the process. A comparison between WAAM and HF-WAAM was performed, and it was concluded that the difference between them is about one order of magnitude. Closer to the torch the vibrations are higher, and along the robotic arm they decrease due to their absorption and damping. When the deposition is performed by a three-dimensional movement of the torch, the vibration values along the robotic arm increase comparatively to the two-dimensional movement, however, in this research, this difference is not significant because the torch was not very inclined due to the difficulty of controlling it in three-dimensional movement. Overall, it was deduced that this vibration values,

acquired during the process, do not compromise the quality of the deposited material and the final component.

#### 4.6.1 Magnetic Pulse Forming vibration comparison

After acquiring vibration data from the WAAM and HF-WAAM processes, it was collected vibration values from Magnetic Pulse Forming process using the same robot, so that it is possible to compare values from different processes in the same robot.

Magnetic Pulse Forming is a process which uses the pulse magnetic force to produce high speed plastic deformation in a sheet metal, to obtain a specific shape. This process uses a mold, and can improve the material formability, reduce thinning, and inhibit rupture or cracking associated to the conventional metal sheet forming processes [58].

This procedure uses an Aluminum 2219, 2 mm thickness sheet as raw material. The part to be built has a bowl shape and the robot follows a spiral movement from the center to the outside. When it finishes one spiral layer, it returns to the center and restarts, until the shape is obtained. In total, it requires 36 layers. The voltage is 8600 V, and the discharges happen every 10 s. The movement starts in a point, discharging the magnetic pulse, then the tool goes 30 mm up, goes on and goes 30 mm down to the next point, repeating the process. The distance between two consecutive points is 20 mm, in a straight line. The magnetic tool is fixed to the robot by four springs.

In Table 4.16, it is possible to visualize the vibration values during the Magnetic Pulse Forming. The strategy to obtain the reference and the maximum values is the same used previously. The reference values were obtained directly in this process. As seen, the maximum values are one order of magnitude lower compared to HF-WAAM, although they are similar when compared to WAAM. The vibration of accelerometer 4 is similar to the vibration of accelerometers 1 and 2. This suggests that, in spite of the high voltage discharging, the springs absorb the vibration, and since the accelerometers are not attached to the tool, only to the robot, the vibration captured is reduced. So, the main source of vibration is the movement of the robot, as in WAAM, leading to uniform vibration values along the robotic arm and similar values between WAAM and Magnetic Pulse Forming.

Table 4.15 - Values of the vibration during Magnetic Pulse Forming, in g (9.81 m/s<sup>2</sup>).

Accelerometer	1	2	3	4
Reference values	-0.003	0.031	-0.006	-0.040
Maximum values	0.377	0.368	0.096	0.384

As demonstrated in Fig. 4.17, the vibration is not constant during the process. First, the angle of the robotic arm when manufacturing the edge side of the part lead to differences in the graphical direction of the maximum values, either positive or negative. Furthermore, in the center of the shape, the vibration is higher because the raw material is not completely leaning against the wall, having a clearance. In the borders, this clearance is reduced and so the vibration, because the borders are the first areas to be molded.

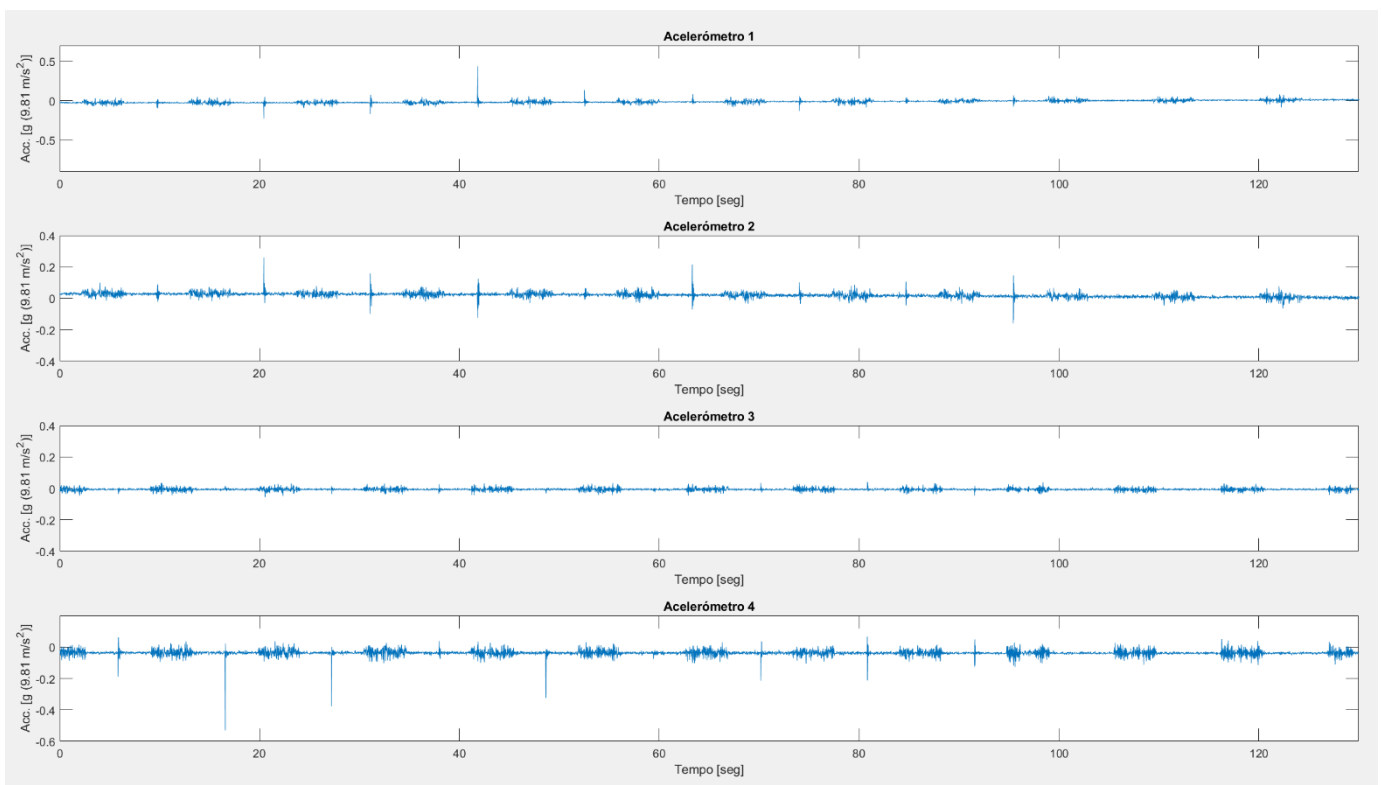


Figure 4.19 - Graph of the vibration acquired during Magnetic Pulse Forming.



This analysis is important to compare different processes, even so different features, but using the same robot. Because of the vibration absorption by the springs, the vibration values are reduced and similar to the ones from WAAM. The built parts are high quality, suggesting this range of values is adequate to the processes. Finding new strategies to reduce and mitigate vibrations is fundamental to have high quality components and to extend the shelf life of the manipulator.

## CONCLUSIONS AND FUTURE WORK

This Chapter presents the main conclusions obtained during this research, summarizing the knowledge acquired during the experiments, and presents purposes for future work to be developed following these results.

### 5.1 Conclusions

This study aimed to build a torch and validate its usage incorporated in an AM robotic system to produce parts with different geometries. Thus, it was studied the behavior of the system during deposition with two-dimensional and three-dimensional torch movement, so that it was possible to develop a methodology to write a robot code, offline, with the best AM process parameters to build a part. Also, the vibration data of the robotic system during the AM process was acquired to study the influence of the vibration in the part quality. Several conclusions were obtained and summarized:

- The developed customized welding torch to forge accomplished the requirements and demonstrated to be adequate to the WAAM and HF-WAAM processes, producing parts with no visible pores and excessive deformations.
- The proof-of-concept showed to be possible and achievable to take advantage of the forging immediately after the deposition to obtain a uniform deformation on the upper surface of the deposited layer, using a 6-DoF robot as a manipulator.

- The torch speed, during the direction's changes, must be kept constant to avoid excessive heat points, which could affect the layer quality and damage the tool.
- It is important to keep a correct CTWD, appropriate to the torch speed, in order to have a constant deposition, without the melting of the welding tip.
- The acquired vibration values revealed not to affect the parts quality, whereby they can be included in a range of admissible values to the process.
- During the three-dimensional deposition movement, the increasing of the distance from the robot's base to the torch increases the maximum vibration values, therefore it is necessary to configure them, aligning the axis of action of the forces to the larger joint (A1, Fig. 2.9), so that the larger joint can withstand the efforts.
- Programming the robot point-by-point is not an adequate strategy to produce parts in an industrial environment, because it is time consuming and can only produce simple geometry parts. It should be used a software that can build the part from its CAD model, controlling the robot's movement.

Concluding, this research is an important contribution to the development of WAAM and HF-WAAM so that it is possible to take full advantage of their potential and they can be complete implemented in the industry.

## 5.2 Future work

Despite of the positive results achieved in this dissertation, some improvements and investigations can be performed in the future:

- To validate the usage of the AM robotic system and the torch in different materials in addition to the 316LSi stainless steel used, such as aluminum, magnesium, or titanium alloys.
- To validate the usage of the AM robotic system and the torch to build parts with hollow cavities.

- To develop a numerical model that allows to simulate the deposition of material, so that it is possible to select the best parameters along the deposition path.
- To develop a hybrid AM robotic system, allowing to perform WAAM and HF-WAAM processes and the milling process in the same station.
- To use a software capable of generating the robot code from the CAD model of the part to build and validate its usage in the AM robotic system and torch to build high quality parts.
- Incorporate in the robotic system online parameter variation during the execution of the AM process without having to stop the system to do so.
- To study the behavior of the robotic process when there are large variations in the torch orientations during the execution of the processes.
- To study the manufacture of thick parts.



## REFERENCES

- [1] J. Butt, "Exploring the interrelationship between additive manufacturing and industry 4.0," *Designs*, vol. 4, no. 2. MDPI AG, pp. 1–33, Jun. 01, 2020. doi: 10.3390/designs4020013.
- [2] U. M. Dilberoglu, B. Gharehpapagh, U. Yaman, and M. Dolen, "The Role of Additive Manufacturing in the Era of Industry 4.0," *Procedia Manuf*, vol. 11, pp. 545–554, 2017, doi: 10.1016/j.promfg.2017.07.148.
- [3] T. A. Rodrigues, V. Duarte, R. M. Miranda, T. G. Santos, and J. P. Oliveira, "Current status and perspectives on wire and arc additive manufacturing (WAAM)," *Materials*, vol. 12, no. 7, 2019, doi: 10.3390/ma12071121.
- [4] K. Treutler and V. Wesling, "The current state of research of wire arc additive manufacturing (Waam): A review," *Applied Sciences (Switzerland)*, vol. 11, no. 18. MDPI, Sep. 01, 2021. doi: 10.3390/app11188619.
- [5] V. R. Duarte, T. A. Rodrigues, N. Schell, R. M. Miranda, J. P. Oliveira, and T. G. Santos, "Hot forging wire and arc additive manufacturing (HF-WAAM)," *Addit Manuf*, vol. 35, Oct. 2020, doi: 10.1016/j.addma.2020.101193.
- [6] S. Williams, "REPORT Wire +arc additive manufacturing vs. traditional machining from solid: a cost comparison," 2015.
- [7] K. v. Wong and A. Hernandez, "A Review of Additive Manufacturing," *ISRN Mechanical Engineering*, vol. 2012, pp. 1–10, Aug. 2012, doi: 10.5402/2012/208760.
- [8] M. Yakout, M. A. Elbestawi, and S. C. Veldhuis, "A review of metal additive manufacturing technologies," in *Solid State Phenomena*, 2018, vol. 278 SSP, pp. 1–14. doi: 10.4028/www.scientific.net/SSP.278.1.
- [9] S. R. Singh and P. Khanna, "Wire arc additive manufacturing (WAAM): A new process to shape engineering materials," in *Materials Today: Proceedings*, 2021, vol. 44, pp. 118–128. doi: 10.1016/j.matpr.2020.08.030.

- [10] M. Mehrpouya, A. Dehghanghadikolaei, B. Fotovvati, A. Vosooghnia, S. S. Emamian, and A. Gisario, "The potential of additive manufacturing in the smart factory industrial 4.0: A review," *Applied Sciences (Switzerland)*, vol. 9, no. 18. MDPI AG, Sep. 01, 2019. doi: 10.3390/app9183865.
- [11] A. Vafadar, F. Guzzomi, A. Rassau, and K. Hayward, "Advances in metal additive manufacturing: A review of common processes, industrial applications, and current challenges," *Applied Sciences (Switzerland)*, vol. 11, no. 3. MDPI AG, pp. 1–33, Feb. 01, 2021. doi: 10.3390/app11031213.
- [12] J. Liu, Y. Xu, Y. Ge, Z. Hou, and S. Chen, "Wire and arc additive manufacturing of metal components: a review of recent research developments", doi: 10.1007/s00170-020-05966-8/Published.
- [13] N. Kladovasilakis, P. Charalampous, I. Kostavelis, D. Tzetzis, and D. Tzovaras, "Impact of metal additive manufacturing parameters on the powder bed fusion and direct energy deposition processes: a comprehensive review," *Progress in Additive Manufacturing*, vol. 6, no. 3. Springer Science and Business Media Deutschland GmbH, pp. 349–365, Aug. 01, 2021. doi: 10.1007/s40964-021-00180-8.
- [14] "Powder Bed Fusion | Additive Manufacturing Research Group | Loughborough University." <https://www.lboro.ac.uk/research/amrg/about/the7categoriesofadditivemanufacturing/powderbedfusion/> (accessed Feb. 17, 2022).
- [15] V. R. Duarte, "Developments in directed energy deposition additive manufacturing: In-situ Hot-Forging and indirect cooling," NOVA School of Science and Technology, NOVA University Lisbon, 2022.
- [16] A. Saboori, A. Aversa, G. Marchese, S. Biamino, M. Lombardi, and P. Fino, "Application of directed energy deposition-based additive manufacturing in repair," *Applied Sciences (Switzerland)*, vol. 9, no. 16. MDPI AG, Aug. 01, 2019. doi: 10.3390/app9163316.
- [17] W. Gao *et al.*, "The status, challenges, and future of additive manufacturing in engineering," *CAD Computer Aided Design*, vol. 69, pp. 65–89, Dec. 2015, doi: 10.1016/j.cad.2015.04.001.
- [18] C. R. Cunningham, J. M. Flynn, A. Shokrani, V. Dhokia, and S. T. Newman, "Invited review article: Strategies and processes for high quality wire arc additive

- manufacturing," *Additive Manufacturing*, vol. 22. Elsevier B.V., pp. 672–686, Aug. 01, 2018. doi: 10.1016/j.addma.2018.06.020.
- [19] D. Ding, Z. Pan, D. Cuiuri, H. Li, S. van Duin, and N. Larkin, "Bead modelling and implementation of adaptive MAT path in wire and arc additive manufacturing," *Robot Comput Integr Manuf*, vol. 39, pp. 32–42, Jun. 2016, doi: 10.1016/j.rcim.2015.12.004.
  - [20] D. Ding, Z. Pan, D. Cuiuri, and H. Li, "Wire-feed additive manufacturing of metal components: technologies, developments and future interests," *International Journal of Advanced Manufacturing Technology*, vol. 81, no. 1–4. Springer London, pp. 465–481, Oct. 26, 2015. doi: 10.1007/s00170-015-7077-3.
  - [21] N. Chernovol, B. Lauwers, and P. van Rymenant, "Development of low-cost production process for prototype components based on Wire and Arc Additive Manufacturing (WAAM)," in *Procedia CIRP*, 2020, vol. 95, pp. 60–65. doi: 10.1016/j.procir.2020.01.188.
  - [22] V. Rebelo Duarte, "Additive manufacturing of a high resistance steel by MIG/MAG," NOVA School of Science and Technology, NOVA University Lisbon, 2016.
  - [23] D. Lopes, "Monitorização e ensaios não destrutivos para peças metálicas produzidas por WAAM," Faculdade de Ciência e Tecnologia, Universidade Nova de Lisboa, 2021.
  - [24] M. Dinovitzer, X. Chen, J. Laliberte, X. Huang, and H. Frei, "Effect of wire and arc additive manufacturing (WAAM) process parameters on bead geometry and microstructure," *Addit Manuf*, vol. 26, pp. 138–146, Mar. 2019, doi: 10.1016/j.addma.2018.12.013.
  - [25] J. G. Lopes, C. M. Machado, V. R. Duarte, T. A. Rodrigues, T. G. Santos, and J. P. Oliveira, "Effect of milling parameters on HSLA steel parts produced by Wire and Arc Additive Manufacturing (WAAM)," *J Manuf Process*, vol. 59, pp. 739–749, Nov. 2020, doi: 10.1016/j.jmapro.2020.10.007.
  - [26] X. Bai, H. Zhang, and G. Wang, "Modeling of the moving induction heating used as secondary heat source in weld-based additive manufacturing," *International*



- Journal of Advanced Manufacturing Technology*, vol. 77, no. 1–4, pp. 717–727, Mar. 2015, doi: 10.1007/s00170-014-6475-2.
- [27] F. Montevercchi, G. Venturini, N. Grossi, A. Scippa, and G. Campatelli, "Idle time selection for wire-arc additive manufacturing: A finite element-based technique," *Addit Manuf*, vol. 21, pp. 479–486, May 2018, doi: 10.1016/j.addma.2018.01.007.
  - [28] X. Cao, W. Wallace, J. P. Immarigeon, and C. Poon, "Research and progress in laser welding of wrought aluminum alloys. II. Metallurgical microstructures, defects, and mechanical properties," *Materials and Manufacturing Processes*, vol. 18, no. 1, pp. 23–49, Jan. 2003, doi: 10.1081/AMP-120017587.
  - [29] K. P. Karunakaran, S. Suryakumar, V. Pushpa, and S. Akula, "Low cost integration of additive and subtractive processes for hybrid layered manufacturing," *Robot Comput Integr Manuf*, vol. 26, no. 5, pp. 490–499, 2010, doi: 10.1016/j.rcim.2010.03.008.
  - [30] Y. H. Chen and Y. Song, "The development of a layer based machining system." [Online]. Available: [www.elsevier.com/locate/cad](http://www.elsevier.com/locate/cad)
  - [31] D. Ding *et al.*, "Towards an automated robotic arc-welding-based additive manufacturing system from CAD to finished part," *CAD Computer Aided Design*, vol. 73, pp. 66–75, Apr. 2016, doi: 10.1016/j.cad.2015.12.003.
  - [32] V. Dhinakaran, B. Stalin, M. Ravichandran, M. Balasubramanian, C. Anand Chairman, and D. Pritima, "Wire Arc Additive Manufacturing Perspectives and Recent Developments," in *IOP Conference Series: Materials Science and Engineering*, Dec. 2020, vol. 988, no. 1. doi: 10.1088/1757-899X/988/1/012102.
  - [33] C. Y. Zhu, J. N. Pires, and A. Azar, "A novel multi-brand robotic software interface for industrial additive manufacturing cells," *Industrial Robot*, vol. 47, no. 4, pp. 581–592, Jun. 2020, doi: 10.1108/IR-11-2019-0237.
  - [34] A. Taşdemir and S. Nohut, "An overview of wire arc additive manufacturing (WAAM) in shipbuilding industry," *Ships and Offshore Structures*. Taylor and Francis Ltd., pp. 1–18, 2020. doi: 10.1080/17445302.2020.1786232.
  - [35] P. Kazanas, P. Deherkar, P. Almeida, H. Lockett, and S. Williams, "Fabrication of geometrical features using wire and arc additive manufacture," *Proc Inst Mech*

- Eng B J Eng Manuf*, vol. 226, no. 6, pp. 1042–1051, Jun. 2012, doi: 10.1177/0954405412437126.
- [36] F. Rafael Pereira Dos Santos, "Hot-Forging WAAM de aço de baixa liga," Faculdade de Ciências e Tecnologia, Universidade Nova de Lisboa, 2021.
  - [37] Y. Cui, S. Kara, and K. C. Chan, "Manufacturing big data ecosystem: A systematic literature review," *Robotics and Computer-Integrated Manufacturing*, vol. 62. Elsevier Ltd, Apr. 01, 2020. doi: 10.1016/j.rcim.2019.101861.
  - [38] H. Lockett, J. Ding, S. Williams, and F. Martina, "Design for wire + Arc additive manufacture: Design rules and build orientation selection," *Journal of Engineering Design*, vol. 28, no. 7–9, pp. 568–598, Aug. 2017, doi: 10.1080/09544828.2017.1365826.
  - [39] Y. K. Bandari, T. O. H. Charrett, F. Michel, J. Ding, S. W. Williams, and R. P. Tatam, "Compensation strategies for robotic motion errors for additive manufacturing (AM)," in *27th Annual International Solid Freeform Fabrication Symposium*, Aug. 2016.
  - [40] P. Urhal, A. Weightman, C. Diver, and P. Bartolo, "Robot assisted additive manufacturing: A review," *Robot Comput Integr Manuf*, vol. 59, pp. 335–345, Oct. 2019, doi: 10.1016/j.rcim.2019.05.005.
  - [41] F. M. Ribeiro, J. N. Pires, and A. S. Azar, "Implementation of a robot control architecture for additive manufacturing applications," *Industrial Robot*, vol. 46, no. 1, pp. 73–82, Apr. 2019, doi: 10.1108/IR-11-2018-0226.
  - [42] D. Ding, Z. Pan, D. Cuiuri, and H. Li, "Process planning for robotic wire and arc additive manufacturing," in *10th, IEEE Conference on Industrial Electronics Society, Auckland*, Jun. 2015.
  - [43] B. Freire, M. Babcsinski, L. Ferreira, B. Señaris, F. Vidal, and P. Neto, "Direct energy deposition: A complete workflow for the additive manufacturing of complex shape parts," in *Procedia Manufacturing*, 2020, vol. 51, pp. 671–677. doi: 10.1016/j.promfg.2020.10.094.
  - [44] M. Babcsinski *et al.*, "An integrated and interoperable AutomationML-based platform for the robotic process of metal additive manufacturing," in *Procedia Manufacturing*, 2020, vol. 51, pp. 26–31. doi: 10.1016/j.promfg.2020.10.005.

- [45] D. Ding, Z. Pan, D. Cuiuri, and H. Li, "A tool-path generation strategy for wire and arc additive manufacturing," *International Journal of Advanced Manufacturing Technology*, vol. 73, no. 1–4, pp. 173–183, 2014, doi: 10.1007/s00170-014-5808-5.
- [46] T. B. Ionescu, "Leveraging graphical user interface automation for generic robot programming," *Robotics*, vol. 10, no. 1, pp. 1–23, 2021, doi: 10.3390/robotics10010003.
- [47] M. Babcsinschi, B. Freire, P. Neto, L. Ferreira, B. Senaris, and F. Vidal, "AutomationML for Data Exchange in the Robotic Process of Metal Additive Manufacturing," in *24th, IEEE International Conference on Emerging Technologies and Factory Automation*, Sep. 2019.
- [48] F. Xu *et al.*, "Realisation of a multi-sensor framework for process monitoring of the wire arc additive manufacturing in producing Ti-6Al-4V parts," *Int J Comput Integr Manuf*, vol. 31, no. 8, pp. 785–798, Aug. 2018, doi: 10.1080/0951192X.2018.1466395.
- [49] B. Guo, Y. Shi, G. Yu, B. Liang, and K. Wang, "Weld deviation detection based on wide dynamic range vision sensor in MAG welding process," *International Journal of Advanced Manufacturing Technology*, vol. 87, no. 9–12, pp. 3397–3410, Dec. 2016, doi: 10.1007/s00170-016-8721-2.
- [50] Y. Guo, Z. Zhao, J. Han, and L. Bai, "Quality monitoring in Wire-Arc additive manufacturing based on spectrum," in *ACM International Conference Proceeding Series*, Dec. 2018, pp. 240–244. doi: 10.1145/3301506.3301534.
- [51] M. Chaturvedi, E. Scutelnicu, C. C. Rusu, L. R. Mistodie, D. Mihailescu, and S. Arungalai Vendan, "Wire arc additive manufacturing: Review on recent findings and challenges in industrial applications and materials characterization," *Metals*, vol. 11, no. 6. MDPI AG, Jun. 01, 2021. doi: 10.3390/met11060939.
- [52] B. Claudiu, C. Mehdi, G. Alain, and N. Jean-Yves, "Dynamic behavior analysis for a six axis industrial machining robot," University Bordeaux, Talence, France, Sep. 2011.

- [53] S. Erkaya, "Analysis of joint clearance effects on dynamics of six DOF robot manipulators," in *Mechanisms and Machine Science*, 2015, vol. 24, pp. 307–314. doi: 10.1007/978-3-319-09411-3\_33.
- [54] V. Nguyen, J. Johnson, and S. Melkote, "Active vibration suppression in robotic milling using optimal control," *Int J Mach Tools Manuf*, vol. 152, May 2020, doi: 10.1016/j.ijmachtools.2020.103541.
- [55] K. B. Kaldestad, I. Tyapin, and G. Hovland, "Robotic face milling path correction and vibration reduction," in *IEEE/ASME International Conference on Advanced Intelligent Mechatronics, AIM*, Aug. 2015, vol. 2015-August, pp. 543–548. doi: 10.1109/AIM.2015.7222591.
- [56] "Bakelite | chemical compound | Britannica." <https://www.britannica.com/science/Bakelite> (accessed Jul. 27, 2022).
- [57] H. Barros, "Desenvolvimento e avaliação de célula robótica para Wire Arc Additive Manufacturing e Hot-Forging Wire Arc Additive Manufacturing," Faculdade de Ciência e Tecnologia, Universidade Nova de Lisboa, 2022.
- [58] H. Yu, Q. Zheng, S. Wang, and Y. Wang, "The deformation mechanism of circular hole flanging by magnetic pulse forming," *J Mater Process Technol*, vol. 257, pp. 54–64, Jul. 2018, doi: 10.1016/j.jmatprotec.2018.02.022.

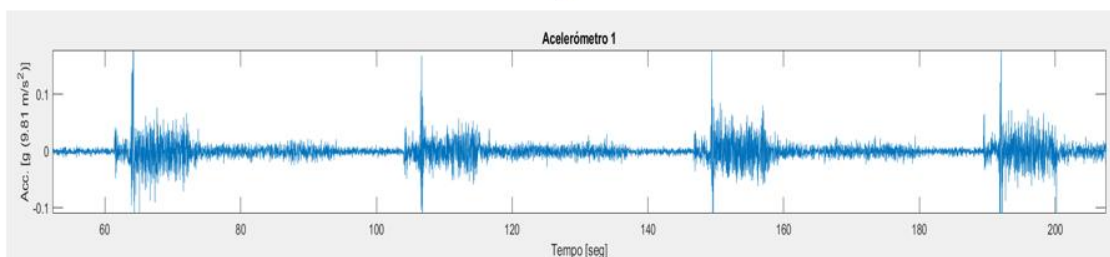
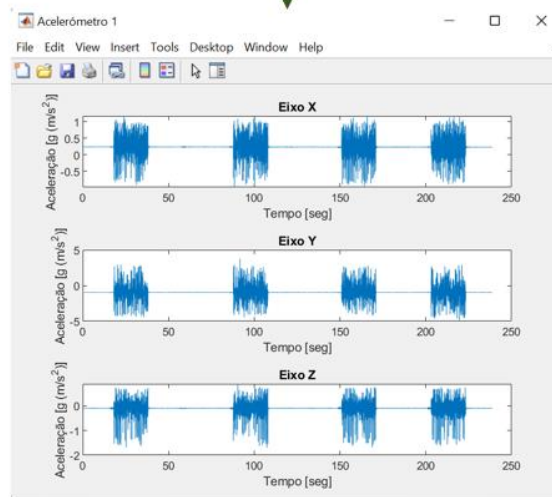
## APPENDIX A

## A.1 acquiring and processing of vibration data

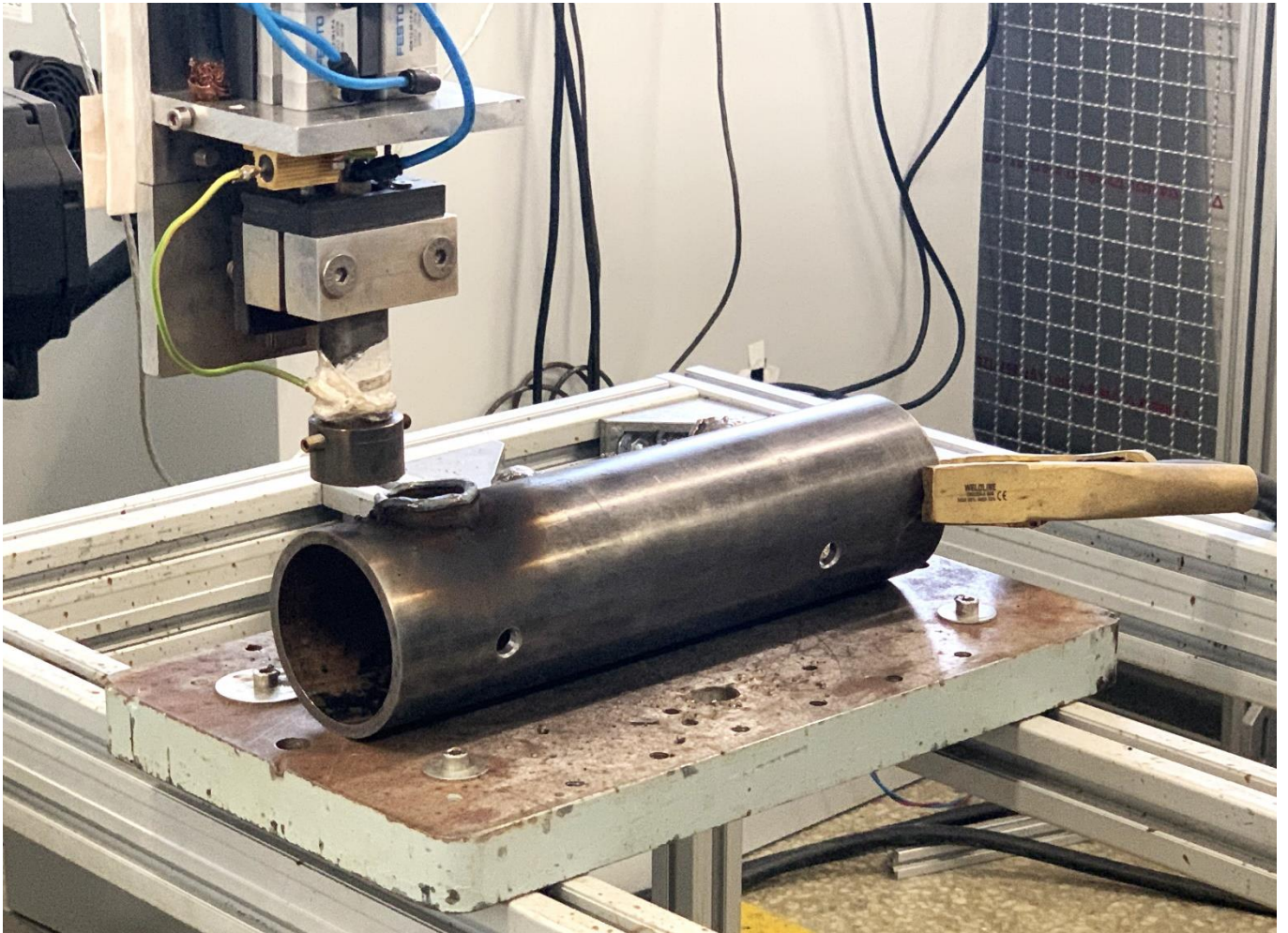
```

2022/07/12 10:41:43:911 AcX1 AcY1 AcZ1 GyX1 GyY1 GyZ1 AcX2 AcY2 AcZ2 GyX2 GyY2 GyZ2 Tmp1 Tmp2
2022/07/12 10:41:45:404 479 -1978 -211 -1547 -741 -247 2101 542 141 -614 -68 6 -2576
2022/07/12 10:41:45:436 493 -1984 -201 -1551 -749 -265 2093 551 130 -578 -68 -20 -2560
2022/07/12 10:41:45:436 484 -1975 -177 -1557 -745 -235 2097 536 130 -595 -54 -41 -2560
2022/07/12 10:41:45:476 484 -1973 -204 -1551 -747 -248 2102 559 129 -563 -49 10 -2560
2022/07/12 10:41:45:476 505 -1973 -198 -1567 -753 -247 2104 541 125 -571 -73 15 -2576
2022/07/12 10:41:45:500 492 -1975 -207 -1556 -718 -261 2092 554 124 -586 -64 -22 -2576
2022/07/12 10:41:45:524 492 -1970 -207 -1561 -751 -262 2095 539 126 -593 -63 4 -2560
2022/07/12 10:41:45:556 476 -1965 -196 -1571 -764 -248 2086 545 113 -600 -60 -3 -2528
2022/07/12 10:41:45:556 488 -1969 -201 -1560 -756 -237 2093 557 130 -579 -56 -7 -2528
2022/07/12 10:41:45:572 493 -1961 -215 -1553 -756 -239 2108 539 131 -585 -58 6 -2544
2022/07/12 10:41:45:596 487 -1972 -206 -1548 -742 -242 2102 554 118 -619 -85 -23 -2608
2022/07/12 10:41:45:596 489 -1972 -208 -1554 -747 -247 2110 532 119 -593 -93 4 -2544
2022/07/12 10:41:45:628 495 -1968 -217 -1558 -752 -250 2105 543 128 -559 -79 19 -2592
2022/07/12 10:41:45:644 478 -1990 -207 -1550 -756 -240 2096 540 138 -590 -80 -8 -2592
2022/07/12 10:41:45:676 492 -1979 -215 -1566 -729 -223 2095 546 118 -563 -89 -17 -2576
2022/07/12 10:41:45:676 495 -1983 -196 -1557 -751 -247 2100 538 129 -601 -79 -13 -2576
2022/07/12 10:41:45:708 491 -1978 -224 -1557 -748 -249 2095 530 137 -582 -72 17 -2592
2022/07/12 10:41:45:708 493 -1974 -235 -1550 -763 -243 2103 545 120 -574 -77 11 -2560
2022/07/12 10:41:45:724 496 -1978 -209 -1552 -760 -253 2100 530 138 -570 -64 9 -2560
2022/07/12 10:41:45:756 486 -1979 -218 -1569 -756 -244 2095 547 135 -568 -77 -1 -2560

```



## A.2 Developed WAAM torch to forge



## APPENDIX B - ROBOT'S CODE OF THE PART FROM TEST 8

### B.1 Robot's code - Part 1

```

&ACCESS RVP
&REL 8
&PARAM TEMPLATE = C:\KRC\Roboter\Template\vorgabe
&PARAM EDITMASK = *
DEF cilindro3( )
;FOLD INI;%{PE}%V3.2.0,%MKUKATPBASIS,%CINIT,%VCOMMON,%P
;FOLD BAS INI;%{E}%V3.2.0,%MKUKATPBASIS,%CINIT,%VINIT,%P
GLOBAL INTERRUPT DECL 3 WHEN $STOPMESS==TRUE DO IR_STOPM ( )
INTERRUPT ON 3
BAS (#INITMOV,0 )
;ENDFOLD (BAS INI)
;FOLD A20 INI;%{E}%V3.2.0,%MKUKATPA20,%CINIT,%VINIT,%P
IF ARC20==TRUE THEN
A20 (ARC_INI)
INTERRUPT DECL 6 WHEN $CYCFLAG[3]==FALSE DO A20(TECH_STOP2)
ENDIF
;ENDFOLD (A20 INI)
;FOLD A10 INI;%{E}%V3.2.0,%MKUKATPARC,%CINIT,%VINIT,%P
IF A10_OPTION==#ACTIVE THEN
INTERRUPT DECL 4 WHEN $CYCFLAG[2]==FALSE DO A10 (#APPL_ERROR)
INTERRUPT DECL 7 WHEN A_ARC_SWI==#ACTIVE DO A10 (#ARC_SEAM)
INTERRUPT DECL 5 WHEN A_FLY_ARC==TRUE DO A10 (#HPU_ARC)
INTERRUPT ON 5
A10_INI ( )
ENDIF
;ENDFOLD (A10 INI)
;FOLD GRIPPER INI;%{E}%V3.2.0,%MKUKATPGRIPPER,%CINIT,%VINIT,%P
USER_GRP(0,DUMMY,DUMMY,GDEFAULT)
;ENDFOLD (GRIPPER INI)
;FOLD SPOT INI;%{E}%V3.2.0,%MKUKATPSPOT,%CINIT,%VINIT,%P
USERSPOT(#INIT)
;ENDFOLD (SPOT INI)
;FOLD TOUCHSENSE INI;%{E}%V3.2.0,%MKUKATPTS,%CINIT,%VINIT,%P
IF H70_OPTION THEN
INTERRUPT DECL 15 WHEN $MEAS_PULSE[TOUCH_I[TOUCH_ACTIVE].IN_NR] DO H70 (6,CD0 )
INTERRUPT DECL 16 WHEN $ZERO_MOVE DO H70 (7,CD0 )
INTERRUPT DECL 17 WHEN $TECHPAR_C[FG_TOUCH,8]>0.5 DO H70 (8,CD0)
H70 (1,CD0 )

```

```

ENDIF
;ENDFOLD (TOUCHSENSE INI)
;FOLD USER INI;%{E}%V3.2.0,%MKUKATPUSER,%CINIT,%VINIT,%P
;Make your modifications here
;ENDFOLD (USER INI)
;ENDFOLD (INI)

;FOLD OUT 1 'gas' State= FALSE CONT;%{PE}%R 4.1.7,%MKUKATPBASIS,%COUT,%VOUTX,%P 2:1, 3:'gas', 5:FALSE,
6:CONTINUE
CONTINUE
$OUT[1]=FALSE
;ENDFOLD
;FOLD OUT 2 'soldadura' State= FALSE CONT;%{PE}%R 4.1.7,%MKUKATPBASIS,%COUT,%VOUTX,%P 2:2, 3:'solda-
dura', 5:FALSE, 6:CONTINUE
CONTINUE
$OUT[2]=FALSE
;ENDFOLD
;FOLD OUT 3 'martelo' State= FALSE CONT;%{PE}%R 4.1.7,%MKUKATPBASIS,%COUT,%VOUTX,%P 2:3, 3:'martelo',
5:FALSE, 6:CONTINUE
CONTINUE
$OUT[3]=FALSE
;ENDFOLD
;FOLD OUT 4 'motor_fio' State= FALSE CONT;%{PE}%R 4.1.7,%MKUKATPBASIS,%COUT,%VOUTX,%P 2:4, 3:'mo-
tor_fio', 5:FALSE, 6:CONTINUE
CONTINUE
$OUT[4]=FALSE
;ENDFOLD

Z1=1.7
Z2=1.2
Z3=3.5

;FOLD PTP HOME Vel= 7 % DEFAULT;%{PE}%R 4.1.7,%MKUKATPBASIS,%CMOVE,%VPTP,%P 1:PTP, 2:HOME, 3:, 5:7,
7:DEFAULT
$BWDSTART = FALSE
PDAT_ACT=PDEFAULT
BAS(#PTP_DAT)
FDAT_ACT=FHOME
BAS(#FRAMES)
BAS(#VEL_PTP,7)
$H_POS=XHOME
PTP XHOME
;ENDFOLD

A1 = XP3
A2 = XP4
A3 = XP5
A4 = XP6
A5 = XP7
A6 = XP8
A7 = XP9
A8 = XP10
A10 = XP12
A11 = XP13
A12 = XP14
A13 = XP15

```



```
;FOLD PTP P1 Vel= 5 % PDAT1 Tool[14]:HF_WAAM_BERNARDO Base[8]:MESA_MA_BERN;%{PE}%R
4.1.7,%MKUKATPBASIS,%CMOVE,%VPTP,%P 1:PTP, 2:P1, 3:, 5:5, 7:PDAT1
$BWDSTART = FALSE
PDAT_ACT=PPDAT1
BAS(#PTP_DAT)
FDAT_ACT=FP1
BAS(#FRAMES)
BAS(#VEL_PTP,5)
PTP XP1
;ENDFOLD
```

```
;FOLD PTP P2 Vel= 5 % PDAT2 Tool[14]:HF_WAAM_BERNARDO Base[8]:MESA_MA_BERN;%{PE}%R
4.1.7,%MKUKATPBASIS,%CMOVE,%VPTP,%P 1:PTP, 2:P2, 3:, 5:5, 7:PDAT2
$BWDSTART = FALSE
PDAT_ACT=PPDAT2
BAS(#PTP_DAT)
FDAT_ACT=FP2
BAS(#FRAMES)
BAS(#VEL_PTP,5)
PTP XP2
;ENDFOLD
```

```
;FOLD LIN P3 Vel= 0.03 m/s CPDAT1 Tool[14]:HF_WAAM_BERNARDO Base[8]:MESA_MA_BERN;%{PE}%R
4.1.7,%MKUKATPBASIS,%CMOVE,%VLIN,%P 1:LIN, 2:P3, 3:, 5:0.03, 7:CPDAT1
$BWDSTART = FALSE
LDAT_ACT=LCPDAT1
BAS(#CP_DAT)
FDAT_ACT=FP3
BAS(#FRAMES)
BAS(#VEL_CP,0.03)
LIN XP3
;ENDFOLD
```

```
;FOLD LIN P4 Vel= 0.01 m/s CPDAT2 Tool[14]:HF_WAAM_BERNARDO Base[8]:MESA_MA_BERN;%{PE}%R
4.1.7,%MKUKATPBASIS,%CMOVE,%VLIN,%P 1:LIN, 2:P4, 3:, 5:0.01, 7:CPDAT2
$BWDSTART = FALSE
LDAT_ACT=LCPDAT2
BAS(#CP_DAT)
FDAT_ACT=FP4
BAS(#FRAMES)
BAS(#VEL_CP,0.01)
LIN XP4
;ENDFOLD
```

```
;FOLD SYN OUT 1 'gas' State= TRUE at START Delay= 0 ms;%{PE}%R
4.1.7,%MKUKATPBASIS,%COUT,%VSYNOUT,%P 2:1, 3:'gas', 5:TRUE, 7:0, 9:0, 12:0
TRIGGER WHEN DISTANCE=0 DELAY=0 DO $OUT[1]=TRUE
;ENDFOLD
```

```
;FOLD LIN P5 Vel= 0.006 m/s CPDAT3 Tool[14]:HF_WAAM_BERNARDO Base[8]:MESA_MA_BERN;%{PE}%R
4.1.7,%MKUKATPBASIS,%CMOVE,%VLIN,%P 1:LIN, 2:P5, 3:, 5:0.006, 7:CPDAT3
$BWDSTART = FALSE
LDAT_ACT=LCPDAT3
BAS(#CP_DAT)
FDAT_ACT=FP5
```

BAS(#FRAMES)  
BAS(#VEL\_CP,0.006)  
LIN XP5  
;ENDFOLD

;FOLD SYN OUT 2 'soldadura' State= TRUE at START Delay= 0 ms;%{PE}%R  
4.1.7,%MKUKATPBASIS,%COUT,%VSYNOUT,%P 2:2, 3:'soldadura', 5:TRUE, 7:0, 9:0, 12:0  
TRIGGER WHEN DISTANCE=0 DELAY=0 DO \$OUT[2]=TRUE  
;ENDFOLD

;FOLD SYN OUT 4 'motor\_fio' State= TRUE at START Delay= 0 ms;%{PE}%R  
4.1.7,%MKUKATPBASIS,%COUT,%VSYNOUT,%P 2:4, 3:'motor\_fio', 5:TRUE, 7:0, 9:0, 12:0  
TRIGGER WHEN DISTANCE=0 DELAY=0 DO \$OUT[4]=TRUE  
;ENDFOLD

;FOLD LIN P6 CONT Vel= 0.006 m/s CPDAT4 Tool[14]:HF\_WAAM\_BERNARDO Base[8]:MESA\_MA\_BERN;%{PE}%R  
4.1.7,%MKUKATPBASIS,%CMOVE,%VLIN,%P 1:LIN, 2:P6, 3:C\_DIS, 5:0.006, 7:CPDAT4  
\$BWDSTART = FALSE  
LDAT\_ACT=LCPDAT4  
BAS(#CP\_DAT)  
FDAT\_ACT=FP6  
BAS(#FRAMES)  
BAS(#VEL\_CP,0.006)  
LIN XP6 C\_DIS  
;ENDFOLD

;FOLD CIRC P7 P8 CONT Vel= 0.006 m/s CPDAT5 Tool[14]:HF\_WAAM\_BERNARDO Base[8]:MESA\_MA\_BERN;%{PE}%R  
4.1.7,%MKUKATPBASIS,%CMOVE,%VCIRC,%P 1:CIRC, 2:P7, 3:P8, 4:C\_DIS, 6:0.006, 8:CPDAT5  
\$BWDSTART = FALSE  
LDAT\_ACT=LCPDAT5  
BAS(#CP\_DAT)  
FDAT\_ACT=FP8  
BAS(#FRAMES)  
BAS(#VEL\_CP,0.006)  
CIRC XP7, XP8 C\_DIS  
;ENDFOLD

;FOLD CIRC P9 P10 CONT Vel= 0.006 m/s CPDAT6 Tool[14]:HF\_WAAM\_BERNARDO  
Base[8]:MESA\_MA\_BERN;%{PE}%R 4.1.7,%MKUKATPBASIS,%CMOVE,%VCIRC,%P 1:CIRC, 2:P9, 3:P10, 4:C\_DIS,  
6:0.006, 8:CPDAT6  
\$BWDSTART = FALSE  
LDAT\_ACT=LCPDAT6  
BAS(#CP\_DAT)  
FDAT\_ACT=FP10  
BAS(#FRAMES)  
BAS(#VEL\_CP,0.006)  
CIRC XP9, XP10 C\_DIS  
;ENDFOLD

;FOLD SYN OUT 4 'motor\_fio' State= FALSE at START Delay= 0 ms;%{PE}%R  
4.1.7,%MKUKATPBASIS,%COUT,%VSYNOUT,%P 2:4, 3:'motor\_fio', 5:FALSE, 7:0, 9:0, 12:0  
TRIGGER WHEN DISTANCE=0 DELAY=0 DO \$OUT[4]=FALSE  
;ENDFOLD

;FOLD SYN OUT 2 'soldadura' State= FALSE at START Delay= 0 ms;%{PE}%R  
4.1.7,%MKUKATPBASIS,%COUT,%VSYNOUT,%P 2:2, 3:'soldadura', 5:FALSE, 7:0, 9:0, 12:0  
TRIGGER WHEN DISTANCE=0 DELAY=0 DO \$OUT[2]=FALSE

;ENDFOLD

;FOLD LIN P5 Vel= 0.006 m/s CPDAT3 Tool[14]:HF\_WAAM\_BERNARDO Base[8]:MESA\_MA\_BERN;{%PE}%R  
4.1.7,%MKUKATPBASIS,%CMOVE,%VLIN,%P 1:LIN, 2:P5, 3:, 5:0.006, 7:CPDAT3  
\$BWDSTART = FALSE  
LDAT\_ACT=LCPDAT3  
BAS(#CP\_DAT)  
FDAT\_ACT=FP5  
BAS(#FRAMES)  
BAS(#VEL\_CP,0.006)  
LIN XP5  
;ENDFOLD

;FOLD SYN OUT 1 'gas' State= FALSE at START Delay= 0 ms;{%PE}%R  
4.1.7,%MKUKATPBASIS,%COUT,%VSYNOUT,%P 2:1, 3:'gas', 5:FALSE, 7:0, 9:0, 12:0  
TRIGGER WHEN DISTANCE=0 DELAY=0 DO \$OUT[1]=FALSE  
;ENDFOLD

;FOLD LIN P4 Vel= 0.01 m/s CPDAT2 Tool[14]:HF\_WAAM\_BERNARDO Base[8]:MESA\_MA\_BERN;{%PE}%R  
4.1.7,%MKUKATPBASIS,%CMOVE,%VLIN,%P 1:LIN, 2:P4, 3:, 5:0.01, 7:CPDAT2  
\$BWDSTART = FALSE  
LDAT\_ACT=LCPDAT2  
BAS(#CP\_DAT)  
FDAT\_ACT=FP4  
BAS(#FRAMES)  
BAS(#VEL\_CP,0.01)  
LIN XP4  
;ENDFOLD

;FOLD LIN P3 Vel= 0.03 m/s CPDAT1 Tool[14]:HF\_WAAM\_BERNARDO Base[8]:MESA\_MA\_BERN;{%PE}%R  
4.1.7,%MKUKATPBASIS,%CMOVE,%VLIN,%P 1:LIN, 2:P3, 3:, 5:0.03, 7:CPDAT1  
\$BWDSTART = FALSE  
LDAT\_ACT=LCPDAT1  
BAS(#CP\_DAT)  
FDAT\_ACT=FP3  
BAS(#FRAMES)  
BAS(#VEL\_CP,0.03)  
LIN XP3  
;ENDFOLD

;FOLD WAIT Time= 30 sec;{%PE}%R 4.1.7,%MKUKATPBASIS,%CWAIT,%VWAIT,%P 2:30  
WAIT SEC 30  
;ENDFOLD  
XP3.Z = XP3.Z + Z1  
XP4.Z = XP4.Z + Z1  
XP5.Z = XP5.Z + Z1  
XP6.Z = XP6.Z + Z1  
XP7.Z = XP7.Z + Z1  
XP8.Z = XP8.Z + Z1  
XP9.Z = XP9.Z + Z1  
XP10.Z = XP10.Z + Z1  
XP12.Z = XP12.Z + Z1  
XP13.Z = XP13.Z + Z1  
XP14.Z = XP14.Z + Z1  
XP15.Z = XP15.Z + Z1

```
;FOLD LIN P3 Vel= 0.03 m/s CPDAT1 Tool[14]:HF_WAAM_BERNARDO Base[8]:MESA_MA_BERN;{%PE}%R
4.1.7,%MKUKATPBASIS,%CMOVE,%VLIN,%P 1:LIN, 2:P3, 3:, 5:0.03, 7:CPDAT1
$BWDSTART = FALSE
LDAT_ACT=LCPDAT1
BAS(#CP_DAT)
FDAT_ACT=FP3
BAS(#FRAMES)
BAS(#VEL_CP,0.03)
LIN XP3
;ENDFOLD
```

```
;FOLD LIN P4 Vel= 0.01 m/s CPDAT2 Tool[14]:HF_WAAM_BERNARDO Base[8]:MESA_MA_BERN;{%PE}%R
4.1.7,%MKUKATPBASIS,%CMOVE,%VLIN,%P 1:LIN, 2:P4, 3:, 5:0.01, 7:CPDAT2
$BWDSTART = FALSE
LDAT_ACT=LCPDAT2
BAS(#CP_DAT)
FDAT_ACT=FP4
BAS(#FRAMES)
BAS(#VEL_CP,0.01)
LIN XP4
;ENDFOLD
```

```
;FOLD SYN OUT 1 'gas' State= TRUE at START Delay= 0 ms;{%PE}%R
4.1.7,%MKUKATPBASIS,%COUT,%VSYNOUT,%P 2:1, 3:'gas', 5:TRUE, 7:0, 9:0, 12:0
TRIGGER WHEN DISTANCE=0 DELAY=0 DO $OUT[1]=TRUE
;ENDFOLD
```

```
;FOLD LIN P5 Vel= 0.006 m/s CPDAT3 Tool[14]:HF_WAAM_BERNARDO Base[8]:MESA_MA_BERN;{%PE}%R
4.1.7,%MKUKATPBASIS,%CMOVE,%VLIN,%P 1:LIN, 2:P5, 3:, 5:0.006, 7:CPDAT3
$BWDSTART = FALSE
LDAT_ACT=LCPDAT3
BAS(#CP_DAT)
FDAT_ACT=FP5
BAS(#FRAMES)
BAS(#VEL_CP,0.006)
LIN XP5
;ENDFOLD
```

```
;FOLD SYN OUT 2 'soldadura' State= TRUE at START Delay= 0 ms;{%PE}%R
4.1.7,%MKUKATPBASIS,%COUT,%VSYNOUT,%P 2:2, 3:'soldadura', 5:TRUE, 7:0, 9:0, 12:0
TRIGGER WHEN DISTANCE=0 DELAY=0 DO $OUT[2]=TRUE
;ENDFOLD
;FOLD SYN OUT 4 'motor_fio' State= TRUE at START Delay= 0 ms;{%PE}%R
4.1.7,%MKUKATPBASIS,%COUT,%VSYNOUT,%P 2:4, 3:'motor_fio', 5:TRUE, 7:0, 9:0, 12:0
TRIGGER WHEN DISTANCE=0 DELAY=0 DO $OUT[4]=TRUE
;ENDFOLD
```

```
;FOLD LIN P6 CONT Vel= 0.006 m/s CPDAT4 Tool[14]:HF_WAAM_BERNARDO Base[8]:MESA_MA_BERN;{%PE}%R
4.1.7,%MKUKATPBASIS,%CMOVE,%VLIN,%P 1:LIN, 2:P6, 3:C_DIS, 5:0.006, 7:CPDAT4
$BWDSTART = FALSE
LDAT_ACT=LCPDAT4
BAS(#CP_DAT)
FDAT_ACT=FP6
BAS(#FRAMES)
BAS(#VEL_CP,0.006)
LIN XP6 C_DIS
```

;ENDFOLD

;FOLD CIRC P12 P13 CONT Vel= 0.006 m/s CPDAT7 Tool[14]:HF\_WAAM\_BERNARDO  
Base[8]:MESA\_MA\_BERN;%{PE}%R 4.1.7,%MKUKATPBASIS,%CMOVE,%VCIRC,%P 1:CIRC, 2:P12, 3:P13, 4:C\_DIS,  
6:0.006, 8:CPDAT7  
\$BWDSTART = FALSE  
LDAT\_ACT=LCPDAT7  
BAS(#CP\_DAT)  
FDAT\_ACT=FP13  
BAS(#FRAMES)  
BAS(#VEL\_CP,0.006)  
CIRC XP12, XP13 C\_DIS  
;ENDFOLD

;FOLD CIRC P14 P15 CONT Vel= 0.006 m/s CPDAT8 Tool[14]:HF\_WAAM\_BERNARDO  
Base[8]:MESA\_MA\_BERN;%{PE}%R 4.1.7,%MKUKATPBASIS,%CMOVE,%VCIRC,%P 1:CIRC, 2:P14, 3:P15, 4:C\_DIS,  
6:0.006, 8:CPDAT8  
\$BWDSTART = FALSE  
LDAT\_ACT=LCPDAT8  
BAS(#CP\_DAT)  
FDAT\_ACT=FP15  
BAS(#FRAMES)  
BAS(#VEL\_CP,0.006)  
CIRC XP14, XP15 C\_DIS  
;ENDFOLD

;FOLD SYN OUT 4 'motor\_fio' State= FALSE at START Delay= 0 ms;%{PE}%R  
4.1.7,%MKUKATPBASIS,%COUT,%VSYNOUT,%P 2:4, 3:'motor\_fio', 5:FALSE, 7:0, 9:0, 12:0  
TRIGGER WHEN DISTANCE=0 DELAY=0 DO \$OUT[4]=FALSE  
;ENDFOLD

;FOLD SYN OUT 2 'soldadura' State= FALSE at START Delay= 0 ms;%{PE}%R  
4.1.7,%MKUKATPBASIS,%COUT,%VSYNOUT,%P 2:2, 3:'soldadura', 5:FALSE, 7:0, 9:0, 12:0  
TRIGGER WHEN DISTANCE=0 DELAY=0 DO \$OUT[2]=FALSE  
;ENDFOLD

;FOLD LIN P5 Vel= 0.006 m/s CPDAT3 Tool[14]:HF\_WAAM\_BERNARDO Base[8]:MESA\_MA\_BERN;%{PE}%R  
4.1.7,%MKUKATPBASIS,%CMOVE,%VLIN,%P 1:LIN, 2:P5, 3:, 5:0.006, 7:CPDAT3  
\$BWDSTART = FALSE  
LDAT\_ACT=LCPDAT3  
BAS(#CP\_DAT)  
FDAT\_ACT=FP5  
BAS(#FRAMES)  
BAS(#VEL\_CP,0.006)  
LIN XP5  
;ENDFOLD

;FOLD SYN OUT 1 'gas' State= FALSE at START Delay= 0 ms;%{PE}%R  
4.1.7,%MKUKATPBASIS,%COUT,%VSYNOUT,%P 2:1, 3:'gas', 5:FALSE, 7:0, 9:0, 12:0  
TRIGGER WHEN DISTANCE=0 DELAY=0 DO \$OUT[1]=FALSE  
;ENDFOLD

;FOLD LIN P4 Vel= 0.01 m/s CPDAT2 Tool[14]:HF\_WAAM\_BERNARDO Base[8]:MESA\_MA\_BERN;%{PE}%R  
4.1.7,%MKUKATPBASIS,%CMOVE,%VLIN,%P 1:LIN, 2:P4, 3:, 5:0.01, 7:CPDAT2  
\$BWDSTART = FALSE  
LDAT\_ACT=LCPDAT2

BAS(#CP\_DAT)  
FDAT\_ACT=FP4  
BAS(#FRAMES)  
BAS(#VEL\_CP,0.01)  
LIN XP4  
;ENDFOLD

;FOLD LIN P3 Vel= 0.03 m/s CPDAT1 Tool[14]:HF\_WAAM\_BERNARDO Base[8]:MESA\_MA\_BERN;{%PE}%R  
4.1.7,%MKUKATPBASIS,%CMOVE,%VLIN,%P 1:LIN, 2:P3, 3:, 5:0.03, 7:CPDAT1

\$BWDSTART = FALSE  
LDAT\_ACT=LCPDAT1  
BAS(#CP\_DAT)  
FDAT\_ACT=FP3  
BAS(#FRAMES)  
BAS(#VEL\_CP,0.03)  
LIN XP3  
;ENDFOLD

;FOLD WAIT Time= 30 sec;{%PE}%R 4.1.7,%MKUKATPBASIS,%CWAIT,%VWAIT,%P 2:30  
WAIT SEC 30  
;ENDFOLD

XP3.Z = XP3.Z + Z1  
XP4.Z = XP4.Z + z1  
XP5.Z = XP5.Z + Z1  
XP6.Z = XP6.Z + Z1

XP7.Z = XP7.Z + Z3

XP8.Z = XP8.Z + Z1  
XP9.Z = XP9.Z + Z1  
XP10.Z = XP10.Z + Z1

XP12.Z = XP12.Z + Z3

XP13.Z = XP13.Z + Z1  
XP14.Z = XP14.Z + Z1  
XP15.Z = XP15.Z + Z1

FOR I=1 TO 20

;FOLD LIN P3 Vel= 0.03 m/s CPDAT1 Tool[14]:HF\_WAAM\_BERNARDO Base[8]:MESA\_MA\_BERN;{%PE}%R  
4.1.7,%MKUKATPBASIS,%CMOVE,%VLIN,%P 1:LIN, 2:P3, 3:, 5:0.03, 7:CPDAT1

\$BWDSTART = FALSE  
LDAT\_ACT=LCPDAT1  
BAS(#CP\_DAT)  
FDAT\_ACT=FP3  
BAS(#FRAMES)  
BAS(#VEL\_CP,0.03)  
LIN XP3  
;ENDFOLD

;FOLD LIN P4 Vel= 0.01 m/s CPDAT2 Tool[14]:HF\_WAAM\_BERNARDO Base[8]:MESA\_MA\_BERN;{%PE}%R  
4.1.7,%MKUKATPBASIS,%CMOVE,%VLIN,%P 1:LIN, 2:P4, 3:, 5:0.01, 7:CPDAT2

\$BWDSTART = FALSE  
LDAT\_ACT=LCPDAT2

```
BAS(#CP_DAT)
FDAT_ACT=FP4
BAS(#FRAMES)
BAS(#VEL_CP,0.01)
LIN XP4
;ENDFOLD
```

```
;FOLD SYN OUT 1 'gas' State= TRUE at START Delay= 0 ms;%{PE}%R
4.1.7,%MKUKATPBASIS,%COUT,%VSYNOUT,%P 2:1, 3:'gas', 5:TRUE, 7:0, 9:0, 12:0
TRIGGER WHEN DISTANCE=0 DELAY=0 DO $OUT[1]=TRUE
;ENDFOLD
```

```
;FOLD LIN P5 Vel= 0.006 m/s CPDAT3 Tool[14]:HF_WAAM_BERNARDO Base[8]:MESA_MA_BERN;%{PE}%R
4.1.7,%MKUKATPBASIS,%CMOVE,%VLIN,%P 1:LIN, 2:P5, 3:, 5:0.006, 7:CPDAT3
$BWDSTART = FALSE
LDAT_ACT=LCPDAT3
BAS(#CP_DAT)
FDAT_ACT=FP5
BAS(#FRAMES)
BAS(#VEL_CP,0.006)
LIN XP5
;ENDFOLD
```

```
;FOLD SYN OUT 2 'soldadura' State= TRUE at START Delay= 0 ms;%{PE}%R
4.1.7,%MKUKATPBASIS,%COUT,%VSYNOUT,%P 2:2, 3:'soldadura', 5:TRUE, 7:0, 9:0, 12:0
TRIGGER WHEN DISTANCE=0 DELAY=0 DO $OUT[2]=TRUE
;ENDFOLD
;FOLD SYN OUT 4 'motor_fio' State= TRUE at START Delay= 0 ms;%{PE}%R
4.1.7,%MKUKATPBASIS,%COUT,%VSYNOUT,%P 2:4, 3:'motor_fio', 5:TRUE, 7:0, 9:0, 12:0
TRIGGER WHEN DISTANCE=0 DELAY=0 DO $OUT[4]=TRUE
;ENDFOLD
```

```
;FOLD SYN OUT 3 'martelo' State= TRUE at START Delay= 0 ms;%{PE}%R
4.1.7,%MKUKATPBASIS,%COUT,%VSYNOUT,%P 2:3, 3:'martelo', 5:TRUE, 7:0, 9:0, 12:0
TRIGGER WHEN DISTANCE=0 DELAY=0 DO $OUT[3]=TRUE
;ENDFOLD
```

```
;FOLD LIN P6 CONT Vel= 0.006 m/s CPDAT4 Tool[14]:HF_WAAM_BERNARDO Base[8]:MESA_MA_BERN;%{PE}%R
4.1.7,%MKUKATPBASIS,%CMOVE,%VLIN,%P 1:LIN, 2:P6, 3:C_DIS, 5:0.006, 7:CPDAT4
$BWDSTART = FALSE
LDAT_ACT=LCPDAT4
BAS(#CP_DAT)
FDAT_ACT=FP6
BAS(#FRAMES)
BAS(#VEL_CP,0.006)
LIN XP6 C_DIS
;ENDFOLD
```

```
;FOLD CIRC P7 P8 CONT Vel= 0.006 m/s CPDAT5 Tool[14]:HF_WAAM_BERNARDO Base[8]:MESA_MA_BERN;%{PE}%R
4.1.7,%MKUKATPBASIS,%CMOVE,%VCIRC,%P 1:CIRC, 2:P7, 3:P8, 4:C_DIS, 6:0.006, 8:CPDAT5
$BWDSTART = FALSE
LDAT_ACT=LCPDAT5
BAS(#CP_DAT)
FDAT_ACT=FP8
BAS(#FRAMES)
BAS(#VEL_CP,0.006)
```

CIRC XP7, XP8 C\_DIS  
;ENDFOLD

;FOLD CIRC P9 P10 CONT Vel= 0.006 m/s CPDAT6 Tool[14]:HF\_WAAM\_BERNARDO  
Base[8]:MESA\_MA\_BERN;%{PE}%R 4.1.7,%MKUKATPBASIS,%CMOVE,%VCIRC,%P 1:CIRC, 2:P9, 3:P10, 4:C\_DIS,  
6:0.006, 8:CPDAT6  
\$BWDSTART = FALSE  
LDAT\_ACT=LCPDAT6  
BAS(#CP\_DAT)  
FDAT\_ACT=FP10  
BAS(#FRAMES)  
BAS(#VEL\_CP,0.006)  
CIRC XP9, XP10 C\_DIS  
;ENDFOLD

;FOLD SYN OUT 4 'motor\_fio' State= FALSE at START Delay= 0 ms;%{PE}%R  
4.1.7,%MKUKATPBASIS,%COUT,%VSYNOUT,%P 2:4, 3:'motor\_fio', 5:FALSE, 7:0, 9:0, 12:0  
TRIGGER WHEN DISTANCE=0 DELAY=0 DO \$OUT[4]=FALSE  
;ENDFOLD

;FOLD SYN OUT 2 'soldadura' State= FALSE at START Delay= 0 ms;%{PE}%R  
4.1.7,%MKUKATPBASIS,%COUT,%VSYNOUT,%P 2:2, 3:'soldadura', 5:FALSE, 7:0, 9:0, 12:0  
TRIGGER WHEN DISTANCE=0 DELAY=0 DO \$OUT[2]=FALSE  
;ENDFOLD

;FOLD LIN P5 Vel= 0.006 m/s CPDAT3 Tool[14]:HF\_WAAM\_BERNARDO Base[8]:MESA\_MA\_BERN;%{PE}%R  
4.1.7,%MKUKATPBASIS,%CMOVE,%VLIN,%P 1:LIN, 2:P5, 3:, 5:0.006, 7:CPDAT3  
\$BWDSTART = FALSE  
LDAT\_ACT=LCPDAT3  
BAS(#CP\_DAT)  
FDAT\_ACT=FP5  
BAS(#FRAMES)  
BAS(#VEL\_CP,0.006)  
LIN XP5  
;ENDFOLD

;FOLD SYN OUT 1 'gas' State= FALSE at START Delay= 0 ms;%{PE}%R  
4.1.7,%MKUKATPBASIS,%COUT,%VSYNOUT,%P 2:1, 3:'gas', 5:FALSE, 7:0, 9:0, 12:0  
TRIGGER WHEN DISTANCE=0 DELAY=0 DO \$OUT[1]=FALSE  
;ENDFOLD

;FOLD LIN P4 Vel= 0.01 m/s CPDAT2 Tool[14]:HF\_WAAM\_BERNARDO Base[8]:MESA\_MA\_BERN;%{PE}%R  
4.1.7,%MKUKATPBASIS,%CMOVE,%VLIN,%P 1:LIN, 2:P4, 3:, 5:0.01, 7:CPDAT2  
\$BWDSTART = FALSE  
LDAT\_ACT=LCPDAT2  
BAS(#CP\_DAT)  
FDAT\_ACT=FP4  
BAS(#FRAMES)  
BAS(#VEL\_CP,0.01)  
LIN XP4  
;ENDFOLD

;FOLD SYN OUT 3 'martelo' State= FALSE at START Delay= 0 ms;%{PE}%R  
4.1.7,%MKUKATPBASIS,%COUT,%VSYNOUT,%P 2:3, 3:'martelo', 5:FALSE, 7:0, 9:0, 12:0  
TRIGGER WHEN DISTANCE=0 DELAY=0 DO \$OUT[3]=FALSE  
;ENDFOLD



```
;FOLD LIN P3 Vel= 0.03 m/s CPDAT1 Tool[14]:HF_WAAM_BERNARDO Base[8]:MESA_MA_BERN;{%PE}%R
4.1.7,%MKUKATPBASIS,%CMOVE,%VLIN,%P 1:LIN, 2:P3, 3:, 5:0.03, 7:CPDAT1
$BWDSTART = FALSE
LDAT_ACT=LCPDAT1
BAS(#CP_DAT)
FDAT_ACT=FP3
BAS(#FRAMES)
BAS(#VEL_CP,0.03)
LIN XP3
;ENDFOLD
```

```
;FOLD WAIT Time= 30 sec;{%PE}%R 4.1.7,%MKUKATPBASIS,%CWAIT,%VWAIT,%P 2:30
WAIT SEC 30
;ENDFOLD
XP3.Z = XP3.Z + Z2
XP4.Z = XP4.Z + Z2
XP5.Z = XP5.Z + Z2
XP6.Z = XP6.Z + Z2
XP7.Z = XP7.Z + Z2
XP8.Z = XP8.Z + Z2
XP9.Z = XP9.Z + Z2
XP10.Z = XP10.Z + Z2
XP12.Z = XP12.Z + Z2
XP13.Z = XP13.Z + Z2
XP14.Z = XP14.Z + Z2
XP15.Z = XP15.Z + Z2
```

```
;FOLD LIN P3 Vel= 0.03 m/s CPDAT1 Tool[14]:HF_WAAM_BERNARDO Base[8]:MESA_MA_BERN;{%PE}%R
4.1.7,%MKUKATPBASIS,%CMOVE,%VLIN,%P 1:LIN, 2:P3, 3:, 5:0.03, 7:CPDAT1
$BWDSTART = FALSE
LDAT_ACT=LCPDAT1
BAS(#CP_DAT)
FDAT_ACT=FP3
BAS(#FRAMES)
BAS(#VEL_CP,0.03)
LIN XP3
;ENDFOLD
```

```
;FOLD LIN P4 Vel= 0.01 m/s CPDAT2 Tool[14]:HF_WAAM_BERNARDO Base[8]:MESA_MA_BERN;{%PE}%R
4.1.7,%MKUKATPBASIS,%CMOVE,%VLIN,%P 1:LIN, 2:P4, 3:, 5:0.01, 7:CPDAT2
$BWDSTART = FALSE
LDAT_ACT=LCPDAT2
BAS(#CP_DAT)
FDAT_ACT=FP4
BAS(#FRAMES)
BAS(#VEL_CP,0.01)
LIN XP4
;ENDFOLD
```

```
;FOLD SYN OUT 1 'gas' State= TRUE at START Delay= 0 ms;{%PE}%R
4.1.7,%MKUKATPBASIS,%COUT,%VSYNOUT,%P 2:1, 3:'gas', 5:TRUE, 7:0, 9:0, 12:0
TRIGGER WHEN DISTANCE=0 DELAY=0 DO $OUT[1]=TRUE
;ENDFOLD
;FOLD LIN P5 Vel= 0.006 m/s CPDAT3 Tool[14]:HF_WAAM_BERNARDO Base[8]:MESA_MA_BERN;{%PE}%R
4.1.7,%MKUKATPBASIS,%CMOVE,%VLIN,%P 1:LIN, 2:P5, 3:, 5:0.006, 7:CPDAT3
$BWDSTART = FALSE
```

```

LDAT_ACT=LCPDAT3
BAS(#CP_DAT)
FDAT_ACT=FP5
BAS(#FRAMES)
BAS(#VEL_CP,0.006)
LIN XP5
;ENDFOLD
;FOLD SYN OUT 2 'soldadura' State= TRUE at START Delay= 0 ms;%{PE}%R
4.1.7,%MKUKATPBASIS,%COUT,%VSYNOUT,%P 2:2, 3:'soldadura', 5:TRUE, 7:0, 9:0, 12:0
TRIGGER WHEN DISTANCE=0 DELAY=0 DO $OUT[2]=TRUE
;ENDFOLD
;FOLD SYN OUT 4 'motor_fio' State= TRUE at START Delay= 0 ms;%{PE}%R
4.1.7,%MKUKATPBASIS,%COUT,%VSYNOUT,%P 2:4, 3:'motor_fio', 5:TRUE, 7:0, 9:0, 12:0
TRIGGER WHEN DISTANCE=0 DELAY=0 DO $OUT[4]=TRUE
;ENDFOLD

;FOLD SYN OUT 3 'martelo' State= TRUE at START Delay= 0 ms;%{PE}%R
4.1.7,%MKUKATPBASIS,%COUT,%VSYNOUT,%P 2:3, 3:'martelo', 5:TRUE, 7:0, 9:0, 12:0
TRIGGER WHEN DISTANCE=0 DELAY=0 DO $OUT[3]=TRUE
;ENDFOLD

;FOLD LIN P6 CONT Vel= 0.006 m/s CPDAT4 Tool[14]:HF_WAAM_BERNARDO Base[8]:MESA_MA_BERN;%{PE}%R
4.1.7,%MKUKATPBASIS,%CMOVE,%VLIN,%P 1:LIN, 2:P6, 3:C_DIS, 5:0.006, 7:CPDAT4
$BWDSTART = FALSE
LDAT_ACT=LCPDAT4
BAS(#CP_DAT)
FDAT_ACT=FP6
BAS(#FRAMES)
BAS(#VEL_CP,0.006)
LIN XP6 C_DIS
;ENDFOLD
;FOLD CIRC P12 P13 CONT Vel= 0.006 m/s CPDAT7 Tool[14]:HF_WAAM_BERNARDO
Base[8]:MESA_MA_BERN;%{PE}%R 4.1.7,%MKUKATPBASIS,%CMOVE,%VCIRC,%P 1:CIRC, 2:P12, 3:P13, 4:C_DIS,
6:0.006, 8:CPDAT7
$BWDSTART = FALSE
LDAT_ACT=LCPDAT7
BAS(#CP_DAT)
FDAT_ACT=FP13
BAS(#FRAMES)
BAS(#VEL_CP,0.006)
CIRC XP12, XP13 C_DIS
;ENDFOLD
;FOLD CIRC P14 P15 CONT Vel= 0.006 m/s CPDAT8 Tool[14]:HF_WAAM_BERNARDO
Base[8]:MESA_MA_BERN;%{PE}%R 4.1.7,%MKUKATPBASIS,%CMOVE,%VCIRC,%P 1:CIRC, 2:P14, 3:P15, 4:C_DIS,
6:0.006, 8:CPDAT8
$BWDSTART = FALSE
LDAT_ACT=LCPDAT8
BAS(#CP_DAT)
FDAT_ACT=FP15
BAS(#FRAMES)
BAS(#VEL_CP,0.006)
CIRC XP14, XP15 C_DIS
;ENDFOLD
;FOLD SYN OUT 4 'motor_fio' State= FALSE at START Delay= 0 ms;%{PE}%R
4.1.7,%MKUKATPBASIS,%COUT,%VSYNOUT,%P 2:4, 3:'motor_fio', 5:FALSE, 7:0, 9:0, 12:0
TRIGGER WHEN DISTANCE=0 DELAY=0 DO $OUT[4]=FALSE

```

```

;ENDFOLD
;FOLD SYN OUT 2 'soldadura' State= FALSE at START Delay= 0 ms;%{PE}%R
4.1.7,%MKUKATPBASIS,%COUT,%VSYNOUT,%P 2:2, 3:'soldadura', 5:FALSE, 7:0, 9:0, 12:0
TRIGGER WHEN DISTANCE=0 DELAY=0 DO $OUT[2]=FALSE
;ENDFOLD

;FOLD LIN P5 Vel= 0.006 m/s CPDAT3 Tool[14]:HF_WAAM_BERNARDO Base[8]:MESA_MA_BERN;%{PE}%R
4.1.7,%MKUKATPBASIS,%CMOVE,%VLIN,%P 1:LIN, 2:P5, 3:, 5:0.006, 7:CPDAT3
$BWDSTART = FALSE
LDAT_ACT=LCPDAT3
BAS(#CP_DAT)
FDAT_ACT=FP5
BAS(#FRAMES)
BAS(#VEL_CP,0.006)
LIN XP5
;ENDFOLD
;FOLD SYN OUT 1 'gas' State= FALSE at START Delay= 0 ms;%{PE}%R
4.1.7,%MKUKATPBASIS,%COUT,%VSYNOUT,%P 2:1, 3:'gas', 5:FALSE, 7:0, 9:0, 12:0
TRIGGER WHEN DISTANCE=0 DELAY=0 DO $OUT[1]=FALSE
;ENDFOLD
;FOLD LIN P4 Vel= 0.01 m/s CPDAT2 Tool[14]:HF_WAAM_BERNARDO Base[8]:MESA_MA_BERN;%{PE}%R
4.1.7,%MKUKATPBASIS,%CMOVE,%VLIN,%P 1:LIN, 2:P4, 3:, 5:0.01, 7:CPDAT2
$BWDSTART = FALSE
LDAT_ACT=LCPDAT2
BAS(#CP_DAT)
FDAT_ACT=FP4
BAS(#FRAMES)
BAS(#VEL_CP,0.01)
LIN XP4
;ENDFOLD

;FOLD SYN OUT 3 'martelo' State= FALSE at START Delay= 0 ms;%{PE}%R
4.1.7,%MKUKATPBASIS,%COUT,%VSYNOUT,%P 2:3, 3:'martelo', 5:FALSE, 7:0, 9:0, 12:0
TRIGGER WHEN DISTANCE=0 DELAY=0 DO $OUT[3]=FALSE
;ENDFOLD

;FOLD LIN P3 Vel= 0.03 m/s CPDAT1 Tool[14]:HF_WAAM_BERNARDO Base[8]:MESA_MA_BERN;%{PE}%R
4.1.7,%MKUKATPBASIS,%CMOVE,%VLIN,%P 1:LIN, 2:P3, 3:, 5:0.03, 7:CPDAT1
$BWDSTART = FALSE
LDAT_ACT=LCPDAT1
BAS(#CP_DAT)
FDAT_ACT=FP3
BAS(#FRAMES)
BAS(#VEL_CP,0.03)
LIN XP3
;ENDFOLD
;FOLD WAIT Time= 30 sec;%{PE}%R 4.1.7,%MKUKATPBASIS,%CWAIT,%VWAIT,%P 2:30
WAIT SEC 30
;ENDFOLD

XP3.Z = XP3.Z + Z2
XP4.Z = XP4.Z + Z2
XP5.Z = XP5.Z + Z2
XP6.Z = XP6.Z + Z2
XP7.Z = XP7.Z + Z2
XP8.Z = XP8.Z + Z2

```

```
XP9.Z = XP9.Z + Z2
XP10.Z = XP10.Z + Z2
XP12.Z = XP12.Z + Z2
XP13.Z = XP13.Z + Z2
XP14.Z = XP14.Z + Z2
XP15.Z = XP15.Z + Z2
```

```
ENDFOR
```

```
;FOLD PTP P11 Vel= 5 % PDAT3 Tool[14]:HF_WAAM_BERNARDO Base[8]:MESA_MA_BERN;{%PE}%R
4.1.7,%MKUKATPBASIS,%CMOVE,%VPTP,%P 1:PTP, 2:P11, 3:, 5:5, 7:PDAT3
```

```
$BWDSTART = FALSE
```

```
PDAT_ACT=PPDAT3
```

```
BAS(#PTP_DAT)
```

```
FDAT_ACT=FP11
```

```
BAS(#FRAMES)
```

```
BAS(#VEL_PTP,5)
```

```
PTP XP11
```

```
;ENDFOLD
```

```
XP3 = A1
```

```
XP4 = A2
```

```
XP5 = A3
```

```
XP6 = A4
```

```
XP7 = A5
```

```
XP8 = A6
```

```
XP9 = A7
```

```
XP10 = A8
```

```
XP12 = A10
```

```
XP13 = A11
```

```
XP14 = A12
```

```
XP15 = A13
```

```
;FOLD PTP HOME Vel= 7 % DEFAULT;{%PE}%R 4.1.7,%MKUKATPBASIS,%CMOVE,%VPTP,%P 1:PTP, 2:HOME, 3:, 5:7,
7:DEFAULT
```

```
$BWDSTART = FALSE
```

```
PDAT_ACT=PDEFAULT
```

```
BAS(#PTP_DAT)
```

```
FDAT_ACT=FHOME
```

```
BAS(#FRAMES)
```

```
BAS(#VEL_PTP,7)
```

```
$H_POS=XHOME
```

```
PTP XHOME
```

```
;ENDFOLD
```

```
END
```

## B.2 Robot's code - Part 2 - Coordinates

```
&ACCESS RVP
&REL 8
&PARAM TEMPLATE = C:\KRC\Roboter\Template\vorgabe
&PARAM EDITMASK = *
DEFDAT CILINDRO3
;FOLD EXTERNAL DECLARATIONS;%{PE}%V3.2.0,%MKUKATPBASIS,%CEXT,%VCOMMON,%P
;FOLD BAS EXT;%{PE}%V3.2.0,%MKUKATPBASIS,%CEXT,%VEXT,%P
EXT BAS (BAS_COMMAND :IN,REAL :IN )
DECL INT SUCCESS
;ENDFOLD
;FOLD A10 EXT;%{E}%V3.2.0,%MKUKATPARC,%CEXT,%VEXT,%P
EXT A10 (A_CMD_T :IN,A_STRT_T :IN,A_WELD_T :IN,A_END_T :IN,INT :IN )
;ENDFOLD
;FOLD A20 EXT;%{E}%V3.2.0,%MKUKATPA20,%CEXT,%VEXT,%P
EXT A20 (INT :IN,WELD_ST :IN,WELD_FI :IN,INT :IN )
;ENDFOLD
;FOLD GRIPPER EXT;%{E}%V3.2.0,%MKUKATPGRIPPER,%CEXT,%VEXT,%P
EXT H50 (INT :IN,INT :IN,INT :IN,GRP_TYP :IN )
;ENDFOLD
;FOLD SPOT EXT;%{E}%V3.2.0,%MKUKATPSPOT,%CEXT,%VEXT,%P
EXT USERSPOT (S_COMMAND :IN,SPOT_TYPE :IN )
;ENDFOLD
;FOLD TOUCHSENSE EXT;%{E}%V3.2.0,%MKUKATPTS,%CEXT,%VEXT,%P
EXT H70 (INT :IN,SRCH_TYP_2 :OUT,E6POS :IN,SRCH_TYP_3 :IN,SRCH_TYP_2 :IN,SRCH_TYP_2 :IN,SRCH_TYP_2 :IN,SRCH_TYP_2 :IN,INT :IN )
;ENDFOLD
;FOLD USER EXT;%{E}%V3.2.0,%MKUKATPUSER,%CEXT,%VEXT,%P
;Make here your modifications
;ENDFOLD
;ENDFOLD

DECL INT I,Z1,Z2,Z3
DECL E6POS A1,A2,A3,A4,A5,A6,A7,A8,A10,A11,A12,A13

DECL BASIS_SUGG_T LAST_BASIS={POINT1[] "P14          ",POINT2[] "P15          ",CP_PARAMS[]
"CPDAT8          ",PTP_PARAMS[] "PDAT3          ",CONT[] "          ",CP_VEL[] "0.006
",PTP_VEL[] "5          ")DECL E6POS XP1={x 54.0545883,y 171.543106,z 147.870804,a 179.997894,b
0.911103129,c 179.998199,s 2,t 10,e1 0.0,e2 0.0,e3 0.0,e4 0.0,e5 0.0,e6 0.0}
DECL FDAT FP1={TOOL_NO 14,BASE_NO 8,IPO_FRAME #BASE}
DECL PDAT PPDAT1={VEL 100.0,ACC 100.0,APO_DIST 100.0}
DECL E6POS XP2={x 23.2235508,y 186.779205,z 110.554199,a -179.997299,b 0.906233013,c -179.205902,s 2,t
2,e1 0.0,e2 0.0,e3 0.0,e4 0.0,e5 0.0,e6 0.0}
DECL FDAT FP2={TOOL_NO 14,BASE_NO 8,IPO_FRAME #BASE}
DECL PDAT PPDAT2={VEL 100.0,ACC 100.0,APO_DIST 100.0}
```

DECL E6POS XP3={x 96.7583466,y 185.494507,z 110.560997,a -179.992294,b 0.906879306,c -179.206406,s 2,t  
2,e1 0.0,e2 0.0,e3 0.0,e4 0.0,e5 0.0,e6 0.0}  
DECL FDAT FP3={TOOL\_NO 14,BASE\_NO 8,IPO\_FRAME #BASE}  
DECL LDAT LCPDAT1={VEL 2.0,ACC 100.0,APO\_DIST 100.0,APO\_FAC 50.0}  
DECL E6POS XP4={x 96.7570724,y 191.365005,z 110.561996,a -179.990204,b 0.907289922,c -179.205902,s 2,t  
2,e1 0.0,e2 0.0,e3 0.0,e4 0.0,e5 0.0,e6 0.0}  
DECL FDAT FP4={TOOL\_NO 14,BASE\_NO 8,IPO\_FRAME #BASE}  
DECL LDAT LCPDAT2={VEL 2.0,ACC 100.0,APO\_DIST 100.0,APO\_FAC 50.0}  
DECL E6POS XP5={x 96.7702637,y 195.701797,z 110.569397,a -179.992096,b 0.908546925,c -179.206207,s 2,t  
2,e1 0.0,e2 0.0,e3 0.0,e4 0.0,e5 0.0,e6 0.0}  
DECL FDAT FP5={TOOL\_NO 14,BASE\_NO 8,IPO\_FRAME #BASE}  
DECL LDAT LCPDAT3={VEL 2.0,ACC 100.0,APO\_DIST 100.0,APO\_FAC 50.0}  
DECL E6POS XP6={x 96.7756271,y 199.811707,z 110.573502,a -179.995193,b 0.909212172,c -179.205994,s 2,t  
2,e1 0.0,e2 0.0,e3 0.0,e4 0.0,e5 0.0,e6 0.0}  
DECL FDAT FP6={TOOL\_NO 14,BASE\_NO 8,IPO\_FRAME #BASE}  
DECL LDAT LCPDAT4={VEL 2.0,ACC 100.0,APO\_DIST 0.0,APO\_FAC 50.0}  
DECL E6POS XP7={x 77.5550919,y 219.048904,z 105.559097,a -179.989304,b 0.909577727,c -179.2052,s 2,t  
2,e1 0.0,e2 0.0,e3 0.0,e4 0.0,e5 0.0,e6 0.0}  
DECL E6POS XP8={x 92.3370209,y 237.640305,z 109.8731,a -179.994995,b 0.908925712,c -179.205597,s 2,t  
2,e1 0.0,e2 0.0,e3 0.0,e4 0.0,e5 0.0,e6 0.0}  
DECL FDAT FP8={TOOL\_NO 14,BASE\_NO 8,IPO\_FRAME #BASE}  
DECL LDAT LCPDAT5={VEL 2.0,ACC 100.0,APO\_DIST 0.0,APO\_FAC 50.0}  
DECL E6POS XP9={x 112.9636,y 218.391403,z 105.590698,a -179.9944,b 0.910759628,c -179.205399,s 2,t 2,e1  
0.0,e2 0.0,e3 0.0,e4 0.0,e5 0.0,e6 0.0}  
DECL E6POS XP10={x 100.156303,y 199.814102,z 109.874802,a -179.994598,b 0.910532176,c -179.206207,s  
2,t 2,e1 0.0,e2 0.0,e3 0.0,e4 0.0,e5 0.0,e6 0.0}  
DECL FDAT FP10={TOOL\_NO 14,BASE\_NO 8,IPO\_FRAME #BASE}  
DECL LDAT LCPDAT6={VEL 2.0,ACC 100.0,APO\_DIST 0.0,APO\_FAC 50.0}  
DECL E6POS XP11={x -69.2939072,y 192.954498,z 241.526398,a -179.992599,b 0.910327971,c 179.998795,s  
2,t 10,e1 0.0,e2 0.0,e3 0.0,e4 0.0,e5 0.0,e6 0.0}  
DECL FDAT FP11={TOOL\_NO 14,BASE\_NO 8,IPO\_FRAME #BASE}  
DECL PDAT PPDAT3={VEL 100.0,ACC 100.0,APO\_DIST 100.0}  
DECL E6POS XP12={x 113.079903,y 218.354797,z 105.604698,a -179.987,b 0.90912497,c -179.2061,s 2,t 2,e1  
0.0,e2 0.0,e3 0.0,e4 0.0,e5 0.0,e6 0.0}  
DECL E6POS XP13={x 92.3334198,y 237.675903,z 109.877502,a 179.998398,b 0.90809077,c -179.205505,s 2,t  
2,e1 0.0,e2 0.0,e3 0.0,e4 0.0,e5 0.0,e6 0.0}  
DECL FDAT FP13={TOOL\_NO 14,BASE\_NO 8,IPO\_FRAME #BASE}  
DECL LDAT LCPDAT7={VEL 2.0,ACC 100.0,APO\_DIST 0.0,APO\_FAC 50.0}  
DECL E6POS XP14={x 77.5479202,y 219.064301,z 105.555,a -179.999298,b 0.908674717,c -179.205795,s 2,t  
2,e1 0.0,e2 0.0,e3 0.0,e4 0.0,e5 0.0,e6 0.0}  
DECL E6POS XP15={x 92.5837479,y 199.320297,z 110.5746,a -179.9935,b 0.908797026,c -179.205994,s 2,t  
2,e1 0.0,e2 0.0,e3 0.0,e4 0.0,e5 0.0,e6 0.0}  
DECL FDAT FP15={TOOL\_NO 14,BASE\_NO 8,IPO\_FRAME #BASE}  
DECL LDAT LCPDAT8={VEL 2.0,ACC 100.0,APO\_DIST 0.0,APO\_FAC 50.0}  
ENDDAT



2022

Bernardo Cruz Varzielas

ROBOTIZING THE CONVENTIONAL AND HOT FORGING WIRE ARC ADDITIVE  
MANUFACTURING PROCESSES FOR PRODUCING 3D PARTS WITH COMPLEX GEOMETRIES